Exploring altered cortical activity using high-density multi-electrode arrays.

Megan Boucher-Routhier

Thesis submitted to the University of Ottawa

in partial fulfillment of the requirements for the

Doctor of Philosophy in Experimental Psychology

School of Psychology

Faculty of Social Sciences

University of Ottawa

TABLE OF CONTENTS

LIST OF FIGURES

LIST OF ABBREVIATIONS

RT: radiation therapy

hd-MEA: high-density multi-electrode array

4-AP: 4-Aminopyridine

PFC: prefrontal cortex

GAN: generative adversarial network

PI: propidium iodide

GABA: γ-Aminobutyric acid

LTP: long-term potentiation

FLE: frontal lobe epilepsy

CA1: cornu ammonis 1

EEG: electroencephalography

fMRI: functional magnetic resonance imaging

MEG: magnetoencephalography

ECoG: electrocorticography

CMOS: complementary metal oxide semi-conductor

APS: active-pixel sensor

PCA: principal components analysis

FA: factor analysis

DMD: dynamic mode decomposition

WGAN: Wasserstein GAN

EM distance: earth-mover distance

K^+: potassium

Mg^{2+}: magnesium

PE: pro-epileptiform

ACSF: artificial cerebrospinal fluid

PE-ACSF: pro-epileptiform artificial cerebrospinal fluid

ReLU: rectified linear units

htan: hypertan

SD: standard deviation

PR: participation ratio

LBMLE: Levina-Bickel maximum likelihood estimation.

FID: Frechet inception distance

SRS: stereotactic radiosurgery

MUA: multi-unit activity

M2: secondary motor area

PrL: prelimbic cortex

MO: medial orbital cortex

VO: ventral orbital cortex

LO: lateral orbital cortex

DLO: dorsolateral orbital cortex

NMDAR: N-methyl-D-aspartate receptor

EGCG: epigallocatechin-3-gallate

mPFC: medial prefrontal cortex

LTD: long-term depression

VAEs: variational autoencoders

NMDG: N-methyl-D-glucamine

PT: physiological temperature

CT: ice-cold temperature

PV neurons: parvalbumin-expressing interneurons

PREFACE

PUBLISHED WORK

This thesis document is based on the following published work:

Boucher-Routhier, M., & Thivierge, J. P. (2023). A deep generative adversarial network capturing complex spiral waves in disinhibited circuits of the cerebral cortex. *BMC neuroscience*, *24*(1), 22.

Contributions: M.B.R and J.P.T designed the experiment. **M.B.R** performed the experiment. **M.B.R** and J.P.T analyzed and interpreted the data. **M.B.R** and J.P.T wrote the manuscript. All authors discussed the results, revised the manuscript, and approved the final manuscript. All authors read and approved the final manuscript.

As well as the following submitted work:

Boucher-Routhier, M., Szanto, J., Nair, V., & Thivierge, J.P., (2024). High-density multi-electrode platform examining the effects of radiation on activity, functional connectivity, complexity, and survival of in vitro cortical networks. [Manuscript under consideration].

Contributions: M.B.R. and J.P.T. conceived the study. **M.B.R**. and J.S. performed the experiments and data collection. **M.B.R**. and J.P.T. analyzed the data. V.N. and J.P.T. supervised the study. All authors contributed to interpreting the results. All authors contributed to writing the manuscript.

APPROVALS

All experiments were conducted in accordance with the Canadian Council on Animal Care guidelines and all procedures were approved by the University of Ottawa Animal Care and Veterinary Services under protocol CMMe-3604.

ACKNOWLEDGMENTS

The work presented in this thesis represents the most challenging and rewarding period of my life to date. These past few years have allowed me to grow immensely as a researcher and on a personal level. Although this experience has been challenging, I am grateful to have gained a deep level of understanding of the inner workings of conducting research and the resilience required to accomplish such a task.

I owe a great deal of gratitude to my supervisor Dr. Jean-Philippe Thivierge who graciously allowed me to volunteer in his lab many years ago as an undergraduate student despite my having no background in computational or experimental neuroscience. Your support and guidance throughout these years (especially during such an unprecedented time) made this experience one I can reflect on with fond memories. The knowledge and skills that I have acquired under your supervision will no doubt carry me through any future endeavours.

I am extremely thankful for the feedback and insight provided by my committee members Dr. Hélène Plamondon, Dr. Nafissa Ismail, Dr. Sylvain Chartier and my external examiner Dr. Julio Martinez Trujillo. Thank you for pushing me to think more critically about my work and ultimately be the best researcher I can be.

I would also like to thank my lab mates past and present who helped me get my studies off the ground and provided moral support along the way. A special thank you to Dr. Philippe Vincent-Lamare, Dr. Éloïse Giraud, Artem Pilzak, Camille Godin, Judy Chékiée and many more. You all made this experience that much more enjoyable.

To our collaborators at the Ottawa Hospital Cancer Center, Dr. Vimoj Nair and Dr. Janos Szanto, I am extremely grateful for your knowledge and expertise that helped make my thesis possible. Your encouragement throughout this process did not go unnoticed.

To my partner, Casey, thank you for your unwavering love and support throughout the past few years and for always finding a way to brighten my day when I was faced with challenges. Your belief in me never went unnoticed and I am forever grateful to have had you by my side throughout this journey.

To my parents, Debbie and Daniel, and my stepdad Tom, thank you for always believing in my potential and for your ongoing love and support throughout this journey. Without you, none of this would have been possible. A special thank you to my grandma, Carole whose belief in me never faltered. I could not have made it through this without your endless love, support and encouragement. Thank you to the rest of my family for their words of encouragement that kept me going throughout my academic career.

Finally, I would like to express my gratitude to my amazing friends who supported me throughout this journey. Bronwen, I am so glad we met through this program, and I am forever grateful for the friendship we have cultivated throughout the years. Karianne, Kalyn, and Abby, thank you for always checking in on me and for encouraging me throughout my (many) years of school!

ABSTRACT

Altered cortical activity has been associated with several brain states including those following radiation therapy (RT), as well as diseased brain states such as epilepsy. These states often result in activation patterns within neural networks that possess unique spatiotemporal dynamics such as propagating waves. They have also been associated with altered neural activity and a variety of cognitive deficits; however, the network dynamics underlying these changes remain poorly understood. We aimed to explore and compare the neural dynamics of irradiated cortical networks to epileptiform networks which produced a series of spiral waves. We used a large-scale high-density multi-electrode array (hd-MEA) to investigate the network-level neural dynamics underlying both pathological brain states. To induce an epileptic brain state, we applied a pro-epileptiform solution consisting of 4-Aminopyridine (4-AP), increased extracellular potassium, and decreased extracellular magnesium to a subset of acute prefrontal cortex (PFC) slices from rats. Subsequently, we were able to examine the characteristics of spiral waves that propagated across the networks in our slices. These spiral waves possessed stereotypical features whereby they rotated around a fixed center of mass, had a broad distribution of instantaneous phases across electrodes and showed increased complexity compared to baseline networks. We then trained a deep generative adversarial network (GAN) to capture the key aspects of the spiral waves in order to produce novel exemplars of these otherwise rare events. We subsequently irradiated healthy PFC slices with a series of doses ranging from 20 to 100 Gy to examine the acute effects of radiation on cortical networks. We found an increase in the

firing rate and density of functional connectivity within the irradiated slices. In comparison, the pro-epileptiform networks showed an increase in firing rate and the strength of the functional connections amongst neurons, but a lower density of connections due to the spatially localized nature of spiral waves. These differences in functional connectivity highlight the fact that these represent distinct brain states, and that RT is not merely inducing an epileptic state. Finally, we stained a subset of our irradiated slices with propidium iodide (PI) to quantify cell death and found a dose-dependent increase in apoptosis. Together, these results point to hd-MEAs as a promising tool for studying altered brain state dynamics, which can be used to help inform treatment protocols for both epilepsy and to minimize radiation-induced brain injuries.

CHAPTER 1: GENERAL INTRODUCTION

ALTERED CORTICAL ACTIVITY

The brain produces intricate patterns of activity that have a wide range of spatiotemporal dynamics. The variability in network dynamics occurs as a result of signalling, or connections, between individual neurons or with larger neuronal circuits (Faisal et al., 2008; Liu et al., 2019; Stein et al., 2005). This neural signalling unfolds over time across a wide range of spatial and temporal scales (Avena-Koenigsberger et al., 2018; Liu et al., 2019; Muller et al., 2018). These patterns of activation are influenced by a variety of factors such as wakefulness (Constantinople & Bruno, 2011; Poulet & Crochet, 2019), cognitive demands (Nadeau, 2020; Reinhart & Woodman, 2014), as well as pathological or diseased brain states (Northoff, 2018).

The brain has also been shown to enter a variety of altered states which are often accompanied by aberrant increases or decreases in activity across brain regions. These altered brain states frequently occur in diseases of the brain and are associated with several cognitive deficits (Dagher, 2001; Mohajerani et al., 2011; Monchi et al., 2006; Patrikelis et al., 2009; Ramanathan et al., 2018; Ranchet et al., 2020; Sato et al., 2015; Verche et al., 2018). Past research has shown that altered cortical activity is associated with diseases such as epilepsy, Parkinson's, cerebral palsy, and stroke (Braakman et al., 2011; Mohajerani et al., 2011; Monchi et al., 2006; Ramanathan et al., 2018; Ranchet et al., 2020; Sato et al., 2015; Trevarrow et al., 2022). In addition, certain disease states can lead to widespread changes in activation patterns within neural circuits that can extend to unaffected brain

regions such as in the case of strokes (Mohajerani et al., 2011; Sato et al., 2015). It has also been associated with brain states following radiation-therapy (RT) including radiation-induced brain injuries (Zhang et al., 2020).

CORTICAL DISINHIBITION AND TRAVELLING WAVES

Neural disinhibition occurs when the balance of excitation and inhibition becomes disrupted (Ammann et al., 2020; Letzkus et al., 2015). This phenomenon has been linked to deficiencies in inhibitory γ-Aminobutyric acid (GABA) transmission and has been associated with the cognitive impairments seen in several disease states (Bast et al., 2017). Past research has established that cortical disinhibition can lead to complex spatiotemporal patterns of neural activity (X. Huang et al., 2004). As a result, disinhibited cortical networks locally synchronize their activity and produce propagating waves (Figure 1) that travel in a single direction (planar waves) or a circular pattern around a fixed spatial locus (spiral waves). They can also form sink and source patterns that contract or expand from a fixed point, as well as saddle patterns that form when multiple waves interact (Engel & Steinmetz, 2019; X. Huang et al., 2010; Muller et al., 2018; Sato et al., 2012; Townsend et al., 2015; Townsend & Gong, 2018; J.-Y. Wu et al., 2008). In unbalanced networks where excitation dominates, complex wave patterns such as spiral waves propagate more globally across the brain for longer periods of time (X. Huang et al., 2010; Keane & Gong, 2015). In contrast, networks where inhibition dominates produce wave patterns that travel across short distances as they tend fall apart rapidly (Keane & Gong, 2015).

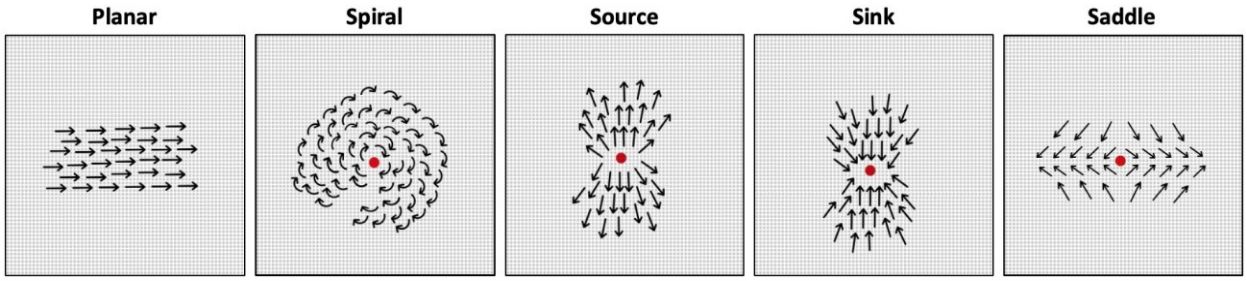

FIGURE 1. REPRESENTATION OF PROPAGATING WAVES THAT OCCUR DURING CORTICAL DISINHIBITION

These waves travel over a wide range of spatial (from single cortical regions to more global patterns) and temporal scales (tens to hundreds of milliseconds) (Muller et al., 2018). Previously, synchronous activity amongst neurons, including neural oscillations, was thought to possess precise zero-lag synchrony whereby the oscillations across brain regions were thought to have perfect temporal alignment (Gray et al., 1989; Muller et al., 2018; Uhlhaas et al., 2009). In contrast, more recent research has shown that travelling waves possess a variety of flexible phase offsets rather than following a precise zero-lag synchrony, which increases in complexity when multiple travelling waves are combined (Muller et al., 2018). Propagating waves are influenced by various brain states and can thus be generated internally, whereas others are generated in response to external stimuli or the sensory conditions of the organism (Muller et al., 2018).

These complex propagating waves are speculated to contribute to cortical function in several ways. To begin, they provide background depolarization in select regions which leads to an increased firing probability and a higher efficacy of synaptic transmission. They may also provide a focus of attention on certain sensory regions as they increase the sensitivity of the network to incoming stimulation (J.-Y. Wu et al., 2008). Finally, it has been

speculated that travelling waves can modulate cortical excitability in a spatially and temporally precise way, which can then impact the future processing of stimuli (Palkar et al., 2023). In contrast to disease states, some changes in localized cortical activity or network activation patterns have been thought to represent potential compensatory mechanisms (Dagher, 2001; Mohajerani et al., 2011; Monchi et al., 2006; Patrikelis et al., 2009). Thus, understanding these network activation patterns will provide important insight into how the brain carries out tasks involving learning, memory, and cognition (Engel & Steinmetz, 2019; Townsend & Gong, 2018).

EPILEPTIFORM BRAIN ACTIVITY – A DISINHIBITED BRAIN STATE

One example of a disinhibited brain state occurs when the brain produces epileptiform activity whereby cortical neurons produce complex propagating waves. Epilepsy is a disease that involves a large variety of pathological network changes that are characterized by recurrent bouts of excessive neural activity (Wenzel et al., 2017). This activity is defined by a transient and abnormal discharge of neurons producing hyperexcitability and hypersynchrony (Grainger et al., 2018; Jiruska et al., 2013), which results from a wide range of underlying causes (Kramer & Cash, 2012). Seizures are typically classified as either focal seizures which originate from a particular region of the brain and can either remain localized or spread to adjacent regions or as primary generalized seizures involving the entire brain or very large regions of the brain (Kramer & Cash, 2012).

There are three stages of seizures beginning with seizure onset, followed by propagation and ending in seizure termination (Kramer & Cash, 2012). Seizure onset

typically involves subtle changes in the voltage of brain activity such that high-frequency oscillations ranging from roughly 20 Hz to over 100 Hz are produced (Bragin et al., 1999; De Curtis & Gnatkovsky, 2009; Kramer & Cash, 2012). These subtle changes often also precede the presentation of clinical symptoms (Kramer & Cash, 2012). In addition, decreases in coupling between brain regions have been shown in higher frequency bands (80-200 Hz), but not in lower frequency bands such as delta (1-4 Hz), alpha (8-13 Hz) and beta (13-30 Hz) frequencies (Grenier et al., 2001; Kramer & Cash, 2012; Schindler et al., 2010). During seizure propagation, there is a transition to slower rhythmic activity with a large amplitude that is more distributed across brain regions and is associated with changes in coupling (Kramer & Cash, 2012). Finally, seizure termination involves large-scale cessation of activity that occurs simultaneously and is thought to be accompanied by increased coupling of neural activity (Kramer et al., 2010; Kramer & Cash, 2012; Schindler et al., 2008).

Recent research has aimed to provide a more thorough understanding of seizure formation and propagation across cortical regions. This research has shown that epileptic activity begins with local neuronal ensembles within an initiation site (micro seizure) followed by a gradual expansion of hyperactivity into neighbouring regions (macro seizure) (Wenzel et al., 2019). Studies have shown that locally induced seizures progress reliably within and across cortical layers displaying consistent spatiotemporal patterns of propagation. In contrast, seizures show greater degrees of variability in terms of their total duration which is thought to be influenced by GABAergic inhibition (Wenzel et al., 2017). Epileptic neural activity has also been associated with changes in synaptic plasticity,

however; the cellular and molecular mechanisms that underlie these changes and sustain seizures remain unclear (Grainger et al., 2018).

Epileptic brain activity is also known to produce travelling waves with complex spatiotemporal patterns of activation. Research has identified the presence of spiral waves during interictal (between seizures) epileptic activity (Dzhala & Staley, 2003; X. Huang et al., 2010; Le Van Quyen et al., 2003; Pinto et al., 2005; Trevelyan et al., 2007). These waves are thought to occur during the expansion of micro seizures into neighbouring cortical regions which produces a widespread macro seizure (Wenzel et al., 2019). They typically arise when local excitatory interactions dominate and can lead to pathological brain activity such as seizures when they are sustained for long periods (X. Huang et al., 2004; X. Huang et al., 2010). In addition, this cortical activity can become trapped in a cycle of recurrent spiral waves whereby the spirals are sustained through re-entrant loops leading to a state of persistent seizures called status epilepticus (Liou et al., 2020; Viventi et al., 2011).

RADIATION-INDUCED BRAIN INJURY AND ALTERED CORTICAL ACTIVITY

Aside from epileptic brain activity, RT can lead to another state of altered cortical activity. RT is known to produce radiation-induced brain injuries within the regions of the brain that are exposed to radiation, consequently producing altered brain states (P. Wu et al., 2012; Zhang et al., 2020). These injuries are thought to be caused by a combination of increased cell death in neurons exposed to radiation as well as dysfunction in surviving brain cells (Zhang et al., 2020). Research has shown that radiation-induced brain injuries can occur on a variety of different timescales following treatment. To illustrate, acute radiation-

induced injuries typically occur within days of RT, whereas early delayed injuries occur within one to six months post-RT, and late delayed injuries occur over 6 months post-RT (Greene-Schloesser et al., 2012; Zhang et al., 2018). Although acute and early delayed injuries have been shown to resolve within months of treatment, late delayed changes are often irreversible and can progress over time (Balentova & Adamkov, 2015). They have also been associated with several cognitive impairments such as memory impairments, attention and executive function deficits, and reduced processing speed, which can occasionally progress to dementia (Brière et al., 2008; Greene-Schloesser et al., 2012; Zhang et al., 2018).

Radiation-induced cell damage and/or death is influenced by a variety of factors including tumour volume, total dose administered, dose per faction, and the duration of radiation treatment (Cuccurullo et al., 2019). RT is known to actively induce cell death through apoptosis, a form of programmed cell death, as well as, passively through necrosis which results in accidental cell death whereby cells with lethally altered DNA undergo mitosis leading to an uncontrolled release of inflammatory contents from the cell (Cohen–Jonathan et al., 1999; Fink & Cookson, 2005). Radiation-induced cell death can be influenced by several direct and indirect effects which are further complicated by the interaction of various brain cell types such as neurons, microglia, astrocytes, and endothelial cells (Cuccurullo et al., 2019; Furuse et al., 2015; Miyatake et al., 2015). For example, radiation can directly cause single- or double-stranded breaks in DNA leading to lethal chromosomal abnormalities (Cohen–Jonathan et al., 1999; Cuccurullo et al., 2019). It has also been shown to impact cell survival indirectly via radiolysis of cellular water which

produces free radicals leading to alterations in DNA as well as metabolic stress in the central nervous system (Cuccurullo et al., 2019). This process has been shown to activate interleukin and tumor necrosis factor alpha causing pro-inflammatory pathways to become upregulated (Cuccurullo et al., 2019; Kam & Banati, 2013). Moreover, this has been shown to lead to a reduction in hippocampal genesis in both human and rodent studies (Cuccurullo et al., 2019; Monje, 2008).

Previous literature has established that irradiated neurons showed significantly increased firing rates (Zhang et al., 2020), changes in synapse morphology (Kempf et al., 2015; Zhang et al., 2020), and inhibited synaptic function and plasticity including deficits in long-term potentiation (LTP) (P. Wu et al., 2012; Zhang et al., 2018). Investigations of late-delayed effects (> 6 months) of radiation doses above 60 Gy have shown decreases in firing rate (Zaer et al., 2022), which may be due to elevated rates of cellular necrosis. Findings from human patients offer some support to this theory as they initially showed an increase in local brain activity followed by higher levels of necrosis in late-delayed stages (Ding et al., 2018). Additionally, there appears to be a dose-dependent response, whereby patients who receive higher doses tend to have worse outcomes later in life (Brière et al., 2008). An age-dependent effect has also been observed where younger patients typically experience poorer outcomes than adult patients (Mulhern et al., 2004), which has been replicated in rodent studies (Zhang et al., 2018). Finally, there is emerging evidence of a sex-dependent effect which suggests that female survivors of brain tumours may experience a higher incidence of cognitive impairments following RT (Armstrong et al., 2007; Carroll et al., 2013; Panwala et al., 2019).

Together, epileptic neural activity and radiation-induced brain injuries represent distinct forms of pathological neural activity that display vastly different neural dynamics. For example, past research has suggested that epileptiform activity is likely associated with an increase in synchronization amongst neurons, which is known to produce spiral waves (Grainger et al., 2018; X. Huang et al., 2010; Jiruska et al., 2013; Viventi et al., 2011). In contrast, RT has been shown to significantly increase firing rates and influence synaptic plasticity and functioning; however, less is known about neural synchrony in networks that are exposed to RT. A recent study has shown a decrease in gamma oscillation synchrony, which is thought to be correlated with cognitive function (Zhang et al., 2020). Thus, it is essential to further develop our understanding of the dynamics underlying both altered cortical states to determine the mechanisms responsible for the known cognitive deficits.

THE PREFRONTAL CORTEX

The PFC was first defined by Rose and Woodley as the region within the cerebral cortex that receives projections from the mediodorsal nucleus located within the thalamus; however, recent research has provided a more nuanced definition of the PFC (Carlén, 2017; Laubach et al., 2018; Rose & Woosley, 1948) Notably, the PFC varies across species and different terminology is used throughout the literature depending on the species being studied. In general, the neocortex, including the PFC, consists of 6 horizontal layers that vary in size, density of neurons and cell types (Amunts & Zilles, 2015; Saberi et al., 2023). Layer I has a low cell density and primarily contains axon terminals and dendrites. Layer II and III primarily contain pyramidal cells and show a size gradient whereby neurons become larger

towards the lower portion of layer III. Layer IV is an input layer that has a high cell density and consists of small pyramidal neurons and stellate cells that make local connections. Layer V is an output layer that targets subcortical regions (Baker et al., 2018). It contains two sub-layers which are composed of small intratelencephalic pyramidal neurons (Layer Va) and large pyramidal neurons that are sparsely distributed (Layer Vb). Finally, Layer VI is also an output layer that contains heterogeneously shaped neurons in addition to corticothalamic pyramidal cells (Baker et al., 2018; Saberi et al., 2023; von Economo et al., 2008).

In humans and non-human primates, the PFC typically refers to the granular and orbital portions of the frontal cortex and is comprised of three anatomically unique subregions which are the lateral (dorsolateral and ventrolateral), medial (ventromedial and ventrolateral) and orbital regions (Carlén, 2017; Fuster, 1997; Laubach et al., 2018; Uylings et al., 2003). In rodents, the PFC is thought to consist of the prelimbic, infralimbic, and anterior cingulate areas of the frontal cortex (Laubach et al., 2018). In comparison to the PFC in humans and non-human primates, all areas of the rodent PFC are agranular meaning they lack a distinct layer IV. It is also worth noting that the terms anterior cingulate cortex and medial prefrontal cortex tend to be used interchangeably in rodent research (Laubach et al., 2018), which highlights the need for a more consistent definition of the rodent PFC.

WHY STUDY PFC?

The PFC is an essential region to study due to its implication in several important brain functions such as decision-making, cognition, executive functioning, motivation,

reward, emotion and working memory (Anastasiades & Carter, 2021; Carlén, 2017; Miller & Cohen, 2001; Robbins & Arnsten, 2009). It sends and receives input from a variety of sensory, motor, and subcortical regions, and is believed to perform "top-down" processing, whereby it influences downstream regions based on internal goals or states (Carlén, 2017; Chini & Hanganu-Opatz, 2021). Moreover, dysregulation and disinhibition of the PFC have been associated with a variety of neuropsychiatric and neurological diseases (Anastasiades & Carter, 2021; Bast et al., 2017; Braakman et al., 2011; Chini & Hanganu-Opatz, 2021; Patrikelis et al., 2009; Yan & Rein, 2022).

Frontal lobe epilepsy (FLE), which often involves regions of the PFC, is the second most common type of partial epilepsy accounting for 20-30% of all cases (Braakman et al., 2011; Manford et al., 1992; Patrikelis et al., 2009). It is often associated with cognitive impairments including deficits in memory, attention, and executive functions such as response inhibition or maintenance, recognizing facial expressions, verbal abstraction, visuoperceptual and visuomotor speed, humour appreciation, social cognition, and gaze perception (Braakman et al., 2011; Patrikelis et al., 2009). It is worth noting that there is a large amount of variability in individual symptomology among FLE patients given the complex connectivity among the frontal lobes and other functionally connected cortical and subcortical regions. As well, one's symptomology will depend on the precise location of one's seizures as well as the hemisphere that is impacted (McGonigal, 2022; Patrikelis et al., 2009). Frontal lobe seizures have been shown to spread very quickly across brain regions due to the complex connectivity in this area, which results in a wide range of simultaneous behavioural changes that can sometimes be volatile in nature (Jobst et al., 2000; McGonigal,

2022). Together, these findings highlight the importance of understanding the underlying network dynamics of regions involved in FLE including the PFC.

Past research on the impact of RT has typically focused on the hippocampus due to its association with memory impairments; however, more recent research has highlighted the importance of studying other brain regions such as the PFC. Notably, research has shown that the highest percentage (~26%) of primary malignant brain tumours occur in the frontal lobes (Gould, 2018). Neurons located within the PFC communicate with one another and adjacent sensory, motor, and subcortical regions through precisely timed action potentials which are believed to be impacted by RT (Miller & Cohen, 2001; Zhang et al., 2020).

One important pathway to study is the direct monosynaptic pathway that originates in the cornu ammonis 1 (CA1)/subiculum fields of the hippocampus and projects to the prelimbic and medial orbital areas of the PFC (Thierry et al., 2000; Zhang et al., 2018). In rats, the hippocampal-PFC pathway has the strongest projections originating from the ventral hippocampus and subiculum and some weaker projections from the intermediate third of the hippocampus (Cenquizca & Swanson, 2007; Godsil et al., 2013; Jay & Witter, 1991; Spedding et al., 2021). These projections terminate in the prelimbic, infralimbic and anterior cingulate regions of the PFC (Cenquizca & Swanson, 2007; Godsil et al., 2013; Hoover & Vertes, 2007; Jay & Witter, 1991; Spedding et al., 2021). In comparison, research on monkeys has shown that the strongest projections originate in the rostral portion of CA1, the subiculum and prosubiculum and project to the orbital and medial PFC (Barbas & Blatt,

1995; Cavada et al., 2000; Godsil et al., 2013; Spedding et al., 2021; Zhong et al., 2006). Although current tract-tracing techniques are too invasive to be applied to humans, diffuser tensor imaging studies have shown that humans have fimbria/fornix fibers that terminate in the orbital and medial PFC suggesting they share a similar hippocampal-PFC pathway with monkeys and rodents (Godsil et al., 2013; Spedding et al., 2021).

Research has shown that radiation can induce a partial block of functional coupling between the PFC and the hippocampus, which leads to abnormal levels of excitation that may play a role in radiation-induced cognitive deficits (Zhang et al., 2020). Additional investigations have shown that RT can impair neuroplasticity, as measured by LTP, along the hippocampal-PFC pathway which was especially pronounced in juvenile rodents. This highlights one example of the age-dependent effects of RT on cortical plasticity (Zhang et al., 2018). Functional imaging studies have also found severe aberrations in the activation, functional coupling and structure in the hippocampal-PFC circuit in patients suffering from a variety of psychiatric disorders (Godsil et al., 2013; Spedding et al., 2021). As a result, it is essential to go beyond the hippocampus and study additional regions such as the PFC to better understand the cognitive impairments that occur following radiation (Zhang et al., 2020).

MULTI-ELECTRODE ARRAYS

The field of neuroscience has strived towards the development of novel electrode and imaging techniques to allow for recordings that are more precise, detailed and operate on a longer timescale (Hong & Lieber, 2019). Several methods are currently used to record

neural activity such as intracellular recordings via patch or sharp electrodes, which can be used to measure the intracellular voltage of individual cells (Obien et al., 2015; Spira & Hai, 2013). Patch-clamp recordings have high spatial and temporal resolution; however, they can only provide recordings of a limited number of neurons per experiment for a limited duration due to biophysical as well as mechanical instabilities of the cells (Hong & Lieber, 2019; Obien et al., 2015; Spira & Hai, 2013). Alternatively, optical imaging technologies that rely on genetically encoded molecular probes or extrinsic fluorescent dyes can be used to measure single-neuron resolution data (Spira & Hai, 2013). Finally, very-large-scale neural populations can be measured via methods such as electroencephalography (EEG), functional magnetic resonance imaging (fMRI), magnetoencephalography (MEG), and electrocorticography (ECoG) (Spira & Hai, 2013). These methods provide a more indirect measure of neural activity in large regions of the brain and can be used to investigate functional connectivity between regions (Obien et al., 2015). They produce recordings with high temporal resolution, but lower spatial resolution (Muller et al., 2018)

These neural recording technologies vary in their spatial and temporal resolution often showing a trade-off between the two. However, multi-electrode arrays (MEAs) offer a middle ground between single-cell recordings and very-large-scale neural activity, which provide the capability to record large populations of neurons over long periods of time without damaging the plasma membranes of the neurons (Berdondini et al., 2009; Spira & Hai, 2013). They also produce recordings of large networks of neurons located in specific cortical regions with very high spatial and temporal resolution (Muller et al., 2018). MEA systems measure extracellular action potentials and local field potentials, which reflect the

global activity of several cortical neurons (Buzsáki et al., 2012; Ferrea et al., 2012; Obien et al., 2015). These systems can vary in terms of the transducers used, the channel count, the type of substrate (e.g., active, passive, complementary metal oxide semiconductor (CMOS) or silicon arrays), the shape of the recording device, the density of electrodes (e.g., high-density arrays with 21 μm between electrodes, or low-density arrays that range from 100-250 μm between electrodes), and the application the arrays are used for (e.g., *in vitro*, *in vivo* or implantable arrays) (Berdondini et al., 2009; Gross et al., 1977; Imfeld et al., 2007, 2008; Obien et al., 2015; Oka et al., 1999; Pine, 1980; Thomas et al., 1972). Recent developments in MEA technology have allowed the number of simultaneously recorded electrodes to steadily double approximately every seven years (Stevenson & Kording, 2011). These systems are now capable of simultaneously recording from thousands of electrodes, which produces extremely rich datasets that can provide a unique insight into the network dynamics of various altered cortical states.

One state-of-the-art MEA system is the BioCamX MEA system (3Brain GmbH) which uses an active-pixel sensor (APS) monolithic CMOS design to simultaneously record from 4,096 (64 x 64) channels with near cellular resolution (Berdondini et al., 2009; Ferrea et al., 2012; Imfeld et al., 2007, 2008). This technology offers a vast improvement in spatial resolution compared to previous systems thus resulting in recordings that have superior spatiotemporal resolution (Ferrea et al., 2012). In contrast, conventional MEAs are typically passive devices that contain fixed wiring without any active circuit elements and are limited in the total number of electrodes that can fit in the array area (Greschner et al 2014; Gross et al 1977; Nisch et al., 1994). Additional on-chip circuitry has since been added to allow for

an increased number of recording channels, but these MEA systems are still limited in electrode density due to the direct wiring of the electrodes to the signal conditioning circuitry (DeBusshere and Kovacs 2001; Gereve et al 2007; Offenhausser et al 1997). Based on this, the BioCamX (3Brain GmbH) is an exceptional MEA system for studying both local and network-level activity in acute brain slices (Figure 2).

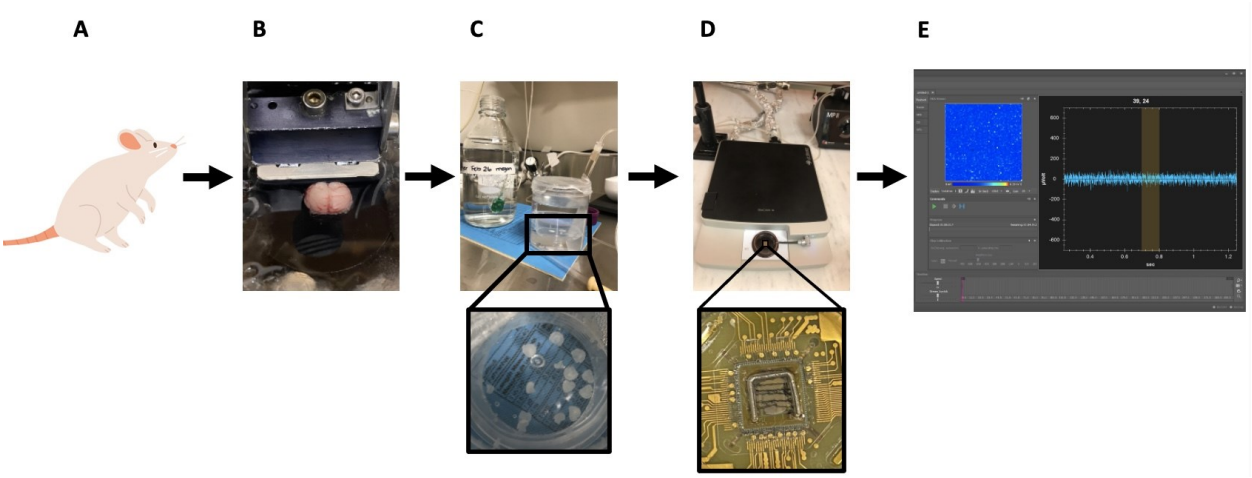

FIGURE 2. MEA RECORDING PROTOCOL FOR BIOCAMX (3BRAIN GMBH) RECORDINGS

A. Sprague Dawley rats aged P14-21, **B**. Brain is extracted and sliced, **C**. Slices are left to recover for one hour prior to recording. **D**. Acute (live) brain slice is placed on MEA chip (zoomed-in panel below), **E**. Simultaneous recording from 4,096 channels.

THE BOTTLENECK PROBLEM

Despite the richness of the data produced by high-density large-scale MEAs, researchers experience the issue of identifying key features within high-dimensional data that offer insight into the nature of network-level activity (Stevenson & Kording, 2011). This issue produces a bottleneck effect whereby we are capable of simultaneously recording from thousands of neurons but lack an understanding of the resulting high-dimensional

data. An additional complication exists in the nature of network-level cortical activity as it typically consists of waves that propagate across various temporal and spatial scales (Engel & Steinmetz, 2019). As such, it is imperative to identify the features of these high-dimensional datasets that will provide simplified and meaningful results (Paninski & Cunningham, 2018; Stevenson & Kording, 2011).

Dimensionality reduction techniques, such as principal components analysis (PCA), factor analysis (FA) or dynamic mode decomposition (DMD) offer a potential solution to this problem as they have been shown to account for neuronal population-level activity using a limited number of dimensions (Cunningham & Yu, 2014; Engel & Steinmetz, 2019; Pang et al., 2016; Paninski & Cunningham, 2018). PCA can be used to convert an N x N covariance matrix of firing rates into a set of activation patterns that account for individual neuronal activity levels and to rank them based on the variance explained by each pattern (Pang et al., 2016). This results in individual snapshots of the original neural activity that are treated independently and produces a one-dimensional dataset that will best preserve the covariance of the data (Cunningham & Yu, 2014; Pang et al., 2016). FA can be used to determine a low-dimensional space where the variance shared across neurons is preserved (firing rate variability) and the variance that is unique to each neuron is discarded (spiking variability) (Cunningham & Yu, 2014). Finally, DMD can be used to determine the spatiotemporal features of the responses of distributed brain regions that unfold across different timescales (Pang et al., 2016).

One question that remains, however, is whether low-dimensional models can also account for disinhibited cortical activity with complex spatiotemporal patterns such as spiral waves. Typically, these patterns of activity cannot be described by broad features such as shared patterns of fluctuation or oscillations (Engel & Steinmetz, 2019). Whereas some studies have shown that spiral waves may contribute to an increase in neural dimensionality due to the presence of complex patterns that propagate across neural tissue, others have suggested that these disinhibited states may decrease dimensionality as they are capable of producing highly stereotypical forms of activity such as the synchronization of neurons (Barbero-Castillo et al., 2021; Xiao et al., 2012). This highlights the importance of further analyzing high-density MEA recordings of disinhibited or altered states of cortical activity to improve our understanding of the dimensionality of these datasets.

GENERATIVE ADVERSARIAL NETWORKS

While dimensionality reduction techniques are primarily aimed at a statistical description of the data, other techniques must be employed to reproduce key aspects of the dataset. These techniques are broadly referred to as generative models, which can produce novel data that closely matches the statistical properties of the set of observations to which they are exposed (Betzel & Bassett, 2017; Harshvardhan et al., 2020). A popular choice of such models is GANs. GANs were developed for use in the field of machine learning, which is a branch of artificial intelligence that is concerned with developing the learning

capabilities of algorithms whereby the model can extract features from raw data (Aggarwal et al., 2021; Gui et al., 2023; Salehi et al., 2020).

Machine learning algorithms are divided into two primary categories based on the type of learning that is used: supervised and unsupervised learning (Salehi et al., 2020). Supervised learning algorithms are typically used to solve classification or regression problems and require a dataset with various features that are labelled. This process tends to be very time-consuming and can prove to be impossible in some circumstances (Salehi et al., 2020). In comparison, unsupervised learning typically involves datasets with multiple similar labels and the network is not instructed on which pattern it should look for. Notably, methods such as data augmentation, which involves creating new samples in the training set or using simple transformations on the images within the training set, have been developed to help mitigate the cost and time it takes to manually label data in supervised learning algorithms (Salehi et al., 2020).

GANs are composed of two competing networks: a generator and a discriminator. The generator is responsible for producing synthetic images based on a given data distribution. The discriminator is responsible for distinguishing between genuine images and those produced by the generator network. The generator is trained in such a way as to maximize the probability that the discriminator will make an error resulting in a "competition" between the two networks (Arjovsky et al., 2017; Goodfellow et al., 2014; Gulrajani et al., 2017). GANs were originally proposed as a hybrid of semi-supervised and unsupervised learning and were used to generate human faces with improved illustration

compared to previous networks (Aggarwal et al., 2021; Jabbar et al., 2021; Salehi et al., 2020). They rely on deep learning methods that are inspired by the many layers that can be observed in biological neural networks and provide a form of representation learning for abstract concepts within a dataset (Aggarwal et al., 2021; Salehi et al., 2020). Moreover, they offer a state-of-the-art form of data augmentation whereby they can produce high-quality training images on a large scale (Salehi et al., 2020).

It is worth noting that traditional GANs face a variety of training difficulties such as mode collapse and training instability due to non-convergence (Aggarwal et al., 2021; Arjovsky et al., 2017; Jabbar et al., 2021; Saxena & Cao, 2021). Mode collapse occurs when the generator only produces a limited distribution of samples by focusing on a single mode within the dataset, or by learning a particular subset of modes which then reduces the diversity of the dataset it produces (Aggarwal et al., 2021; Salehi et al., 2020; Saxena & Cao, 2021). In this context, modes refer to the different classes or categories that are present within the training dataset. Mode collapse thus results in the discriminator learning to continuously reject the samples produced by the generator (Saxena & Cao, 2021). GANs can also suffer from training instability whereby the discriminator can easily differentiate between real samples and those produced by the generator which results in gradient vanishing and leads to non-convergence (Jabbar et al., 2021; Salehi et al., 2020; Saxena & Cao, 2021). Gradient vanishing occurs when the discriminator becomes more powerful than the generator which reduces the probability of generated samples being considered real. Consequently, the weights in earlier layers of the generator's network become increasingly

small and can saturate near zero causing the initial layers to stop learning (Jabbar et al., 2021; Saxena & Cao, 2021)

More recently, the Wasserstein GAN (WGAN) was developed to improve learning stability and prevent mode collapse (Arjovsky et al., 2017). WGANs differ from traditional GANs in the way that the distance between the generator's distribution and the real distribution is defined and measured. The WGAN uses Earth-Mover (EM) distance or Wasserstein-1 as the loss function within the model, which provides a continuous measure of the distance (difference) between data produced by the generator and the real dataset (Arjovsky et al., 2017; Saxena & Cao, 2021). In comparison, the traditional GANs measure the distance between the data produced by the generator and the real dataset based on the Jensen-Shannon divergence, which is not a continuous measure and can lead to non-convergence (Goodfellow et al., 2014; Saxena & Cao, 2021). Traditional GANs use a cross-entropy minimax loss where the generator tries to minimize the function so that it can successfully "fool" the discriminator, and the discriminator tries to maximize it to successfully identify "fake" data from the generator (Goodfellow et al., 2014). This can lead to gradient vanishing if the discriminator can discriminate between real and fake samples too easily (Gulrajani et al., 2017; Saxena & Cao, 2021).

Despite this, GANs have been successfully employed for a variety of tasks in the fields of computer vision, space sciences, traffic control, facial recognition, medicine and most notably neuroscience (Aggarwal et al., 2021; Gui et al., 2023). Within the field of neuroscience, GANs have provided valuable insight into studying neural network dynamics

as well as various diseased brain states. Training GANs using medical images or data allows for the identification and subsequent reproduction of complex non-linear patterns of activity that are present in pathological states (R. Wang et al., 2023). To illustrate, GANs can be used for the classification of disease stages or subtypes even at preclinical stages in diseases such as Alzheimer's, multiple sclerosis, major depressive disorder, and schizophrenia (R. Wang et al., 2023; Zhao et al., 2020). In addition, GANs can be used to detect tumours or other brain anomalies (C. Han et al., 2019; Schlegl et al., 2019; R. Wang et al., 2023). They can also be used to model healthy brain aging and/or disease progression in order to provide early detection of pathological brain states (Rachmadi et al., 2020; Ravi et al., 2022; R. Wang et al., 2023; Wei et al., 2020; T. Xia et al., 2021). Based on GANs' ability to generate novel exemplars from experimental datasets, they offer a unique avenue for creating larger datasets of pathological brain activity that can later be used to determine markers of pathological activity as well as classification systems for brain disorders. In addition, these sets of exemplars can potentially be used to investigate novel intervention techniques such as neural stimulation. This could help provide a guide for interventions or treatment protocols that are later used for human patients.

OVERVIEW OF THESIS

The remainder of this thesis is structured as follows. First, we will investigate disinhibited cortical activity that results following the application of a pro-epileptiform solution. More specifically, we will discuss a variety of properties associated with epileptiform spiral waves including neural complexity, spatial correlations within the

network, the center of mass and phase distribution. We will then compare the experimental results to novel exemplars generated by a GAN trained on snapshots of the experimental data. Finally, we will discuss how we can modify the amplitude and variance of the GAN's input to produce a wide range of activation patterns that span both healthy and pathological states of cortical activity.

Following the discussion of complex spiral waves that occur in disinhibited cortical networks, we will discuss the impact of ablative RT on healthy cortical neurons. We will describe the changes in network dynamics as measured by firing rates and functional connectivity that occur following escalating doses of radiation. In addition, we will discuss the rate of apoptosis that accompanies each dose of radiation. We will also provide a comparison of the results from the radiated networks and those from the pro-epileptiform networks. Finally, we will highlight the differences and similarities in neural activity that occur in both conditions. Following the description of the results from both studies, we will discuss the broader implications for understanding epileptiform activity as well as the effects of RT. To end, we will offer avenues or clinical implications and future directions that may be taken.

CHAPTER 2: A DEEP GENERATIVE ADVERSARIAL NETWORK CAPTURING COMPLEX SPIRAL WAVES IN DISINHIBITED CIRCUITS OF THE CEREBRAL CORTEX

Boucher-Routhier, M., & Thivierge, J. P. (2023). A deep generative adversarial network capturing complex spiral waves in disinhibited circuits of the cerebral cortex. *BMC neuroscience*, *24*(1), 22.

ABSTRACT

Background: In the cerebral cortex, disinhibited activity is characterized by propagating waves that spread across neural tissue. In this pathological state, a widely reported form of activity are spiral waves that travel in a circular pattern around a fixed spatial locus termed the center of mass. Spiral waves exhibit stereotypical activity and involve broad patterns of co-fluctuations, suggesting that they may be of lower complexity than healthy activity.

Results: To evaluate this hypothesis, we performed dense multi-electrode recordings of cortical networks where disinhibition was induced by perfusing a pro-epileptiform solution containing 4-Aminopyridine as well as increased potassium and decreased magnesium. Spiral waves were identified based on a spatially delimited center of mass and a broad distribution of instantaneous phases across electrodes. Individual waves were decomposed into “snapshots” that captured instantaneous neural activation across the entire network. The complexity of these snapshots was examined using a measure termed the participation ratio. Contrary to our expectations, an eigenspectrum analysis of these snapshots revealed a broad distribution of eigenvalues and an increase in complexity compared to baseline networks. A deep generative adversarial network was trained to generate novel exemplars of snapshots that closely captured cortical spiral waves. These

synthetic waves replicated key features of experimental data including a tight center of mass, a broad eigenvalue distribution, spatially-dependent correlations, and a high complexity. By adjusting the input to the model, new samples were generated that deviated in systematic ways from the experimental data, thus allowing the exploration of a broad range of states from healthy to pathologically disinhibited neural networks.

Conclusions: Together, results show that the complexity of population activity serves as a marker along a continuum from healthy to disinhibited brain states. The proposed generative adversarial network opens avenues for replicating the dynamics of cortical seizures and accelerating the design of optimal neurostimulation aimed at suppressing pathological brain activity.

Keywords: deep neural network, multi electrodes, epilepsy, complexity

BACKGROUND

In disinhibited cortical circuits, neural activity is characterized by patterns that propagate across widespread networks (X. Huang et al., 2004). These patterns take on different forms, including planar waves traveling in a single direction, saddle waves emerging from the interaction between multiple sites of propagation, and spiral waves that evolve in a circular motion around a fixed spatial locus (Engel & Steinmetz, 2019; X. Huang et al., 2010; Muller et al., 2018; Sato et al., 2012; Townsend et al., 2015; Townsend & Gong, 2018; J.-Y. Wu et al., 2008). These spiral waves are found during interictal epileptic activity (Dzhala & Staley, 2003; Le Van Quyen et al., 2003; Pinto et al., 2005; Trevelyan et al., 2007) and are reported in cortical networks both *in vitro* (X. Huang et al., 2004) and *in vivo* (Viventi

et al., 2011). Their origin and characteristics, however, remain to be fully elucidated, as they constitute rare events relative to background activity and cannot be captured by simple computational models including classic balanced excitation/inhibition networks (C. Huang et al., 2019).

A promising avenue to describe patterns of activity is to examine their *complexity*, indicative of the number of distinct factors needed to capture neural fluctuations. In many instances, the activity of large networks can be closely approximated using only a small number of factors that capture much of the variance across neurons (Engel & Steinmetz, 2019). This low complexity suggests that a few broad features, such as oscillations or shared patterns of fluctuation, may explain most population-level activity, thus greatly simplifying descriptions of neural dynamics and providing a strong guidance to theories of brain function (Ecker et al., 2014; Lin et al., 2015; Rabinowitz et al., 2015).

While alterations in neural complexity are expected in disinhibited brain networks (Barbero-Castillo et al., 2021; Xiao et al., 2012), diverging lines of evidence point to either an increase or decrease in complexity, thus leaving unresolved the relation between complexity and pathological brain states. Previous work suggests that pathologically disinhibited states are accompanied by a decrease in complexity given that they exhibit highly stereotypical forms of activity. More specifically, disinhibiting cortical neurons by blocking $GABA_A$ transmission increases synchronization and reduces the complexity of oscillations (Barbero-Castillo et al., 2021; Xiao et al., 2012). Other work, however, suggests that disinhibited waves contribute to an increase in neural complexity as they form intricate

patterns that extend both in time and across neuronal tissue (Araújo et al., 2022; El Boustani & Destexhe, 2010; C. Huang et al., 2019). Examining the complexity of spiral waves is key to disambiguating these viewpoints.

In this work, we studied cortical population activity in disinhibited slices recorded with a high-density multi-electrode array (hd-MEA) (Ferrea et al., 2012). Disinhibited neural activity exhibited spiral waves whose amplitude was concentrated in the delta frequency range (1-4 Hz). These waves were analyzed by extracting "snapshots" that captured the instantaneous neural activation across whole cortical networks. The complexity of these snapshots was analyzed using a measure termed the participation ratio (PR) (Altan et al., 2021; Hu & Sompolinsky, 2020; Litwin-Kumar et al., 2017; Mazzucato et al., 2016).

To capture spiral waves and account for their complexity, a deep generative adversarial network (GAN) was trained to generate snapshots of activity that matched those obtained experimentally (Goodfellow et al., 2014). After training, the GAN model produced synthetic snapshots that closely captured the experimental data in terms of their high complexity, tight center of mass, and spatially-dependent correlations. Going further, the model was employed to generate a range of new samples that deviated from the data in systematic ways and covered a broad spectrum of conditions where complexity ranged from pathological to healthy states.

Taken together, results suggest that the complexity of population activity provides a marker of neural fluctuations along a continuum of states from healthy to pathologically disinhibited. Furthermore, deep GAN networks offer a promising avenue to study the

dynamic control of disinhibited neural activity using brain-computer interfaces with implications for diseases that impact brain networks.

RESULTS

SPIRAL WAVES

Activity from coronal prefrontal cortex (PFC) was recorded in acute slices (Figure 3A) using a hd-MEA after the application of a pro-epileptiform (PE) solution that included 4-Aminopyridine (4-AP) as well as reduced extracellular magnesium (Mg^{2+}) and increased extracellular potassium (K^{+}). A total of 219 spiral waves were identified across three slices following a set of criteria (see Methods). These waves were broadly distributed across electrodes, generating slow fluctuations in activity across recording sites (Figure 3B). The spatiotemporal evolution of these waves displayed a rotating pattern characteristic of a spiral (Figure 3C and Supplementary Movie). While spiral waves were not the only form of activity present in these recordings, they formed a prominent and repeatable pattern over time. Spiral waves were detected at an average rate of 7.3 per minute and their mean voltage amplitude was concentrated in delta frequencies, with lower amplitude found in higher bands (Figure 3D). The duration of spiral waves was estimated by counting the number of consecutive snapshots (1 ms windows of instantaneous activity) where a wave was identified. The average duration of waves was 2.52 sec with standard deviation (SD) of 1.00 sec, with both shorter and longer waves present (Figure 3E). While these values are inherently imprecise due to the manual identification of time windows surrounding spiral

waves, they provide an indication that these waves represent slow-evolving events whose timecourse largely exceeds synaptic time constants (Cavanagh et al., 2020).

By comparison, related work has reported spirals with relatively short durations (<1 sec) (X. Huang et al., 2004; Viventi et al., 2011). These events, however, were primarily limited to a single cycle, whereas manual inspection of spirals in our data revealed that approximately one third of events had more than a single cycle (one cycle: 63.79%; two cycles: 31.03%; three or more cycles: 3.45% of all spiral waves). The presence of two or more cycles prolonged the duration of spiral event compared with previous accounts and is consistent with *in vivo* cortical waves (X. Huang et al., 2010)

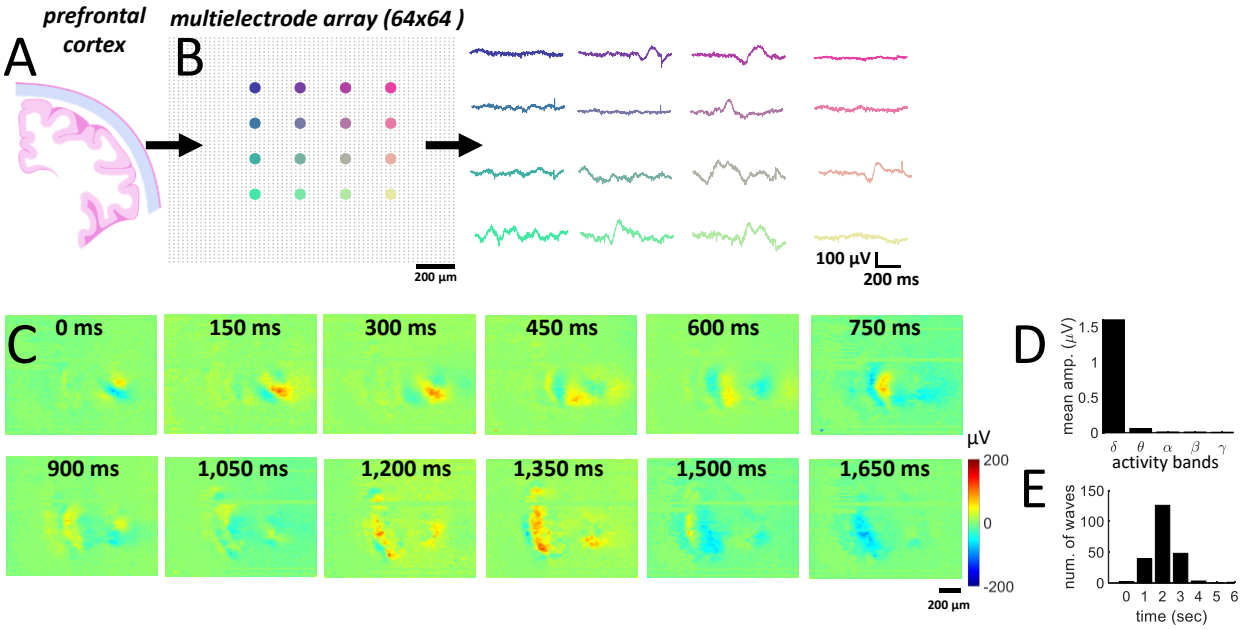

FIGURE 3. ROTATING SPIRAL WAVES IN DISINHIBITED CORTICAL ACTIVITY

(**A**) Rodent PFC acute slice recorded with a hd-MEA. (**B**) Voltage traces across individual channels. Colors correspond to spatial locations of electrodes. (**C**) Example of spiral wave observed after bath application of PE solution. See movie in Supplementary Material.

(**D**) Mean band-filtered voltage across delta (δ, 0-4 Hz), theta (θ, 4-7 Hz), alpha (α, 7-12 Hz), beta (β, 12-30 Hz), and gamma (γ, 30-80 Hz) frequencies. (**E**) Distribution of spiral wave durations.

CENTER OF MASS

Next, the center of mass of each spiral wave was computed by averaging together the central row and column of individual snapshots (Methods Eqs. 1-2). The center of mass was highly consistent across repeated waves of the same slice (Figure 4A). Variability across waves was primarily delimited to the inter-electrode spacing (20 μm) (Figure 4A, inset). An example of average voltage activity during a single wave is shown in Figure 4B. Activity across the network arose in "domains" where groups of neurons were activated over delimited regions of space. Furthermore, voltage activation near the center of mass was lower than surrounding regions (Rule et al., 2018).

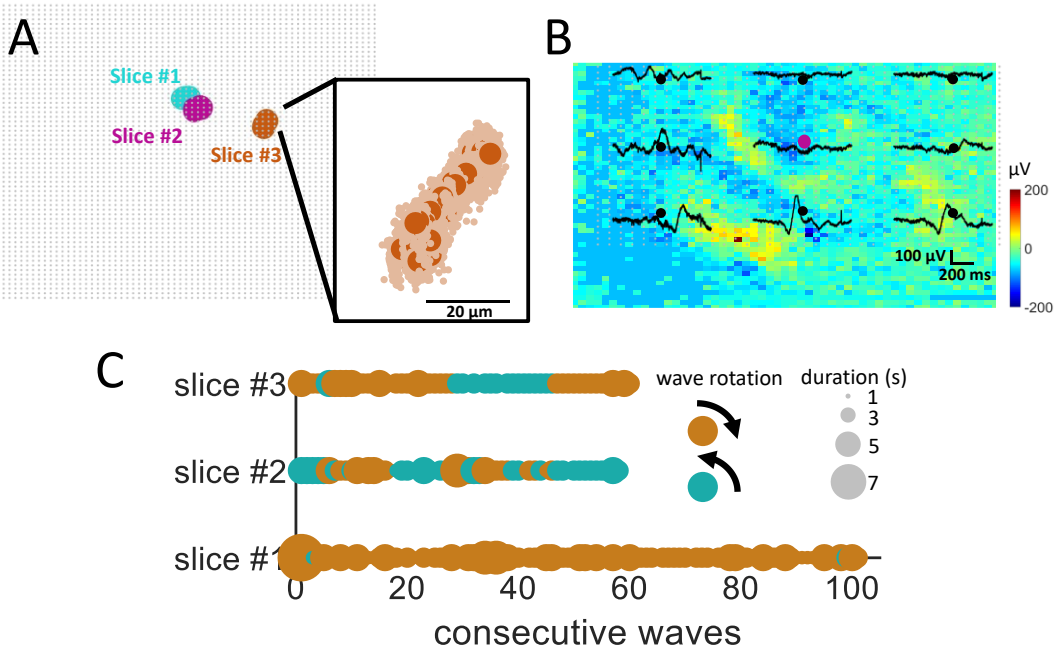

FIGURE 4. SPATIOTEMPORAL ATTRIBUTES OF SPIRAL WAVES

(**A**) Mean center of mass of individual spiral waves across recordings. Inset shows a zoom of center of mass for spiral waves of a single slice (darker color) and individual time frames ("snapshots") of each wave (lighter color). (**B**) Solid black lines are voltage traces at individual electrodes on the array. The center of mass is colored according to slice #2 in panel "a". (**C**) Rotational direction and duration of spiral waves across three *in vitro* cortical slices.

DIRECTION OF ROTATION

Each spiral wave was assigned a clockwise or counter-clockwise direction of rotation by visual inspection. Overall, 161 waves rotated clockwise and 58 waves counter-clockwise. Because spiral waves may arise by planar waves colliding into each other (X. Huang et al., 2004), it is possible that the direction of rotation depends upon the exact arrival times of these simpler waves, which is subject to variability over time. Therefore, we speculated that

the angle of rotation may change over the course of a given recording. Consistent with this idea, the direction of rotation alternated across individual waves in two of the slices (Figure 4C, slices #2 and #3). In these recordings, waves repeated the same rotation several times before switching direction (Viventi et al., 2011). By comparison, another slice yielded rotational directions that remained mostly consistent over the entire recording (Figure 4C, slice #1). Thus, cortical networks could exhibit spiral waves with both alternating directions of rotation and waves with more stable patterns characterized by a preferred direction.

INSTANTANEOUS PHASE

Another key feature of spiral waves is the broad distribution of instantaneous phases across individual electrodes (X. Huang et al., 2004). Instantaneous phases were computed by applying a Hilbert transform to delta band-filtered snapshots of activity at a resolution of 1 ms. An example of instantaneous phase obtained at a given time point (Figure 5A) revealed the presence of a phase gradient radiating from the center of mass of the spiral wave (Figure 5B). Across all waves, the distribution of instantaneous phases exhibited a broad range of values (Figure 5C). Thus, snapshots of activity displayed a wide distribution of phases in line with a well-documented signature of spiral waves.

Going further, phase maps were employed to generate vector fields using Matlab's quiver function. These vector fields indicate the speed and direction of propagating activity across cortical tissue and were employed to validate the presence of spiral waves in segments of neural data (Townsend & Gong, 2018). Vector fields are shown by arrows that

span a range of orientations representing the flow of spiral waves around a fixed center of mass (Figure 5D).

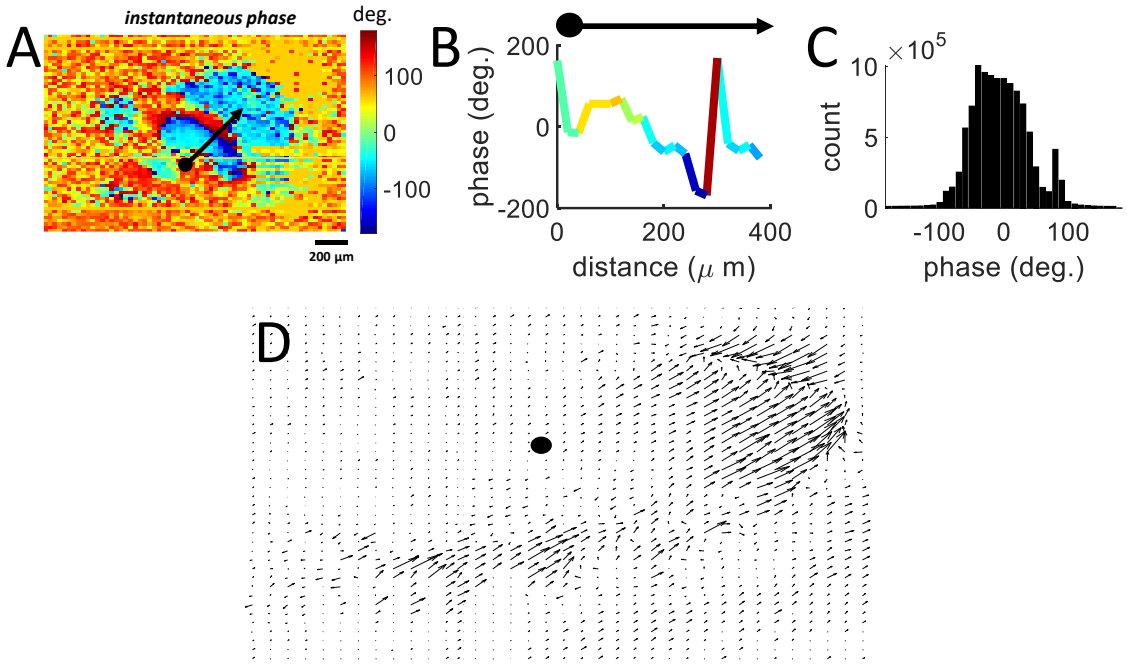

FIGURE 5. INSTANTANEOUS PHASE OF SPIRAL WAVES

(**A**) Spatial distribution of instantaneous phases during a rotating wave. Black arrow: direction of vector field used in panel "B". (**B**) Instantaneous phase along the vector field in "A". (**C**) Global distribution of phases across all spiral waves. (**D**) Quiver plot showing vector fields of an individual spiral wave calculated between consecutive phase maps separated by 10 ms. **Solid black circle**: center of mass.

DISTANCE-DEPENDENT CORRELATIONS

Next, network interactions during spiral waves were examined by computing the Pearson correlation between voltages at all pairs of electrodes. Individual correlation matrices were obtained for each spiral of a given network, then averaged to create a mean

correlation matrix (Figure 6A). A widely reported feature of correlations in cortex is their spatial dependence, whereby neighboring cells are on average more strongly correlated than distant pairs (Song et al., 2005). This spatial ordering is also observed in synaptic connectivity where the probability of a monosynaptic contact falls off exponentially with physical distance between neurons (Horvát et al., 2016; Levy & Reyes, 2012; Mariño et al., 2005). Therefore, we reasoned that correlations should decrease with physical distance between pairs of electrodes. Consistent with this prediction, we found a lower mean correlation with increased distance on the array (Pearson correlation test, R^2= 0.8789, p=2.5193e-07) (Figure 6B). This analysis was repeated by focusing on the correlation between the center of mass and surrounding points on the array (Figure 6C). As expected, correlations decreased with increased physical distance from the center of mass (R^2=0.3, p=4.5221e-241) (Figure 6D). Thus, spiral waves displayed distance-dependent interactions consistent with prior findings on functional and structural cortical connectivity.

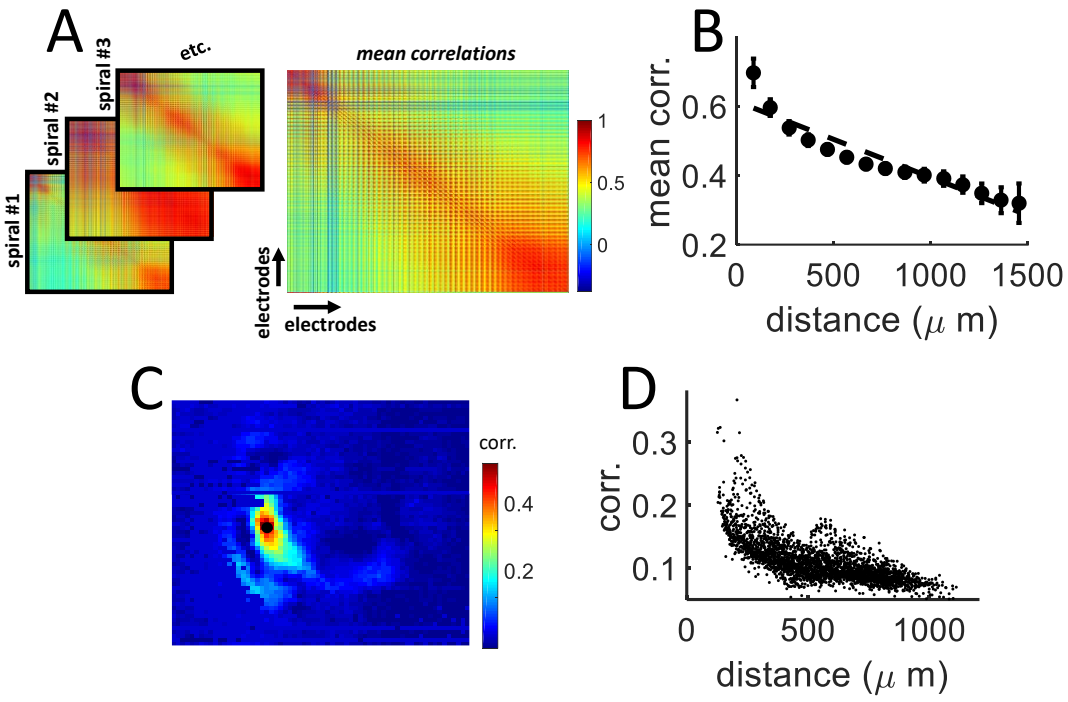

FIGURE 6. SPATIAL DISTRIBUTION OF CORRELATIONS DURING SPIRAL WAVES

(**A**) Pairwise correlations were computed for each spiral wave then averaged to create a matrix of mean correlations. (**B**) The pairwise correlation between electrodes decreased as a function of their spatial distance. Vertical bars: standard error of the mean. Dashed line: best-fitting line of regression. (**C**) Correlation between the center of mass of a spiral and surrounding electrodes. Filled black circle: center of mass. (**D**) Correlations relative to the distance from center of mass.

WAVE COMPLEXITY

The complexity of spiral waves was estimated by first applying an eigenspectrum decomposition to population activity, then computing the PR based on the resulting eigenvalues (see Methods). Eigenvalues followed a skewed distribution with a broad right tail (Hu & Sompolinsky, 2020; Stringer, Pachitariu, Steinmetz, Reddy, et al., 2019; Thivierge,

2020) (Figure 7A). To evaluate whether complexity was altered in disinhibited cortex, the mean PR of slices was compared before and after application of the PE solution. An equivalent number of snapshots was selected across both conditions (Figure 7B). The PR across all snapshots yielded a markedly higher value for disinhibited networks compared to baseline (Student's t-test, T_{436}=2.979, p=0.0032) (Figure 7C). The average PR value for the baseline was 22.2 (SD: 2.1) compared to 34.31 (SD: 4.24) for spirals. Therefore, spiral waves yielded a higher complexity than baseline, strengthening the view that these waves formed a state of high complexity in cortex (Araújo et al., 2022; El Boustani & Destexhe, 2010; C. Huang et al., 2019).

Because the PR is prone to overestimating complexity in neural data (Altan et al., 2021), the above results were compared to an alternative measure termed the Levina-Bickel maximum likelihood estimation (LBMLE) (Levina & Bickel, 2004). This non-linear measure estimates complexity using a geometric approach to calculate the distance between data points. Ten spiral waves and comparable data segments from baseline recordings were selected at random from three cortical slices. For all except one spiral wave, LBMLE complexity was higher with spiral waves than baseline (Figure 7D). The discrepancy between linear and non-linear measures of complexity is comparable with related work (Altan et al., 2021). Hence, both linear (PR) and non-linear (LBMLE) approaches showed that spiral waves yield increased complexity compared to baseline cortical circuits.

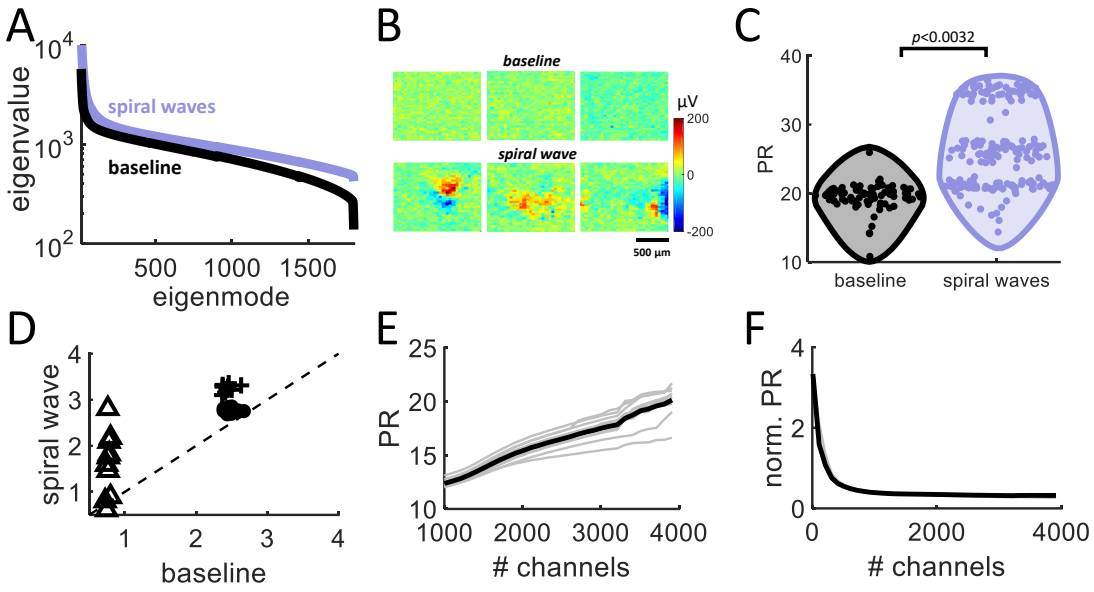

FIGURE 7. EIGENVALUES AND COMPLEXITY OF SPIRAL WAVES

(**A**) Distribution of ranked eigenvalues for spiral waves in disinhibited slices treated with a PE solution compared to baseline recordings. (**B**) Examples of snapshots from baseline data vs. spiral wave. (**C**) Participation ratio of baseline recordings and spiral waves. (**D**) LBMLE across 10 individual spiral waves and baseline activity of three cortical slices (filled circle, cross, and triangle markers). Dashed line shows unity. (**E-F**) Complexity (PR and normalized PR) versus number of randomly selected multi-electrode channels. **Grey lines**: individual spirals; **solid black line**: average over 10 spirals.

Next, we examined how the number of channels (N) impacted the PR. Random subsets of channels were selected from 10 spiral waves and the PR of those channels was computed. Results show an increase in the PR as the number of selected channels increased (Figure 7E). This increase could be compensated by scaling the PR by $\sqrt{N}$, resulting in a stable estimate of the PR when at least a few hundred channels were included

(Figure 7F). This effect does not alter our conclusions regarding the increased complexity of spiral waves (Figure 7C) given that the same number of channels was employed relative to baseline. However, it may be relevant in cases where N varies across conditions.

Finally, the complexity of baseline activity was compared to planar waves characterized by vector fields that were mainly aligned along a single direction (Figure 8A). A set of 12 planar waves were manually identified from PE activity. These waves exhibited significantly lower PR than baseline (Student's t-test, T_{87}=14.4365, p=8.1302e-25) (Figure 8B). Thus, disinhibited activity was comprised of a mixture of high complexity spiral waves as well as lower complexity planar waves. Other forms of activity, including saddle waves, were likely present but not explicitly detected here.

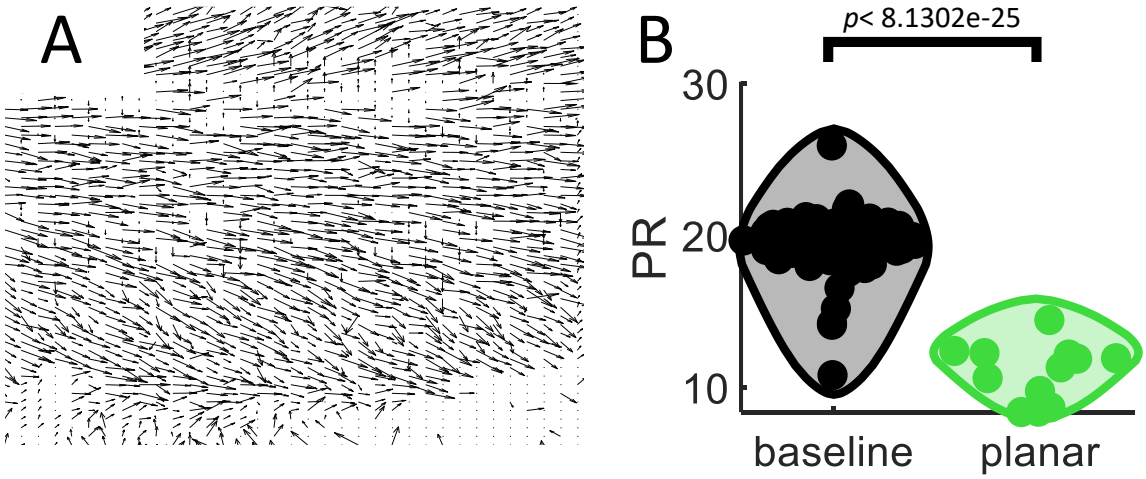

FIGURE 8. COMPLEXITY OF PLANAR WAVES

(**A**) Quiver plot showing vector fields of an individual planar wave. (**B**) PR of baseline activity compared to planar waves.

CAPTURING SPIRAL WAVES IN A DEEP GAN

A deep GAN (Goodfellow et al., 2014) was trained to produce snapshots that closely matched spiral waves obtained in disinhibited cortical networks (see Methods). This model is comprised of a generative network that produces synthetic samples, and a discriminator network whose goal is to distinguish between real and synthetic data (Figure 9A). The GAN was trained for 10,000 epochs, at which point the performance of both the generator and discriminator networks saturated (Figure 9B).

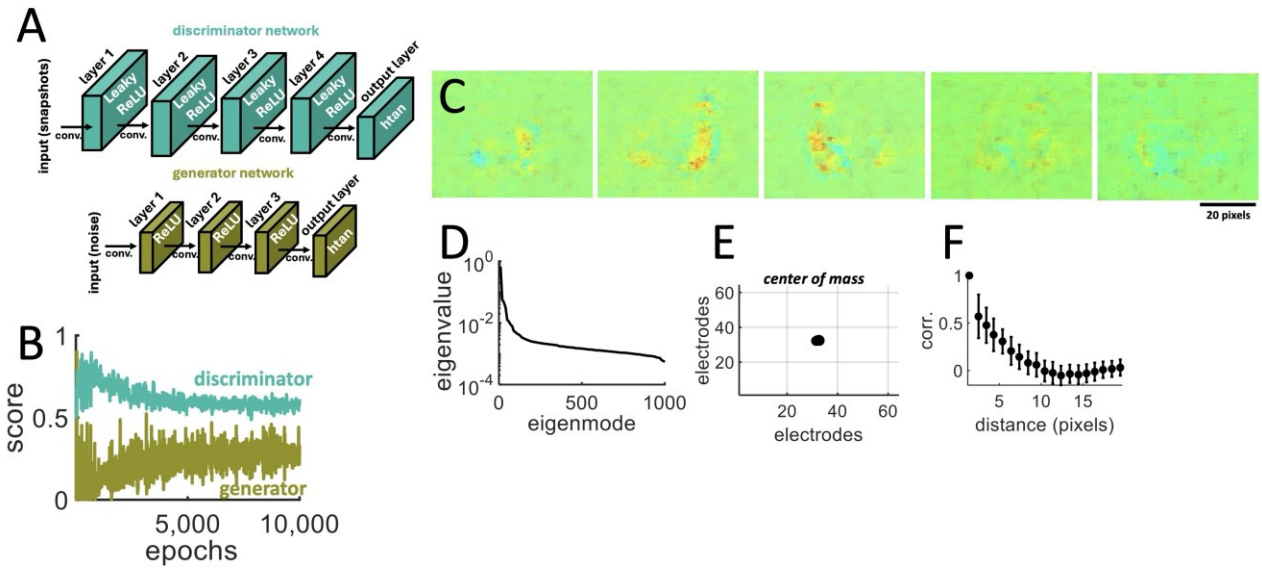

FIGURE 9. GENERATIVE ADVERSARIAL NETWORK TRAINED TO CAPTURE SNAPSHOTS OF SPATIAL ACTIVITY

(**A**) Architecture of the GAN model including both a generator and discriminator network. "conv.": convolution operator. (**B**) Performance of the discriminator and generator networks. (**C**) Snapshots generated by the network after training. (**D**) Distribution of eigenvalues across 1,000 snapshots generated by the network. (**E**) Center of mass across

all snapshots. (**F**) Pairwise correlations decreased with spatial distance across the GAN snapshots.

Once training was completed, noisy input (mean of zero and SD of 25) was injected to the generator network to produce synthetic exemplars of spiral waves (Figure 9C). A total of 1,000 novel snapshots of dimensions 64x64 pixels matching the size of the hd-MEA were generated in this fashion. Synthetic snapshots were analyzed similarly to experimental data using their eigenspectrum, center of mass, spatial correlations, and PR.

First, applying an eigenspectrum decomposition to the GAN snapshots yielded a broad distribution of eigenvalues (Figure 9D) reminiscent of experimental data (Figure 7A). Second, the center of mass of snapshots was concentrated in a delimited area of space (Figure 9E) as in experiments (Figure 4A). Third, spatial correlations were computed across snapshots of individual waves, then averaged together to yield a 4096x4096 pixels correlation matrix. As with experimental data, synthetic images had higher correlations for nearby spatial regions (Figure 9F). This is expected given that the model generated spatially delimited “regions” where activity was highly correlated (Figure 9C).

Next, a series of analyses examined the PR of snapshots generated by the GAN model. To study a broad range of synthetic images, we varied the SD of the noise injected as input to the generator network. By increasing the noise SD, waves of activity began to break apart into smaller spatial clusters (Figure 10A) and yielded a more diffuse center of mass (Figure 10B). Increasing noise SD resulted in higher values of PR, which began to saturate around an SD of 500 (Figure 10C). PR values obtained from baseline and PE experimental

data were included in Figure 10C as points of comparison, showing that manipulating noise SD yielded a continuum of PRs covering the range of experimental data as well as more extreme cases. Manipulating the mean of the injected noise also yielded a broad range of PR values capturing the scope of experimental data (Figure 10D).

To compare the results of GAN with experimental data, the effect of noise on PR values was directly assessed by adding Gaussian noise with different means and SD to snapshots of a given cortical spiral wave and computing the resulting PR value. This analysis yielded PR distributions that were qualitatively comparable to those obtained by adding noise to GAN networks. Specifically, noise SD increased the PR until an asymptotic value was reached (Figure 10E). Further, altering the mean of the Gaussian noise yielded a distribution of PR values that was maximal at zero (Figure 10F). Hence, GANs provided the ability to not only generate novel samples that were faithful to the statistics of the training data, but also samples that deviated in systematic ways from those statistics. This key feature of GANs could be exploited to study the impact of noise on various measures of neural complexity (Altan et al., 2021) as well as design brain-computer protocols to study the effects of neurostimulation on epileptiform activity (Scheid et al., 2021).

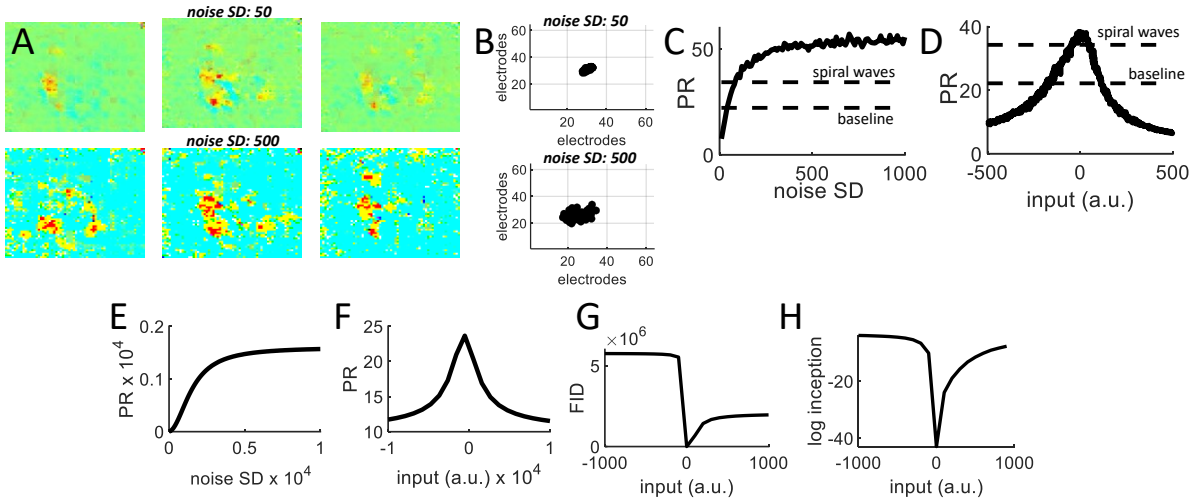

FIGURE 10. THE INPUT PROVIDED TO GENERATIVE NETWORKS CONTROLLED THE STATISTICS OF SNAPSHOTS

(**A**) Examples of snapshots where the SD of the input noise was increased from 50 to 500. (**B**) Center of mass of 1,000 snapshots. (**C**) The participation ratio increased along with the SD of the input noise. Dashed lines show the participation ratio of baseline and disinhibited cortical activity. 100 images were generated for each value of noise SD. (**D**) Effect of input strength on the participation ratio of snapshots. Input strength is in arbitrary units (a.u.). (**E-F**) Additive Gaussian noise to a cortical spiral wave altered the PR. (**G-H**) The Frechet Inception Distance (FID) and Inception Score are impacted by the input strength to the GAN. The log of the Inception Score is shown for ease of visualization.

The performance of the GAN was further assessed using two common performance measures, namely the Inception Score (Salimans et al., 2016) and the Frechet Inception Distance (Heusel et al., 2017). In both instances, we varied the mean of the noise injected to the GAN and found that better matches to the experimental data were obtained when the

noise was near zero (Figure 10G,H). Hence, the goodness-of-fit of snapshots generated by the GAN was dependent upon the statistics of the noise injected into the network.

Finally, we examined how the number of snapshots extracted from each spiral wave affected the PR. For both neural and synthetic data, we extracted a given number of snapshots per spiral and found that increasing the number of snapshots yielded higher values of PR (Figure 11A). A good fit between the GAN and experimental data was found when the noise injected to the GAN had SD=70 (Pearson correlation test, R^2= 0.9795, p=4.9036e-08). Normalizing the PR by the square root of the number of snapshots eliminated most of this effect (Figure 11B). Thus, while PR is influenced by the number of snapshots, this effect can be largely overcome by normalization and does not alter our conclusions given that the number of snapshots remained constant across conditions.

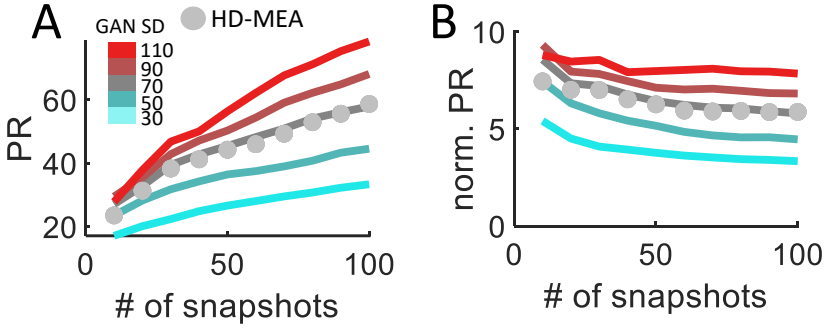

FIGURE 11. COMPLEXITY VERSUS THE NUMBER OF SNAPSHOTS PER SPIRAL WAVE

(**A**) GAN approximated hd-MEA data when the SD of its input was 70. (**B**) Normalizing PR by the square root of the number of snapshots.

In sum, the deep GAN model captured key aspects of spiral waves observed in disinhibited cortical networks. Going further, this model was employed to explore a broad

range of spatiotemporal activity by manipulating the noise injected as input to the generator network. Below, we discuss the implications of these results for the characterization of pathological network states.

Discussion

In this work, spiral waves arose in disinhibited cortical networks and exhibited stereotypical characteristics in terms of phase distribution, center of mass, spatial correlations, and neural complexity. Our main finding is that a deep generative neural network produced novel exemplars that captured these characteristics. Further, by adjusting the amplitude and variance of the GAN's input, the model generated patterns that spanned a broad range of complexity values encompassing both healthy and pathological states of activity.

Practical applications

There are two main avenues where GANs may be applied to neuropathological activity. First, GANs may inform neurostimulation protocols aimed at the suppression of epilepsy (Scheid et al., 2021). Results of the GAN network suggest that it may be possible to control the dynamical state and complexity of neural circuits by adjusting the amplitude and variance of injected input. In line with our results, the effect of noise on reducing episodes of neural synchrony has been suggested in theoretical work (Golomb, 1998; Zirkle & Rubchinsky, 2021). In clinical settings, it remains challenging to find regimes of electrical stimulation that are effective at suppressing seizures (S. Wang et al., 2022). This could be addressed by designing generative networks that produce pathological activity, then tuning

the input of these networks to optimally suppress this activity. Results of simulations could then be applied to deep brain stimulation and brain-machine interfaces.

A second avenue of application for GAN models is the generation of large datasets of plausible exemplars from a known distribution. This is an important application given that certain brain events such as seizures occur infrequently but are key to understanding the underlying neural pathology. The current work is a prime example of such application, where a GAN was employed to generate a dataset of spiral waves that are relatively rare in cortical recordings. This dataset can then be employed to examine the robustness of key properties of neural activity and train decision-based systems that serve as diagnostic aid (Chirasani & Manikandan, 2022; Ilakiyaselvan et al., 2020; Ilias et al., 2023).

RELATED APPROACHES

Our work can be compared to approaches that fall into two categories, namely generative models and biologically-inspired networks. Increasingly sophisticated generative models have emerged in recent years, with the capability to produce realistic images (Brock et al., 2018; Karras et al., 2019; Menick & Kalchbrenner, 2018; Razavi et al., 2019) and videos (Clark et al., 2019; Mathieu et al., 2015; Saito et al., 2017; Tulyakov et al., 2018; Vondrick et al., 2016). Few studies, however, have applied GANs to brain data (Arakaki et al., 2017; Lyamzin et al., 2010; Panzeri et al., 2010; Seeliger et al., 2018), and none thus far have looked at epileptiform brain activity.

Biologically-inspired models have been successful at capturing UP-DOWN states of rhythmic activity (Amit & Brunel, 1997; Compte et al., 2003; Stringer et al., 2016) as well as

spiral waves (Ermentrout & Kleinfeld, 2001; X. Huang et al., 2004; Jirsa et al., 2014; Scheid et al., 2021; Spiegler et al., 2016). A key advantage of these models is that they suggest candidate neural mechanisms to produce spiral waves. Notably, waves are proposed to emerge via three main scenarios: (*i*) an initially localized oscillation that propagates through lateral interactions; (*ii*) a shared input that drives nearby cortical sites with different transmission delays; and (*iii*) several sites that oscillate at similar frequencies and form coherent patterns (Ermentrout & Kleinfeld, 2001). Biologically-inspired models, however, are not designed to function as generative models that capture the statistics of a given dataset. A hybrid approach will hopefully emerge where biologically-inspired GANs can serve as data generators while embodying biological principles. Ideally, this approach would allow GANs to behave as a dynamical system that captures the mechanisms involved in generating seizure activity.

While our work employed PR and LBMLE as measures of complexity, various linear and non-linear alternatives have been proposed (Altan et al., 2021). While non-linear approaches may provide a more accurate estimation of complexity, it is unclear what method best applies to disinhibited neural data compared across experimental conditions. A complete theoretical analysis of PR and related measures will be needed to shed light on the relation between noise, disinhibited activity, and neuronal complexity.

MEASURES OF NEURAL COMPLEXITY

Several measures of neural complexity have been proposed (Altan et al., 2021). Linear methods such as the PR are widely used and straightforward to interpret due to their

simplicity. However, linear methods tend to overestimate the dimensionality of neural data. Hence, we compared the PR to a non-linear LBMLE method (Figure 7D). With both approaches, results consistently showed that spiral waves led to an increase in complexity compared to baseline activity. Another factor to consider is that measures of complexity such as the PR scale with the number of channels (N) analyzed (Figure 7E) and the resolution (i.e., number of snapshots) of the data (Figure 11A). This does not affect our main conclusions given that the number of neurons and snapshots was constant across spiral waves and baseline conditions. However, for applications where the number of channels and resolution may vary, it would be useful to scale the PR by these values. This will yield more stable estimates of complexity (Figure 7F, Figure 11B).

ALTERNATIVES TO GANS

While GANs were successful at capturing several aspects of spiral waves and hold the state-of-the-art for image generation, it is worth considering the advantages and drawbacks of potential alternatives, including diffusion models (Dhariwal & Nichol, 2021), variational autoencoders (Kingma & Welling, 2019), and U-nets (X. Chen et al., 2021). Diffusion models are a class of likelihood-based models that have recently been shown to produce high-quality images and avoid the "collapse" problem associated with GANs that produce images within a limited range of the training space. These models, however, tend to be slower and require more user intervention, in the form of classifier guidance. Variational autoencoders process input data by reducing it to a latent space of lower dimensionality prior to reconstruction. Results are generally inferior in quality than GANs. Finally, U-net is a generative model that uses a segmentation network as the discriminator,

where the goal is to partition an image into several basic constituents. A restriction of this approach, however, is that the input and output dimensions of the network must be the same. How these different generative models compare when trained on neural data is an interesting question for future work.

COMPARISON TO *IN VIVO* SPIRAL WAVES

Despite the *in vitro* nature of the data analysed herein, our results share several characteristics of spiral waves found *in vivo* during sleep-like states (X. Huang et al., 2010), epileptic activity (Viventi et al., 2011), and anaesthesia (Townsend et al., 2015). These characteristics include a broad phase distribution, a low amplitude near the center of mass, and the co-occurrence of spiral waves with other forms of activity including planar waves. The advantage of an *in vitro* approach using an hd-MEA is the ability to monitor spiral waves using a large number of channels simultaneously. The resulting data allowed us to elucidate several aspects of spiral waves that had not previously been explored, including spatial correlations and complexity. These results will benefit from *in vivo* support in future studies.

LIMITATIONS AND FUTURE WORK

While our results suggest increased complexity in disinhibited cortical networks, it is unclear whether these results would generalize to surrounding brain regions. In hippocampus, for instance, chaotic dynamics were mainly confined to the dentate gyrus and subiculum, while lower levels of chaotic activity were found in areas CA1-CA4 (Araújo et al., 2022). It would be worthwhile to explore seizure-like activity across brain regions and capture their differences using generative networks.

Furthermore, disinhibited networks produce various forms of waves that have not been explored here, including saddle patterns formed by the interaction between multiple waves (Engel & Steinmetz, 2019; X. Huang et al., 2010; Muller et al., 2018; Sato et al., 2012; Townsend et al., 2015; Townsend & Gong, 2018; J.-Y. Wu et al., 2008). Future work should be aimed at capturing the diversity of waves produced during healthy and disinhibited cortical states.

Caution should be warranted when attempting to draw general conclusions about neural complexity based strictly on spiral waves without also considering other forms of neural events as well as inter-wave activity. Spiral waves are interleaved with other neuronal patterns, including periods of both synchronized and desynchronized activity (Muller et al., 2018). It is possible that analyzing spiral waves in isolation may suggest increased neural complexity, while a broader range of activity may reveal otherwise. Here, we focused on spiral waves as they constitute an intricate form of neural activity that has thus far eluded a complete characterization. More broadly, neural complexity remains poorly understood as it covaries with many factors including cognitive attention (C. Huang et al., 2019), task demands (Rigotti et al., 2013; Stringer, Pachitariu, Steinmetz, Carandini, et al., 2019), arousal state (Kohn et al., 2020), and neural pathologies (Ferrea et al., 2012).

Finally, the prospects of using artificial neural networks to monitor and dynamically control epileptic events in real time will require the implementation of GANs that can handle continuous input streams and produce time-evolving synthetic data. This field of research

is currently under development and requires a combination of GANs with recurrent neural networks (Esteban et al., 2017; Mogren, 2016).

Conclusions

During states of disinhibited activity, cortical circuits generate propagating waves whose spatial and temporal evolution follows reliable patterns (X. Huang et al., 2004). A deep generative neural network trained on cortical spiral waves captured key aspects of these patterns. Once trained, the model was employed to show that neural complexity varies along a continuum – from lower values in healthy states to higher values in disinhibited states. The complexity of the simulated data was achieved solely by controlling the amplitude and variance of the input fed to the model, suggesting a framework that can be employed to examine the stimulus-driven suppression of aberrant network activity. This work opens the door to novel approaches that derive synthetic exemplars from neuroscience data to study rare forms of activity and probe their causal origins.

Methods

Electrophysiological data collection

Animals. All data were collected using three Sprague Dawley rats of both sexes (2 males and 1 female), aged 14 to 21 days, purchased from Charles River. Animals were housed in standard housing conditions with cage enrichment and *ad libitum* access to water and standard chow. All experiments were conducted in accordance with the Canadian Council on Animal Care guidelines and all procedures were approved by the University of Ottawa Animal Care and Veterinary Services.

ACUTE SLICE PREPARATION. Animals were deeply anaesthetized using isofluorane (Baxter Corporation) and subsequently euthanized via decapitation. Brains of the animals were quickly extracted and submerged into a frozen choline dissection buffer. The buffer consisted of the following: 119.0 mM choline chloride, 2.5 mM KCl, 4.3 mM MgSO4, 1.0 mM CaCl2, 1.0 mM NaH2PO4, 1.3 mM sodium ascorbate, 11.0 mM glucose, 26.2 mM NaHCO3, and was perfused using carbogen (95% O2/5% CO2). Acute cortical slices containing the PFC were produced using a Leica VT1000S vibratome. The brain was sliced coronally at a thickness of 300 μm. Once the slices were collected, they were placed in a recovery chamber filled with a standard artificial cerebrospinal fluid (ACSF) consisting of 119.0 mM NaCl, 2.5 mM KCl, 1.3 mM MgSO4, 2.5 mM CaCl2, 1.0 mM NaH2PO4, 11.0 mM glucose, and 26.2 mM NaHCO3. The ACSF was continuously perfused using carbogen (95% O2/5% CO2) and maintained at a temperature of 37˚C. Following slicing, the chamber was left to recover for 1 hour prior to experiments where it equilibrated to room temperature.

MULTI-ELECTRODE ARRAYS

GENERATION OF EPILEPTIFORM ACTIVITY. Baseline data was recorded using standard ACSF prior to application of the PE solution. Slices were included in the study if they displayed neural activity during baseline recordings, defined as threshold-crossing events in voltage traces on the acquisition software. Following baseline recordings, epileptiform activity was generated by applying a pro-epileptiform ACSF (PE-ACSF) containing the following: 120 mM NaCl, 8.5 mM KCl, 1.25 mM NaH2PO4, 0.25 mM MgSO4, 2 mM CaCl2, 24 mM NaHCO3, 10 mM dextrose, and 0.05 mM 4-AP (Postnikova et al., 2020). The PE-ACSF included a potassium channel blocker (4-AP) as well as reduced extracellular magnesium (Mg^{2+}) and

increased extracellular potassium (K^+), all of which have been reported to induce epileptiform activity (Bear & Lothman, 1993; Grainger et al., 2018; Igelström et al., 2011; Pacico & Mingorance-Le Meur, 2014; Postnikova et al., 2020; Traynelis & Dingledine, 1988; Trevelyan et al., 2006) and increase synchronization (Avoli et al., 1996; D'Antuono et al., 2002). The PE-ACSF solution was applied for 20 minutes prior to beginning the recordings and epileptiform activity was recorded for 10 minutes.

MULTI-ELECTRODE RECORDINGS. Extracellular potentials were collected using an active pixel sensor hd-MEA. This array uses a complementary metal-oxide semiconductor monolithic chip in which the pixels were modified to detect changes in electric voltages from electrogenic tissue. The circuit is designed to provide simultaneous recordings from 4,096 electrodes with a sampling rate of 7.7 kHz per channel. The chips are comprised of 64x64 electrodes arranged as a pixel element array whereby each pixel measures 21 μm x 21 μm with an electrode pitch of 42 μm. The active area of the array is 7.22 mm^2 and has a pixel density of 567 pixels/mm^2 (Ferrea et al., 2012; Imfeld et al., 2008). Data were acquired using BrainWave software (3Brain Gmbh, Switzerland) and imported to Matlab (MathWorks, Natick) for offline analysis.

IDENTIFICATION OF SPIRAL WAVES

Voltages at individual channels were processed by first applying a second order bandpass Butterworth filter in the delta range (1-4 Hz) to the raw voltages in the forward and reverse directions using the filtfilt function in Matlab (Buzsáki et al., 2012; Logothetis et al., 2001; Panzeri et al., 2010). Artefacts were removed by setting time-points with absolute

values greater than 200 μV to the mean of the signal. Data segments containing spiral waves were extracted based on visual inspection and later verified by the following criteria (Rule et al., 2018a): (*i*) a broad distribution of instantaneous phases around the center of mass (Figure 5A-C); (*ii*) rotating vector fields (Figure 5D); (*iii*) a decrease in voltage near the center of mass (Figure 4B); and (*iv*) spatially-dependent correlations between pairs of channels (Figure 6).

CENTER OF MASS. The center of mass of a given spiral wave was obtained as follows (F. Han et al., 2008; W. Xu et al., 2007). Assuming a 64x64 array of elements a_{ij} reflecting the band-filtered voltage at a particular time and spatial location (row i and column j up to N electrodes), the center row (r) and column (c) are given by

$$r = \frac{\sum_{i,j}^{N} i \cdot a_{ij}}{\sum_{i,j}^{N} a_{ij}}, \tag{1}$$

and

$$c = \frac{\sum_{i,j}^{N} j \cdot a_{ij}}{\sum_{i,j}^{N} a_{ij}}. \tag{2}$$

The above expressions were computed for each 1 ms time frame ("snapshot") of a given spiral wave, then averaged to provide the mean center of mass of each wave.

COMPLEXITY. The complexity of a given spiral wave was estimated by applying an eigenspectrum decomposition (Chapin & Nicolelis, 1999; Nicolelis et al., 1995) to 6 evenly-

spaced snapshots of each spiral wave, yielding ranked eigenvalues $\lambda_1, \ldots, \lambda_N$ where N is the total number of channels. Then, complexity was calculated using the PR (Hu & Sompolinsky, 2020; Litwin-Kumar et al., 2017; Mazzucato et al., 2016),

$$\mathrm{PR} = \frac{(\sum_i^N \lambda_i)^2}{\sum_i^N \lambda_i^2}, \tag{3}$$

corresponding to the square of the eigenspectrum's first moment normalized by its second moment. If patterns of neural activity are limited to a few dimensions, only a few eigenvalues will be positive, and the PR will be low. However, more complex, high-dimensional neural activity will be reflected by a broad distribution of eigenvalues and a high PR value.

GENERATIVE ADVERSARIAL NETWORK

In the GAN framework, two artificial neural networks compete against each other (Goodfellow et al., 2014). The "generative model" (*G*) attempts to produce synthetic samples that closely match the original data, while its counterpart, the "discriminative model" (*D*), learns to discriminate these synthetic samples from genuine ones. The competition between these two networks drives the GAN to produce synthetic samples that are indistinguishable from the original data. Once successfully trained, novel samples can be obtained from the generative model by feeding random noise to its input layer.

Here, a GAN was trained to produce synthetic samples of spiral waves. Once cortical spiral waves were identified and verified based on the above criteria, a sample of 6 snapshots were collected per spiral, corresponding to evenly spaced time points between the approximate time of initiation and termination of the wave. The complete dataset consisted of 1,314

images obtained from 219 spiral waves. Each input to the GAN consisted of all 6 snapshots from an individual wave tiled to form a pattern of size 64 pixels x 64 pixels x 6 snapshots.

Formally, assume some real data $\{x^{(i)}\}_{i=1}^{m} \sim \mathbb{P}_r$, where $\mathbb{P}_r$ is the data distribution. The goal was to generate some novel data $\tilde{\boldsymbol{x}}$ whose distribution $\mathbb{P}_g$ is a close approximation of $\mathbb{P}_r$. This was achieved by feeding noise to the generator network, $\tilde{\boldsymbol{x}} = G_\theta(z)$, given noisy priors $\{z^{(i)}\}_{i=1}^{m} \sim p(z)$. The input z to the generator was sampled from a Gaussian distribution.

The generative and discriminative networks were trained according to a minimax objective function,

$$\min_G \max_D V(D,G) = \mathbb{E}_{\boldsymbol{x}\sim p_{data}(\boldsymbol{x})}[logD(\boldsymbol{x})] + \mathbb{E}_{\boldsymbol{z}\sim p_{z(\boldsymbol{z})}}[\log\Big(1 - D\big(G(\boldsymbol{z})\big)\Big)], \tag{4}$$

where $V(D,G)$ is a min-max value function and $\boldsymbol{x}$ is the original data. This objective function was optimized using the Adam optimizer (Kingma & Ba, 2014) with a discriminator network learning rate of α =0.0002. The generator network learning rate was α=0.001. The total number of training iterations was set to 10,000. The generator network was composed of six hidden layers with rectified linear units (ReLU) and a hypertan (htan) output layer. The discriminator network had eight hidden layers with leaky ReLU units and a htan output layer. A convolution step preceded each hidden layer. The full model was trained using the Matlab Deep Learning library with default parameters unless otherwise stated. Output images were 64x64 pixels in size, matching the dimensions of the input snapshots obtained from the hd-MEA.

The performance of the generator network (Figure 9B) was computed by the score

$$S_G = mean\left(\hat{Y}_{generated}\right), \quad (5)$$

where $\hat{Y}_{generated}$ contains the probabilities for the generated images. For the discriminator network, the score was

$$S_D = 0.5\, mean\left(\hat{Y}_{real}\right) + 0.5\, mean\left(1 - \hat{Y}_{generated}\right), \quad (6)$$

where $\hat{Y}_{real}$ contains the discriminator output probabilities for real images. The ideal scenario is where both scores are close to 0.5. However, this is not a requirement to obtain a successful GAN; in fact, several measures were employed to compare the generated images with experimental data, including eigenspectrum distribution (Figure 9D), center of mass (Figure 9E), spatial correlations (Figure 9F), complexity (Figure 10C-F), Frechet Inception Distance (Figure 10G), and Inception Score (Figure 10H).

REFERENCES

Altan, E., Solla, S. A., Miller, L. E., & Perreault, E. J. (2021). Estimating the dimensionality of the manifold underlying multi-electrode neural recordings. *PLoS Computational Biology*, *17*(11), e1008591. https://doi.org/10.1371/journal.pcbi.1008591

Amit, D. J., & Brunel, N. (1997). Model of global spontaneous activity and local structured activity during delay periods in the cerebral cortex. *Cerebral Cortex (New York, N.Y.: 1991)*, *7*(3), 237–252. https://doi.org/10.1093/cercor/7.3.237

Arakaki, T., Barello, G., & Ahmadian, Y. (2017). Capturing the diversity of biological tuning curves using generative adversarial networks. *arXiv Preprint arXiv:1707.04582*.

Araújo, N. S., Reyes-Garcia, S. Z., Brogin, J. A. F., Bueno, D. D., Cavalheiro, E. A., Scorza, C. A., & Faber, J. (2022). Chaotic and stochastic dynamics of epileptiform-like activities in sclerotic hippocampus resected from patients with pharmacoresistant epilepsy. *PLoS Computational Biology*, *18*(4), e1010027. https://doi.org/10.1371/journal.pcbi.1010027

Avoli, M., Barbarosie, M., Lücke, A., Nagao, T., Lopantsev, V., & Köhling, R. (1996). Synchronous GABA-mediated potentials and epileptiform discharges in the rat limbic system in vitro. *The Journal of Neuroscience: The Official Journal of the Society for Neuroscience*, *16*(12), 3912–3924.

Barbero-Castillo, A., Mateos-Aparicio, P., Dalla Porta, L., Camassa, A., Perez-Mendez, L., & Sanchez-Vives, M. V. (2021). Impact of GABAA and GABAB Inhibition on Cortical Dynamics and Perturbational Complexity during Synchronous and Desynchronized States. *The Journal of Neuroscience: The Official Journal of the Society for Neuroscience*, *41*(23), 5029–5044. https://doi.org/10.1523/JNEUROSCI.1837-20.2021

Bear, J., & Lothman, E. W. (1993). An in vitro study of focal epileptogenesis in combined hippocampal-parahippocampal slices. *Epilepsy Research*, *14*(3), 183–193. https://doi.org/10.1016/0920-1211(93)90043-7

Brock, A., Donahue, J., & Simonyan, K. (2018). Large scale GAN training for high fidelity natural image synthesis. *arXiv Preprint arXiv:1809.11096*.

Buzsáki, G., Anastassiou, C. A., & Koch, C. (2012). The origin of extracellular fields and currents—EEG, ECoG, LFP and spikes. *Nature Reviews. Neuroscience*, *13*(6), 407–420. https://doi.org/10.1038/nrn3241

Cavanagh, S. E., Hunt, L. T., & Kennerley, S. W. (2020). A Diversity of Intrinsic Timescales Underlie Neural Computations. *Frontiers in Neural Circuits*, *14*, 615626. https://doi.org/10.3389/fncir.2020.615626

Chapin, J. K., & Nicolelis, M. A. (1999). Principal component analysis of neuronal ensemble activity reveals multidimensional somatosensory representations. *Journal of Neuroscience Methods*, *94*(1), 121–140. https://doi.org/10.1016/s0165-0270(99)00130-2

Chen, X., Li, Y., Yao, L., Adeli, E., & Zhang, Y. (2021). Generative adversarial U-Net for domain-free medical image augmentation. *arXiv Preprint arXiv:2101.04793*.

Chirasani, S. K. R., & Manikandan, S. (2022). A deep neural network for the classification of epileptic seizures using hierarchical attention mechanism. *Soft Computing*, *26*(11), 5389–5397. https://doi.org/10.1007/s00500-022-07122-8

Clark, A., Donahue, J., & Simonyan, K. (2019). Adversarial video generation on complex datasets. *arXiv Preprint arXiv:1907.06571*.

Compte, A., Sanchez-Vives, M. V., McCormick, D. A., & Wang, X.-J. (2003). Cellular and network mechanisms of slow oscillatory activity (<1 Hz) and wave propagations in a cortical network model. *Journal of Neurophysiology*, *89*(5), 2707–2725. https://doi.org/10.1152/jn.00845.2002

D'Antuono, M., Benini, R., Biagini, G., D'Arcangelo, G., Barbarosie, M., Tancredi, V., & Avoli, M. (2002). Limbic network interactions leading to hyperexcitability in a model of temporal lobe epilepsy. *Journal of Neurophysiology*, *87*(1), 634–639. https://doi.org/10.1152/jn.00351.2001

Dhariwal, P., & Nichol, A. (2021). *Diffusion Models Beat GANs on Image Synthesis* (arXiv:2105.05233). arXiv. https://doi.org/10.48550/arXiv.2105.05233

Dzhala, V. I., & Staley, K. J. (2003). Transition from interictal to ictal activity in limbic networks in vitro. *The Journal of Neuroscience: The Official Journal of the Society for Neuroscience*, *23*(21), 7873–7880.

Ecker, A. S., Berens, P., Cotton, R. J., Subramaniyan, M., Denfield, G. H., Cadwell, C. R., Smirnakis, S. M., Bethge, M., & Tolias, A. S. (2014). State dependence of noise correlations in macaque primary visual cortex. *Neuron*, *82*(1), 235–248. https://doi.org/10.1016/j.neuron.2014.02.006

El Boustani, S., & Destexhe, A. (2010). Brain dynamics at multiple scales: Can one reconcile the apparent low-dimensional chaos of macroscopic variables with the seemingly stochastic behavior of single neurons? *International Journal of Bifurcation and Chaos*, *20*(06), 1687–1702. https://doi.org/10.1142/S0218127410026769

Engel, T. A., & Steinmetz, N. A. (2019). New perspectives on dimensionality and variability from large-scale cortical dynamics. *Current Opinion in Neurobiology*, *58*, 181–190. https://doi.org/10.1016/j.conb.2019.09.003

Ermentrout, G. B., & Kleinfeld, D. (2001). Traveling electrical waves in cortex: Insights from phase dynamics and speculation on a computational role. *Neuron*, *29*(1), 33–44. https://doi.org/10.1016/s0896-6273(01)00178-7

Esteban, C., Hyland, S. L., & Rätsch, G. (2017). Real-valued (medical) time series generation with recurrent conditional gans. *arXiv Preprint arXiv:1706.02633*.

Ferrea, E., Maccione, A., Medrihan, L., Nieus, T., Ghezzi, D., Baldelli, P., Benfenati, F., & Berdondini, L. (2012). Large-scale, high-resolution electrophysiological imaging of field potentials in brain slices with microelectronic multielectrode arrays. *Frontiers in Neural Circuits*, *6*, 80. https://doi.org/10.3389/fncir.2012.00080

Golomb, D. (1998). Models of neuronal transient synchrony during propagation of activity through neocortical circuitry. *Journal of Neurophysiology*, *79*(1), 1–12. https://doi.org/10.1152/jn.1998.79.1.1

Goodfellow, I., Pouget-Abadie, J., Mirza, M., Xu, B., Warde-Farley, D., Ozair, S., Courville, A., & Bengio, Y. (2014). Generative adversarial nets. *Advances in Neural Information Processing Systems*, *27*.

Grainger, A. I., King, M. C., Nagel, D. A., Parri, H. R., Coleman, M. D., & Hill, E. J. (2018). In vitro Models for Seizure-Liability Testing Using Induced Pluripotent Stem Cells. *Frontiers in Neuroscience*, *12*, 590. https://doi.org/10.3389/fnins.2018.00590

Han, F., Caporale, N., & Dan, Y. (2008). Reverberation of recent visual experience in spontaneous cortical waves. *Neuron*, *60*(2), 321–327. https://doi.org/10.1016/j.neuron.2008.08.026

Heusel, M., Ramsauer, H., Unterthiner, T., Nessler, B., & Hochreiter, S. (2017). Gans trained by a two time-scale update rule converge to a local nash equilibrium. *Advances in Neural Information Processing Systems*, *30*.

Horvát, S., Gămănuț, R., Ercsey-Ravasz, M., Magrou, L., Gămănuț, B., Van Essen, D. C., Burkhalter, A., Knoblauch, K., Toroczkai, Z., & Kennedy, H. (2016). Spatial Embedding and Wiring Cost Constrain the Functional Layout of the Cortical Network of Rodents and Primates. *PLoS Biology*, *14*(7), e1002512. https://doi.org/10.1371/journal.pbio.1002512

Hu, Y., & Sompolinsky, H. (2020). The spectrum of covariance matrices of randomly connected recurrent neuronal networks. *bioRxiv*.

Huang, C., Ruff, D. A., Pyle, R., Rosenbaum, R., Cohen, M. R., & Doiron, B. (2019). Circuit Models of Low-Dimensional Shared Variability in Cortical Networks. *Neuron*, *101*(2), 337-348.e4. https://doi.org/10.1016/j.neuron.2018.11.034

Huang, X., Troy, W. C., Yang, Q., Ma, H., Laing, C. R., Schiff, S. J., & Wu, J.-Y. (2004). Spiral waves in disinhibited mammalian neocortex. *The Journal of Neuroscience: The Official Journal of the Society for Neuroscience*, *24*(44), 9897–9902. https://doi.org/10.1523/JNEUROSCI.2705-04.2004

Huang, X., Xu, W., Liang, J., Takagaki, K., Gao, X., & Wu, J.-Y. (2010). Spiral wave dynamics in neocortex. *Neuron*, *68*(5), 978–990. https://doi.org/10.1016/j.neuron.2010.11.007

Igelström, K. M., Shirley, C. H., & Heyward, P. M. (2011). Low-magnesium medium induces epileptiform activity in mouse olfactory bulb slices. *Journal of Neurophysiology*, *106*(5), 2593–2605. https://doi.org/10.1152/jn.00601.2011

Ilakiyaselvan, N., Nayeemulla Khan, A., & Shahina, A. (2020). Deep learning approach to detect seizure using reconstructed phase space images. *Journal of Biomedical Research*, *34*(3), 240–250. https://doi.org/10.7555/JBR.34.20190043

Ilias, L., Askounis, D., & Psarras, J. (2023). Multimodal detection of epilepsy with deep neural networks. *Expert Systems with Applications*, *213*, 119010. https://doi.org/10.1016/j.eswa.2022.119010

Imfeld, K., Neukom, S., Maccione, A., Bornat, Y., Martinoia, S., Farine, P.-A., Koudelka-Hep, M., & Berdondini, L. (2008). Large-scale, high-resolution data acquisition system for extracellular recording of electrophysiological activity. *IEEE Transactions on Bio-Medical Engineering*, *55*(8), 2064–2073. https://doi.org/10.1109/TBME.2008.919139

Jirsa, V. K., Stacey, W. C., Quilichini, P. P., Ivanov, A. I., & Bernard, C. (2014). On the nature of seizure dynamics. *Brain: A Journal of Neurology*, *137*(Pt 8), 2210–2230. https://doi.org/10.1093/brain/awu133

Karras, T., Laine, S., & Aila, T. (2019). A style-based generator architecture for generative adversarial networks. *Proceedings of the IEEE/CVF Conference on Computer Vision and Pattern Recognition*, 4401–4410.

Kingma, D. P., & Ba, J. (2014). Adam: A method for stochastic optimization. *arXiv Preprint arXiv:1412.6980*.

Kingma, D. P., & Welling, M. (2019). An introduction to variational autoencoders. *Foundations and Trends® in Machine Learning*, *12*(4), 307–392.

Kohn, A., Jasper, A. I., Semedo, J. D., Gokcen, E., Machens, C. K., & Yu, B. M. (2020). Principles of Corticocortical Communication: Proposed Schemes and Design

Considerations. *Trends in Neurosciences*, *43*(9), 725–737. https://doi.org/10.1016/j.tins.2020.07.001

Le Van Quyen, M., Navarro, V., Martinerie, J., Baulac, M., & Varela, F. J. (2003). Toward a neurodynamical understanding of ictogenesis. *Epilepsia*, *44 Suppl 12*, 30–43. https://doi.org/10.1111/j.0013-9580.2003.12007.x

Levina, E., & Bickel, P. J. (2004). Maximum Likelihood Estimation of Intrinsic Dimension: Neural Information Processing Systems: NIPS. *Vancouver, CA*.

Levy, R. B., & Reyes, A. D. (2012). Spatial profile of excitatory and inhibitory synaptic connectivity in mouse primary auditory cortex. *The Journal of Neuroscience: The Official Journal of the Society for Neuroscience*, *32*(16), 5609–5619. https://doi.org/10.1523/JNEUROSCI.5158-11.2012

Lin, I.-C., Okun, M., Carandini, M., & Harris, K. D. (2015). The Nature of Shared Cortical Variability. *Neuron*, *87*(3), 644–656. https://doi.org/10.1016/j.neuron.2015.06.035

Litwin-Kumar, A., Harris, K. D., Axel, R., Sompolinsky, H., & Abbott, L. F. (2017). Optimal Degrees of Synaptic Connectivity. *Neuron*, *93*(5), 1153-1164.e7. https://doi.org/10.1016/j.neuron.2017.01.030

Logothetis, N. K., Pauls, J., Augath, M., Trinath, T., & Oeltermann, A. (2001). Neurophysiological investigation of the basis of the fMRI signal. *Nature*, *412*(6843), 150–157. https://doi.org/10.1038/35084005

Lyamzin, D. R., Macke, J. H., & Lesica, N. A. (2010). Modeling Population Spike Trains with Specified Time-Varying Spike Rates, Trial-to-Trial Variability, and Pairwise Signal and

Noise Correlations. *Frontiers in Computational Neuroscience*, *4*, 144. https://doi.org/10.3389/fncom.2010.00144

Mariño, J., Schummers, J., Lyon, D. C., Schwabe, L., Beck, O., Wiesing, P., Obermayer, K., & Sur, M. (2005). Invariant computations in local cortical networks with balanced excitation and inhibition. *Nature Neuroscience*, *8*(2), 194–201. https://doi.org/10.1038/nn1391

Mathieu, M., Couprie, C., & LeCun, Y. (2015). Deep multi-scale video prediction beyond mean square error. *arXiv Preprint arXiv:1511.05440*.

Mazzucato, L., Fontanini, A., & La Camera, G. (2016). Stimuli Reduce the Dimensionality of Cortical Activity. *Frontiers in Systems Neuroscience*, *10*, 11. https://doi.org/10.3389/fnsys.2016.00011

Menick, J., & Kalchbrenner, N. (2018). Generating high fidelity images with subscale pixel networks and multidimensional upscaling. *arXiv Preprint arXiv:1812.01608*.

Mogren, O. (2016). *C-RNN-GAN: Continuous recurrent neural networks with adversarial training*. https://doi.org/10.48550/arXiv.1611.09904

Muller, L., Chavane, F., Reynolds, J., & Sejnowski, T. J. (2018). Cortical travelling waves: Mechanisms and computational principles. *Nature Reviews. Neuroscience*, *19*(5), 255–268. https://doi.org/10.1038/nrn.2018.20

Nicolelis, M. A., Baccala, L. A., Lin, R. C., & Chapin, J. K. (1995). Sensorimotor encoding by synchronous neural ensemble activity at multiple levels of the somatosensory system. *Science (New York, N.Y.)*, *268*(5215), 1353–1358. https://doi.org/10.1126/science.7761855

Pacico, N., & Mingorance-Le Meur, A. (2014). New in vitro phenotypic assay for epilepsy: Fluorescent measurement of synchronized neuronal calcium oscillations. *PloS One*, *9*(1), e84755. https://doi.org/10.1371/journal.pone.0084755

Panzeri, S., Brunel, N., Logothetis, N. K., & Kayser, C. (2010). Sensory neural codes using multiplexed temporal scales. *Trends in Neurosciences*, *33*(3), 111–120. https://doi.org/10.1016/j.tins.2009.12.001

Pinto, D. J., Patrick, S. L., Huang, W. C., & Connors, B. W. (2005). Initiation, propagation, and termination of epileptiform activity in rodent neocortex in vitro involve distinct mechanisms. *The Journal of Neuroscience: The Official Journal of the Society for Neuroscience*, *25*(36), 8131–8140. https://doi.org/10.1523/JNEUROSCI.2278-05.2005

Postnikova, T. Y., Amakhin, D. V., Trofimova, A. M., & Zaitsev, A. V. (2020). Calcium-permeable AMPA receptors are essential to the synaptic plasticity induced by epileptiform activity in rat hippocampal slices. *Biochemical and Biophysical Research Communications*, *529*(4), 1145–1150. https://doi.org/10.1016/j.bbrc.2020.06.121

Rabinowitz, N. C., Goris, R. L., Cohen, M., & Simoncelli, E. P. (2015). Attention stabilizes the shared gain of V4 populations. *eLife*, *4*, e08998. https://doi.org/10.7554/eLife.08998

Razavi, A., Van den Oord, A., & Vinyals, O. (2019). Generating diverse high-fidelity images with vq-vae-2. *Advances in Neural Information Processing Systems*, *32*.

Rigotti, M., Barak, O., Warden, M. R., Wang, X.-J., Daw, N. D., Miller, E. K., & Fusi, S. (2013). The importance of mixed selectivity in complex cognitive tasks. *Nature*, *497*(7451), 585–590. https://doi.org/10.1038/nature12160

Rule, M. E., Vargas-Irwin, C., Donoghue, J. P., & Truccolo, W. (2018). Phase reorganization leads to transient β-LFP spatial wave patterns in motor cortex during steady-state movement preparation. *Journal of Neurophysiology*, *119*(6), 2212–2228. https://doi.org/10.1152/jn.00525.2017

Saito, M., Matsumoto, E., & Saito, S. (2017). Temporal generative adversarial nets with singular value clipping. *Proceedings of the IEEE International Conference on Computer Vision*, 2830–2839.

Salimans, T., Goodfellow, I., Zaremba, W., Cheung, V., Radford, A., & Chen, X. (2016, June 10). *Improved Techniques for Training GANs*. arXiv.Org. https://doi.org/10.48550/arXiv.1606.03498

Sato, T. K., Nauhaus, I., & Carandini, M. (2012). Traveling waves in visual cortex. *Neuron*, *75*(2), 218–229. https://doi.org/10.1016/j.neuron.2012.06.029

Scheid, B. H., Ashourvan, A., Stiso, J., Davis, K. A., Mikhail, F., Pasqualetti, F., Litt, B., & Bassett, D. S. (2021). Time-evolving controllability of effective connectivity networks during seizure progression. *Proceedings of the National Academy of Sciences of the United States of America*, *118*(5), e2006436118. https://doi.org/10.1073/pnas.2006436118

Seeliger, K., Güçlü, U., Ambrogioni, L., Güçlütürk, Y., & van Gerven, M. A. (2018). Generative adversarial networks for reconstructing natural images from brain activity. *NeuroImage*, *181*, 775–785.

Song, S., Sjöström, P. J., Reigl, M., Nelson, S., & Chklovskii, D. B. (2005). Highly nonrandom features of synaptic connectivity in local cortical circuits. *PLoS Biology*, *3*(3), e68. https://doi.org/10.1371/journal.pbio.0030068

Spiegler, A., Hansen, E. C. A., Bernard, C., McIntosh, A. R., & Jirsa, V. K. (2016). Selective Activation of Resting-State Networks following Focal Stimulation in a Connectome-Based Network Model of the Human Brain. *eNeuro*, *3*(5), ENEURO.0068-16.2016. https://doi.org/10.1523/ENEURO.0068-16.2016

Stringer, C., Pachitariu, M., Steinmetz, N. A., Okun, M., Bartho, P., Harris, K. D., Sahani, M., & Lesica, N. A. (2016). Inhibitory control of correlated intrinsic variability in cortical networks. *eLife*, *5*, e19695. https://doi.org/10.7554/eLife.19695

Stringer, C., Pachitariu, M., Steinmetz, N., Carandini, M., & Harris, K. D. (2019). High-dimensional geometry of population responses in visual cortex. *Nature*, *571*(7765), 361–365. https://doi.org/10.1038/s41586-019-1346-5

Stringer, C., Pachitariu, M., Steinmetz, N., Reddy, C. B., Carandini, M., & Harris, K. D. (2019). Spontaneous behaviors drive multidimensional, brainwide activity. *Science (New York, N.Y.)*, *364*(6437), 255. https://doi.org/10.1126/science.aav7893

Thivierge, J.-P. (2020). Frequency-separated principal component analysis of cortical population activity. *Journal of Neurophysiology*, *124*(3), 668–681. https://doi.org/10.1152/jn.00167.2020

Townsend, R. G., & Gong, P. (2018). Detection and analysis of spatiotemporal patterns in brain activity. *PLoS Computational Biology*, *14*(12), e1006643. https://doi.org/10.1371/journal.pcbi.1006643

Townsend, R. G., Solomon, S. S., Chen, S. C., Pietersen, A. N. J., Martin, P. R., Solomon, S. G., & Gong, P. (2015). Emergence of complex wave patterns in primate cerebral cortex. *The Journal of Neuroscience: The Official Journal of the Society for Neuroscience*, *35*(11), 4657–4662. https://doi.org/10.1523/JNEUROSCI.4509-14.2015

Traynelis, S. F., & Dingledine, R. (1988). Potassium-induced spontaneous electrographic seizures in the rat hippocampal slice. *Journal of Neurophysiology*, *59*(1), 259–276. https://doi.org/10.1152/jn.1988.59.1.259

Trevelyan, A. J., Sussillo, D., Watson, B. O., & Yuste, R. (2006). Modular propagation of epileptiform activity: Evidence for an inhibitory veto in neocortex. *The Journal of Neuroscience: The Official Journal of the Society for Neuroscience*, *26*(48), 12447–12455. https://doi.org/10.1523/JNEUROSCI.2787-06.2006

Trevelyan, A. J., Sussillo, D., & Yuste, R. (2007). Feedforward inhibition contributes to the control of epileptiform propagation speed. *The Journal of Neuroscience: The Official Journal of the Society for Neuroscience*, *27*(13), 3383–3387. https://doi.org/10.1523/JNEUROSCI.0145-07.2007

Tulyakov, S., Liu, M.-Y., Yang, X., & Kautz, J. (2018). Mocogan: Decomposing motion and content for video generation. *Proceedings of the IEEE Conference on Computer Vision and Pattern Recognition*, 1526–1535.

Viventi, J., Kim, D.-H., Vigeland, L., Frechette, E. S., Blanco, J. A., Kim, Y.-S., Avrin, A. E., Tiruvadi, V. R., Hwang, S.-W., Vanleer, A. C., Wulsin, D. F., Davis, K., Gelber, C. E., Palmer, L., Van der Spiegel, J., Wu, J., Xiao, J., Huang, Y., Contreras, D., … Litt, B. (2011). Flexible, foldable, actively multiplexed, high-density electrode array for mapping brain activity in vivo. *Nature Neuroscience*, *14*(12), 1599–1605. https://doi.org/10.1038/nn.2973

Vondrick, C., Pirsiavash, H., & Torralba, A. (2016). Generating videos with scene dynamics. *Advances in Neural Information Processing Systems*, *29*.

Wang, S., Kfoury, C., Marion, A., Lévesque, M., & Avoli, M. (2022). Modulation of in vitro epileptiform activity by optogenetic stimulation of parvalbumin-positive interneurons. *Journal of Neurophysiology*, *128*(4), 837–846. https://doi.org/10.1152/jn.00192.2022

Wu, J.-Y., Xiaoying Huang, null, & Chuan Zhang, null. (2008). Propagating waves of activity in the neocortex: What they are, what they do. *The Neuroscientist: A Review Journal Bringing Neurobiology, Neurology and Psychiatry*, *14*(5), 487–502. https://doi.org/10.1177/1073858408317066

Xiao, Y., Huang, X.-Y., Van Wert, S., Barreto, E., Wu, J.-Y., Gluckman, B. J., & Schiff, S. J. (2012). The role of inhibition in oscillatory wave dynamics in the cortex. *The European Journal of Neuroscience*, *36*(2), 2201–2212. https://doi.org/10.1111/j.1460-9568.2012.08132.x

Xu, W., Huang, X., Takagaki, K., & Wu, J. (2007). Compression and reflection of visually evoked cortical waves. *Neuron*, *55*(1), 119–129. https://doi.org/10.1016/j.neuron.2007.06.016

Zirkle, J., & Rubchinsky, L. L. (2021). Noise effect on the temporal patterns of neural synchrony. *Neural Networks*, *141*, 30–39.

CHAPTER 3: HIGH-DENSITY MULTI-ELECTRODE PLATFORM EXAMINING THE EFFECTS OF RADIATION ON ACTIVITY, FUNCTIONAL CONNECTIVITY, COMPLEXITY, AND SURVIVAL OF IN VITRO CORTICAL NETWORKS

Boucher-Routhier, M., Szanto, J., Nair, V., & Thivierge, J.P., (2024). A high-density multi-electrode platform to study the neuromodulatory effect of radiation on populations of prefrontal cortical neurons. [Manuscript under consideration].

ABSTRACT

Radiation therapy and stereotactic radiosurgery are common treatments for brain malignancies. However, the impact of radiation on underlying neuronal circuits is poorly understood. In the prefrontal cortex (PFC), neurons communicate via action potentials that control essential processes such as executive function, decision making and working memory, thus it is important to understand the impact of radiation on these circuits. Here we present a novel protocol to investigate the effect of radiation on the activity and survival of dense PFC networks *in vitro*. Escalating doses of radiation were applied to PFC slices using a robotic radiosurgery platform at a standard dose rate of 10 Gy/min. High-density multielectrode array recordings of radiated slices were collected to capture extracellular activity across 4,096 channels. Radiated slices showed an increase in firing rate, functional connectivity, and complexity. These results were compared to pharmacologically-induced epileptic slices where neural complexity was markedly elevated, and functional connections were strong but remained spatially focused. Finally, propidium iodide staining revealed a dose-dependent effect of radiation on apoptosis. These findings provide a novel assay to investigate the impacts of clinically relevant doses of radiation on brain circuits and highlight the acute effects of escalating radiation doses on PFC neurons.

Keywords radiation, multielectrode array, prefrontal cortex, complexity, neuronal activity

INTRODUCTION

Radiation therapy (RT) and stereotactic radiosurgery (SRS) are increasingly used to treat conditions such as primary and metastatic brain tumors, trigeminal neuralgia and intractable epilepsy (Quigg et al., 2012; Zhang et al., 2020). Despite their widespread use, the effects of radiation on surviving neuronal networks remain poorly understood (Zhang et al., 2020). Radiation can produce brain injuries that occur on different timescales following treatment. Acute radiation-induced injuries typically occur within days of radiation, whereas early delayed injuries occur within one to six months post-radiation, and late delayed injuries occur over 6 months post-radiation (Greene-Schloesser et al., 2012; Zhang et al., 2018). Radiation-induced brain injuries have been associated with several cognitive impairments such as memory, attention, and executive function deficits, as well as reduced processing speed, which can occasionally progress to dementia (Brière et al., 2008; Greene-Schloesser et al., 2012; Zhang et al., 2018). These injuries appear to be dose-dependent, whereby patients who receive higher doses tend to have worse long-term outcomes (Brière et al., 2008).

Radiation-induced brain injuries are thought to be caused by a combination of cell death and dysfunction in surviving brain cells. Previous literature examining acute and early delayed effects of radiation has established that irradiated neurons show significantly increased firing rates (Zaer et al., 2022; Zhang et al., 2020), changes in synaptic morphology (Kempf et al., 2015; Zhang et al., 2020), and inhibited synaptic function and plasticity including deficits in long-term potentiation (P. Wu et al., 2012; Zhang et al., 2018). Larger doses of radiation (>60 Gy) in the primary visual cortex of Göttingen minipigs have also

shown significant decreases in firing rate 6-months post-radiation suggesting distinct effects in acute compared to late delayed radiation-induced brain injuries (Zaer et al., 2022).

Past research has primarily focused on the impact of radiation on the hippocampus due to its association with memory impairments. However, more recent work has highlighted the importance of studying other brain regions such as the PFC. The PFC is a key region of interest because it is responsible for several important functions including executive function, decision-making, and working memory (Carlén, 2017). Neurons located within the PFC communicate with one another and with adjacent sensory, motor, and subcortical regions through precisely-timed action potentials that are impacted by radiation therapy (Miller and Cohen, 2001; Zhang et al., 2020). Further, the PFC has close functional connections with the hippocampus through a direct monosynaptic pathway that originates in the cornu ammonis 1 (CA1)/subiculum fields of the hippocampus and projects to the prelimbic and medial orbital areas of the PFC (Thierry et al., 2000; Zhang et al., 2018). Thus, the PFC is a major contributor to inter-regional hippocampal communication and a region of central importance in understanding cognitive impairments following radiation (Gould, 2018; Zhang et al., 2020).

Large-scale, high-density multi-electrode arrays (hd-MEAs) are gaining widespread interest as a tool to monitor brain networks *in vitro* (Stevenson & Kording, 2011). Because of their ability to record from broad networks at high spatial and temporal resolution, hd-MEAs offer a middle ground between single-cell recordings and very large-scale neural activity obtained with electrocorticograms or electroencephalograms. State-of-the-art hd-MEAs

can monitor thousands of neurons simultaneously at sufficient temporal resolution to isolate individual action potentials, providing a rich insight into patterns of network activity during both healthy and altered cortical states (Ferrea et al., 2012).

In this work, a novel assay was developed where hd-MEAs were employed to monitor the neuronal activity of *in vitro* PFC slices following radiation, with a focus on acute radiation-induced dysfunction. To the best of our knowledge, this is the first time that any MEA technology has been used to study the impacts of therapeutic doses of radiation on *in vitro* PFC circuits. Various markers were designed to quantify changes in network dynamics and apoptosis. Comparisons of these markers between radiation and pharmacologically-induced epileptiform activity revealed a distinct signature of radiation-induced changes in network function. These results suggest that hd-MEAs constitute a novel and viable assay to investigate the impact of clinically relevant doses of radiation (Redmond et al., 2021; Tuleasca et al., 2021) on neuronal dysfunction and apoptosis.

MATERIAL AND METHODS

ELECTROPHYSIOLOGICAL DATA COLLECTION

A total of 12 acute PFC slices were assigned to either the pro-epileptiform (PE, 2 slices) or radiation (10 slices) treatment (Figure 12). This number is common for hd-MEA recordings as the statistical sample size is determined by the number of electrodes (n = 4,096) that are simultaneously recorded rather than the total number of slices. Fewer slices were analyzed for the pro-epileptiform treatment given that widespread ictal events constitute rare occurrences and were obtained from a previously published data set

(Boucher-Routhier & Thivierge, 2023). Slices receiving the PE treatment were first recorded at baseline using the hd-MEA, then perfused with the PE solution and recorded again after 20 minutes. Slices receiving the radiation treatment were split into control (4 slices) and radiated (6 slices) groups. Escalating radiation doses of 20 Gy, 50 Gy and 100 Gy were delivered to each of the slices followed by a 45-minute recovery period. These slices were then either recorded on the hd-MEA or imaged using propidium iodide (PI) staining. Control slices received sham radiation followed by 45 minutes of recovery before proceeding to the recording or imaging step. Together, this platform provides a direct comparison between epileptiform- and radiation-induced changes in neural activity, as well as an evaluation of dose-dependent neuronal apoptosis.

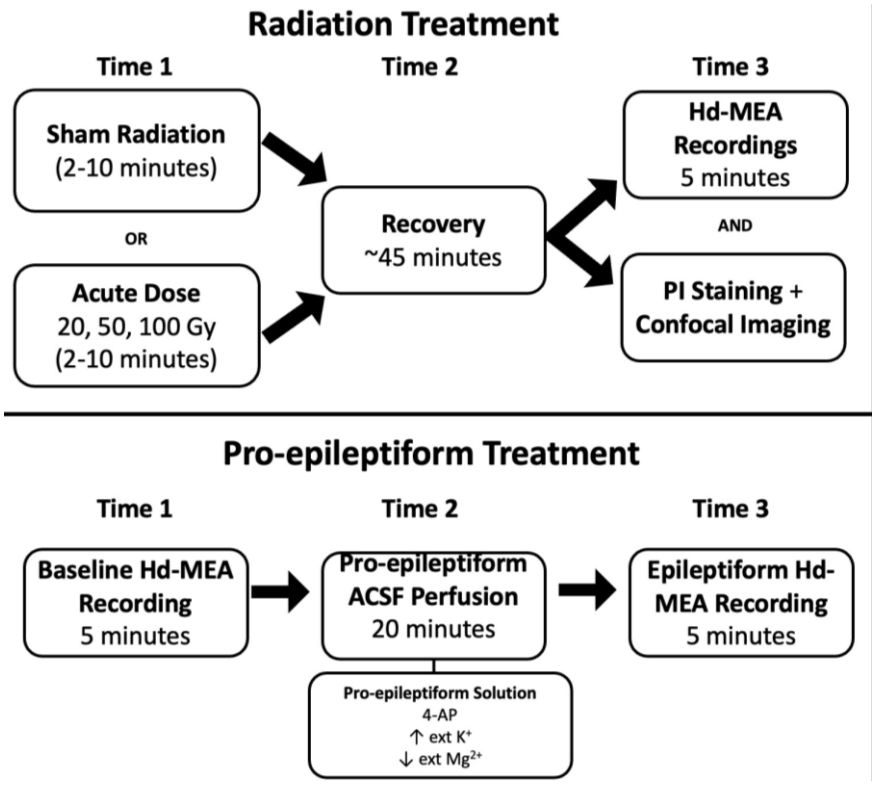

FIGURE 12. COMPARISON OF RADIATION AND PRO-EPILEPTIC TREATMENT PROTOCOLS EMPLOYED IN PREFRONTAL CORTICAL SLICES.

ANIMALS

Data were collected using Sprague Dawley rats of both sexes, aged 14 to 21 days, purchased from Charles River. The rodents used in different conditions were from different litters. We chose to study juvenile animals as past research has shown that brain slices from juveniles attain higher survival rates than later developmental stages (Lipton et al., 1995). The neurons in juvenile slices are also generally more resistant to various insults when compared to adult animals, suggesting that the effects reported in the juvenile slices may be even greater in mature animals (S. Huang & Uusisaari, 2013). Another motivating factor for studying juvenile rodents comes from age-dependent findings in human patients. Past research has shown an age-dependent effect of radiation whereby younger patients typically experience poorer outcomes than adult patients thus highlighting the importance of studying these effects (Mulhern et al., 2004). These findings have also been replicated in rodent studies (Zhang et al., 2018).

Animals were housed in standard housing conditions with cage enrichment and ad libitum access to water and standard chow. All experiments were carried out in accordance with Canadian Council on Animal Care Guidelines and all procedures were approved by the University of Ottawa Animal Care and Veterinary Services.

ACUTE SLICE PREPARATION

Animals were deeply anaesthetized using isoflurane (Baxter Corporation) and were subsequently euthanized via decapitation. The brains of the animals were quickly extracted and submerged into a frozen choline dissection buffer. The buffer consisted of the following: 119.0 mM choline chloride, 2.5 mM KCl, 4.3 mM $MgSO_4$, 1.0 mM $CaCl_2$, 1.0 mM NaH_2PO_4,

1.3 mM sodium ascorbate, 11.0 mM glucose, 26.2 mM NaHCO3, and was perfused with carbogen (95 % O_2/5 % CO_2) for 25 minutes prior to performing the dissection. The brains were sliced coronally at a thickness of 300 µm using a Leica VT1000S vibratome. Acute slices containing the PFC were used for all experiments. Due to the technological limitations of hd-MEA experiments, we were limited to performing a crude identification of the anatomical regions located within our slices. Given that we were unable to determine the exact anatomical localization of the slices, our goal was to understand the impact of radiation on PFC networks more broadly rather than provide localized effects of radiation on specific regions of the PFC.

Once the slices were collected, they were placed in a recovery chamber filled with a standard artificial cerebrospinal fluid (ACSF) consisting of the following: 119.0 mM NaCl, 2.5 mM KCl, 1.3 mM $MgSO_4$, 2.5 mM $CaCl_2$, 1.0 mM NaH_2PO_4, 11.0 mM glucose, and 26.2 mM $NaHCO_3$. The ACSF was continuously perfused using carbogen (95 % O_2/5 % CO_2) and maintained at a temperature of 37˚C. Following slicing, brain slices were left to recover for 1 hour prior to experiments allowing the ACSF to equilibrate to room temperature.

RADIATION

Acute doses of radiation consisting of 20 Gy, 50 Gy, or 100 Gy were administered to a subset of healthy slices using the robotic radiosurgery platform (Cyberknife® G4) at a standard dose rate of 10 Gy/min. The use of non-fractionated doses was selected to serve as a stepping-stone for comparing standard dose rates to ultra-fast delivery methods such as FLASH radiation. These ultra-fast dose rates are several orders of magnitude greater than

those used in conventional RT and have shown promise in maintaining the efficacy of the treatment while reducing radiation-induced injuries (Favaudon et al., 2014; Hughes & Parsons, 2020; Matuszak et al., 2022; Montay-Gruel et al., 2017; Simmons et al., 2019).

While acute PFC brain slices were continuously perfused with carbogen (95 % O_2/5 % CO_2) throughout the experiment, perfusion was temporarily halted while radiation doses were administered (2-10 minutes depending on the dose). The radiation beam was 60 mm in diameter and slices were placed in the center of the beam to ensure a homogeneous dose across the entire brain slice. Control slices were brought over to the same location as the Cyberknife to control for potential mechanical damage during transport. In addition, the carbogen perfusion was temporarily stopped for roughly 2-10 minutes to mimic the experimental conditions. However, no radiation was delivered to these slices. Distinct slices were employed for radiation and controls given that hd-MEAs could not be radiated due to potential damage to the chips. The slices in both conditions were then employed to either record neural activity or were stained with PI to quantify cell death.

EPILEPTIFORM ACTIVITY

We used a pro-epileptiform ACSF (PE-ACSF) containing the following: 120 mM NaCl, 8.5 mM KCl,1.25 mM NaH_2PO_4, 0.25 mM $MgSO_4$, 2 mM $CaCl_2$, 24 mM $NaHCO_3$, 10 mM dextrose, and 0.05 mM to generate interictal-like neural activity (Postnikova et al., 2020). 4-AP is known to act on $GABA_A$ receptors and produce an *in vitro* model of epileptic neural activity (Avoli et al., 2002; Gonzalez-Sulser et al., 2011). In this condition, baseline recordings were taken from the same slices prior to the application of PE-ACSF. Following

baseline recordings, slices were perfused in PE-ACSF for 20 minutes and 10-minute recordings of neural activity were collected. The baseline slices differ slightly from the radiation control slices in that they were not exposed to the same potential mechanical damage caused by transporting the slices to be irradiated.

HD-MEA RECORDINGS

SYSTEM DESCRIPTION

Recordings of network-level neural activity were collected using an active pixel sensor hd-MEA. This hd-MEA used a CMOS-based CCD monolithic chip in which the pixels were modified to detect changes in electric voltages from electrogenic tissues. The array provided simultaneous recordings from 4,096 electrodes with a sampling rate of 18 kHz across the entire array. The hd-MEA chips were comprised of 64x64 electrodes arranged as a pixel element array whereby each pixel measures 21 μm x 21 μm with an electrode pitch of 42 μm. The active area of the array was 7.22 mm^2 and had a pixel density of 567 pixels/mm^2 (Ferrea et al., 2012; Imfeld et al., 2008). Data were acquired using BrainWave software (*3Brain Gmbh, Switzerland*) and imported to MATLAB (MathWorks, Natick) for offline analysis.

MEASURING LARGE-SCALE NEURAL ACTIVITY

A subset of acute PFC slices were placed on the hd-MEA chip, held in place by a harp and bathed in standard ACSF that was continuously perfused with carbogen (95 % O_2/5 % CO_2). Slices were maintained at a temperature of 37˚C throughout the recording period.

Recordings were completed in a dark environment to prevent interference from light artefacts. Five minutes of neural activity was recorded from each slice.

QUANTIFYING CELL DEATH IN IRRADIATED BRAIN SLICES

A different subset of brain slices (4 slices) from each dose condition (20, 50, and 100 Gy) and the control condition were subsequently stained using PI (1 mg/mL, Sigma-Aldrich), a cell death marker that binds to the DNA of neurons with fragmented plasma membranes but remains membrane impermeable in healthy neurons (Kuebler et al., 2015). Following a 15-minute application of PI, serial dilution of the PI-stained ACSF was performed and acute brain slices were imaged using a Zeiss LSM880 confocal microscope. We quantified cell death based on the mean intensity of images taken from PI-stained slices.

DATA PREPARATION

Data collected from all conditions were initially processed using a second-order bandpass Butterworth filter in the forward and reverse directions (300-5,000 Hz) applied to the raw voltages to remove high-frequency noise and slowly changing field potentials (Bullmann et al., 2019). Artefacts were identified as any timepoint where the voltages were greater than 1000 μV. Artefacts were subsequently replaced with the mean of the filtered data. Spike times were then extracted based on their multi-unit activity (MUA) using a voltage-threshold method (Lewicki, 1998) whereby we identified negative signal peaks below a threshold of 5 standard deviations (SD) from the mean of the filtered signal. To determine our final threshold, we first calculated the mean and SD of the filtered control data and then took the difference between the two as our overall threshold. This final

threshold was then applied to voltage data to identify multi-unit spike times, representing the activity of neurons within the vicinity of individual channels on the hd-MEA.

A known limitation associated with MUAs is the possibility of capturing signal redundancies whereby a single channel picks up the activity from multiple neurons or a single neuron's activity is picked up by multiple channels on the array (Hilgen et al., 2017; Prentice et al., 2011; Rossant et al., 2016). Consequently, this method lacks the ground truth necessary to provide single-neuron resolution data. Despite this, broadband signals can be split into slower components (<100 Hz) that represent local field potentials and faster components (300-5000 Hz) that constitute MUA or the sum of activity of the neurons in the vicinity of a single electrode (Bansal et al., 2011; Davis et al., 2022; Legatt et al., 1980; Mitzdorf, 1985; Stark & Abeles, 2007). While inferential methods can be employed to sort the MUA into putative single-cell contributions (Hilgen et al., 2017; Prentice et al., 2011; Rossant et al., 2016), a ground truth comparison is required to provide accurate spike sorting. Even in the absence of direct ground truth validation, studies have shown that MUAs capture key properties of activity in neural circuits and can be used to adequately infer firing rates and correlations amongst neurons (Trautmann et al., 2019).

NEURONAL SPIKE RATES

Spike times were employed to generate rasters that represent the activity of entire networks across time. Rasters were downsampled from 18 kHz to 1 kHz using non-overlapping temporal bins of binary data set to "1" in the presence of one or more spikes, or "0" if no spikes were present. We then computed a peri-stimulus time histogram using a rolling window of 500 ms. Channels without activity were removed from further analyses.

Firing rates were assessed using a Kolmogorov-Smirnov test of normality which revealed non-normal distributions for all conditions ($p < 0.001$). Past research has also established that cortical firing rate distributions follow a log-normal distribution rather than a normal distribution (Buzsáki & Mizuseki, 2014; Song et al., 2005). As such, we opted to compare firing rates (Hz) using a non-parametric Wilcoxon rank sum test, which assumes independence across samples but relaxes the assumption of Gaussian normality (Y. Xia, 2020). Finally, the use of a non-parametric test on global data distributions ensured that we did not overemphasize any minor effects that may have been amplified given the large number of channels (n=4,096) that were simultaneously recorded via the hd-MEA.

FUNCTIONAL CONNECTIVITY

Pearson cross-correlations were computed for each pair of electrodes within the hd-MEA, yielding a 4,096 x 4,096 matrix of interactions. These correlations were subsequently passed through a threshold of r=0.2 to detect the presence or absence of a functional connection between pairs of channels, representing the statistical coincidence of multi-unit spikes at these channels. Data were subsequently assessed for normality using a Kolmogorov-Smirnov test followed by a Wilcoxon rank sum test.

NEURAL COMPLEXITY

Spatiotemporal patterns of activity recorded on the hd-MEA were described by their participation ratio (PR), a measure of neural complexity reflecting the number of factors needed to capture fluctuations in the data (Litwin-Kumar et al., 2017; Mazzucato et al., 2016; Hu and Sompolinsky, 2020; Altan et al., 2021). The PR of population recordings was computed by first extracting 10 brief time segments of data (mean duration: 3,811.5 ms,

SEM: 145.17) across each experimental condition. The PR of each segment was computed by eigenspectrum decomposition (Chapin and Nicolelis, 1999), providing ranked eigenvalues $\lambda_1, \ldots, \lambda_N$ where N denotes the total number of channels on the hd-MEA. Then, the PR was calculated as the first moment of the eigenspectrum normalized by the second moment,

$$\mathrm{PR} = \frac{(\sum_i^N \lambda_i)^2}{\sum_i^N \lambda_i^2}. \quad (1)$$

If patterns of population activity can be described by a limited number of dimensions, only a portion of eigenvalues will be positive, resulting in a low PR. However, patterns of activity with higher complexity would yield a large number of positive eigenvalues and hence a higher PR.

RESULTS

IRRADIATED BRAIN SLICES REVEAL CHANGES IN CORTICAL POPULATION ACTIVITY

Neuronal activity recorded on the hd-MEA was characterized by sharp deflections in voltage at individual channels, indicative of multi-unit spikes amongst clusters of neurons in the vicinity of the electrodes (Figure 13A). These deflections were detected by application of a threshold below the mean of the voltage (see Methods). The rate of neural activity at individual channels was computed as the average number of threshold-crossing events per second and stored as rasters for offline analysis. These rasters revealed an increase in activity among radiated slices compared to controls (Figure 13B). A dose of 20 Gy radiation

yielded a statistically reliable increase in mean firing rate compared to sham radiation (Wilcoxon rank sum test, p = 2.4546e-27), as did 50 Gy (p = 7.2954e-05) and 100 Gy (p = 0.0028935). Examples of individual rasters are shown in Figure 13C, where individual dots identify the times and channels where these events occurred.

A pronounced increase in firing rate was observed following PE treatment (mean rate of 2.25 Hz compared to a baseline firing rate of 0.09 Hz, p = 4.9558e-39). Although the baseline firing rate was quite low (mean rate of 0.09 Hz), past research has shown that slow waves (< 1 Hz) can spontaneously occur in cortical slices that are disconnected from adjacent regions. This has been suggested to be an emergent default pattern of disconnected cortical networks (Compte et al., 2003; Sanchez-Vives & Mattia, 2014; Sanchez-Vives, 2020; Sanchez-Vives et al., 2017; Sanchez-Vives & McCormick, 2000). Further work characterizing epileptiform activity in terms of propagating waves can be found elsewhere (Boucher-Routhier & Thivierge, 2023). These results show that radiation-induced changes in neuronal activity remained markedly lower than epileptiform activity.

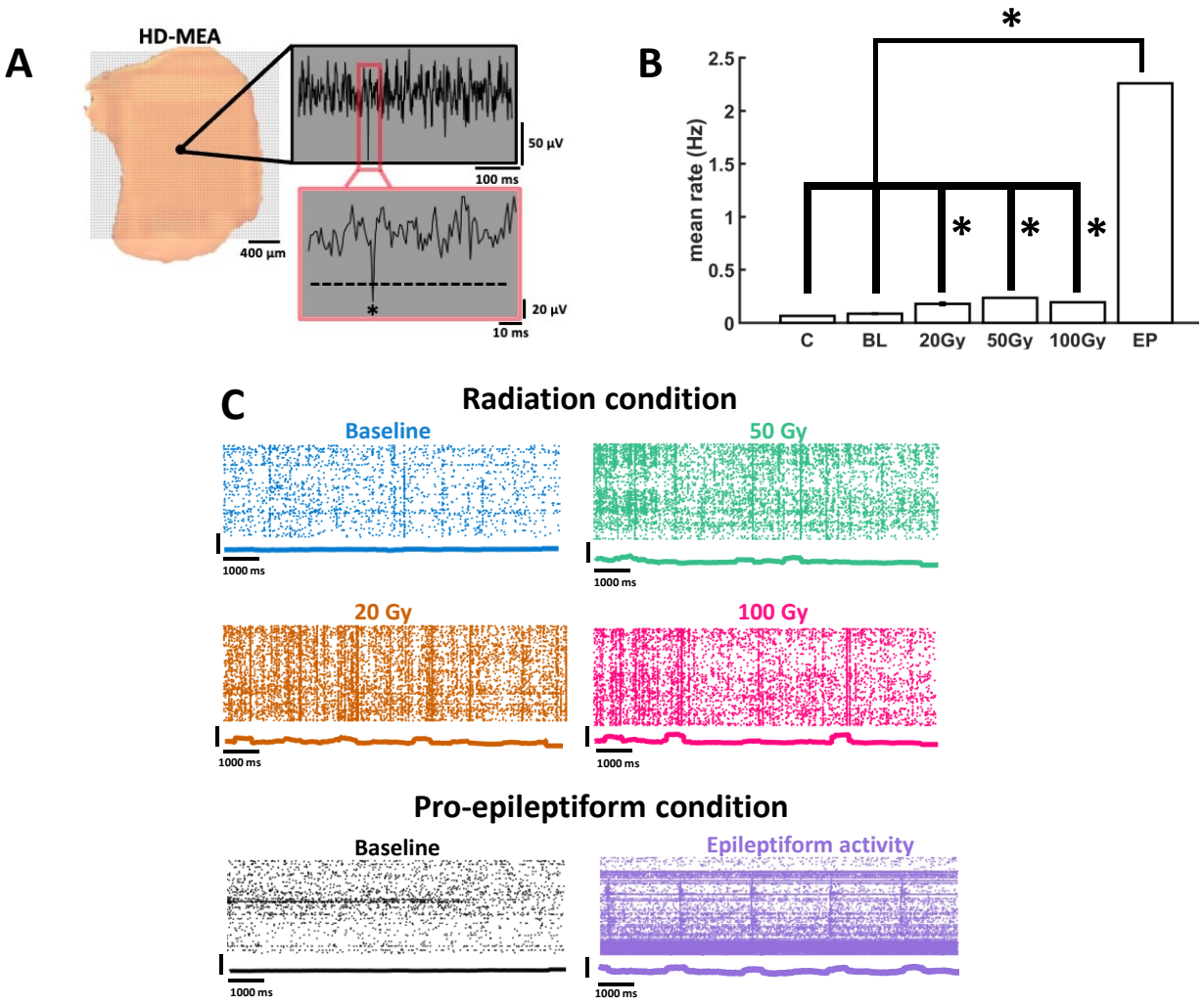

FIGURE 13. NEURONAL ACTIVITY IN POPULATIONS OF PREFRONTAL CORTICAL NEURONS (**A**) *Left*, example of PFC slice placement on the hd-MEA. *Right*, multiunit spike (identified by an asterisk "*") extracted from voltage deflections identified at an individual channel. (**B**) Mean firing rate of prefrontal cortical neurons across various conditions. C=control slices for the radiation treatment; BL=baseline in the PE condition; 20-100 Gy=radiation conditions; EP=epileptiform activity. *indicates statistical significance at $p<0.01$. (**C**) Rasters of activity show spikes across whole populations of neurons following graded doses

of radiation or perfusion of pro-epileptiform solution. Peri-stimulus time histogram underneath each raster shows summated activity using a 500 ms rolling window.

Next, we examined functional connectivity amongst cortical neurons by computing correlations between all pairs of channels on the hd-MEA (Figure 14A, B). To facilitate the interpretation of functional networks, a cut-off of r=0.2 was applied to reject lower correlations amongst pairs of channels. This threshold was selected to ensure connections were observed across all conditions without reaching a saturation point where all connections were present (i.e., the threshold was too low) or all connections were absent (i.e., the threshold was too high).

Connectivity within the brain can be measured via structural (anatomical) links that consist of white matter tracks or functional connections which are represented by statistical dependency between regions (Bringmann et al., 2013; Bullmore & Sporns, 2009; Friston, 2011; Friston et al., 2003; Guye et al., 2008; He & Evans, 2010; Johansen-Berg & Behrens, 2006; Rykhlevskaia et al., 2008; Tournier et al., 2011). Functional connections can be further divided into effective or functional connectivity. Effective connectivity involves the influence that one brain region or node has on another which implies a causal relationship between nodes (Bringmann et al., 2013; Friston, 2011). Functional connectivity, on the other hand, is characterized by the statistical correlation between nodes and does not provide causal relationships between brain regions (Bringmann et al., 2013; Bullmore & Sporns, 2009; Friston, 2011). Functional connectivity is also indicative of the communication amongst

populations of neurons and is known to fluctuate in disease states (Craddock et al., 2009; Konstantinou et al., 2019; Lang et al., 2017; Wang et al., 2007).

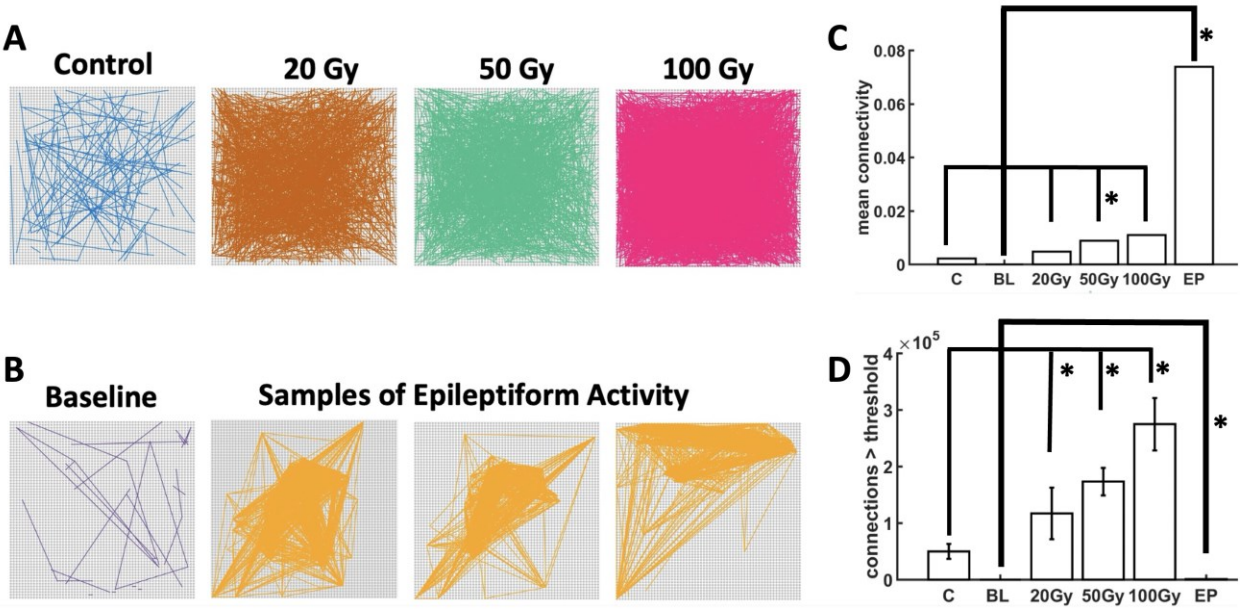

FIGURE 14. FUNCTIONAL CONNECTIVITY OF CORTICAL NETWORKS

(**A**) Irradiated networks, (**B**) Perfusion of a pro-epileptiform (PE) solution, (**C**) Mean strength and **(D**) number of functional connections exceeding a pre-defined threshold.

Two markers of functional connectivity were examined, namely the strength and the number of functional connections across conditions. The strength of functional connectivity following radiation was higher than controls across all doses of radiation delivered to the PFC slices (Figure 14C). Functional connections were significantly stronger than controls for 50 Gy ($p = 0.0014797$) but did not reach statistical significance for 20 Gy ($p = 0.08826$) or 100 Gy ($p = 0.16837$). Despite variability across conditions, the overall impact of radiation was

an increase in the strength of functional connections across PFC networks, indicative of greater synchronization amongst neurons.

In radiated slices, the number of functional connections showed a dose-dependent response, with higher doses yielding more abundant connections than lower doses (Figure 14D). The number of functional connections was higher than controls for 20 Gy ($p = 3.3951e-07$), 50 Gy ($p = 2.2621e-11$) and 100 Gy ($p = 1.9287e-19$). Thus, radiation impacted PFC functional connectivity by increasing the density of connections amongst pairs of channels on the array.

These results were compared to networks that received PE treatment (Figure 14B). The mean strength of functional connectivity was markedly higher in PE compared to radiated slices (20 Gy: $p = 9.543e-14$; 50 Gy: $p = 1.4247e-13$; 100 Gy: $p = 3.3604e-11$), suggesting an increase in synchrony during PE activity. Conversely, the number of functional connections was lower in PE compared to radiated slices (20 Gy: $p = 1.3018e-40$; 50 Gy: $p = 2.6966e-39$; 100 Gy: $p = 3.578e-39$). The lower number of connections obtained under PE treatment is explained by epileptiform activity yielding functional interactions that are focused on a small group of neurons within the broader population recorded on the array (Figure 14B). Indeed, seizure-like events observed under PE are characterized by a spatially-focused propagation of strong and repeatable patterns of activity (Boucher-Routhier & Thivierge, 2023). In sum, radiation induced more abundant functional connections amongst PFC neurons. These results are distinct from epileptiform activity, where strong connections are present but are much sparser due to spatially-focused epileptiform propagation across the array.

Finally, the complexity of population activity was examined in both radiated and PE slices, indicative of the number of factors required to capture the neuronal data (Litwin-Kumar et al., 2017; Mazzucato et al., 2016; Hu and Sompolinsky, 2020; Altan et al., 2021). The complexity of radiated slices was higher than controls across all doses of radiation delivered to PFC (Figure 15A). Complexity was significantly higher than controls for 20 Gy ($p = 1.0116e-15$), 50 Gy ($p = 3.316e-20$), and 100 Gy ($p = 1.0041e-17$). Thus, radiation reliably increased the complexity of neural data recorded on the hd-MEA.

This result was compared to the effect of PE treatment. Relative to baseline activity, slices treated with PE yielded a marked increase in complexity ($p = 4.6426e-38$) (Figure 15B). The magnitude of this effect largely exceeded the complexity of radiated slices, suggesting that while radiation increased the complexity of neural activity, this effect was limited compared to the high complexity obtained from epileptiform activity, thus showing that population activity following radiation is distinct from a regime of PE-induced seizures. Eigenvalue distributions across experimental conditions further supported this point. In controls and radiated slices, a limited number of eigenvalues yielded positive values; by comparison, PE activity was characterized by a broad distribution of eigenvalues spanning at least two orders of magnitude (Figure 15C).

Together, these results show clear distinctions between epileptiform and radiation-induced changes in neuronal activity across populations of cortical cells. While both forms of activity were characterized by an increase in firing rates, radiated slices exhibited markedly weaker neuronal communication and lower complexity than PE-treated slices.

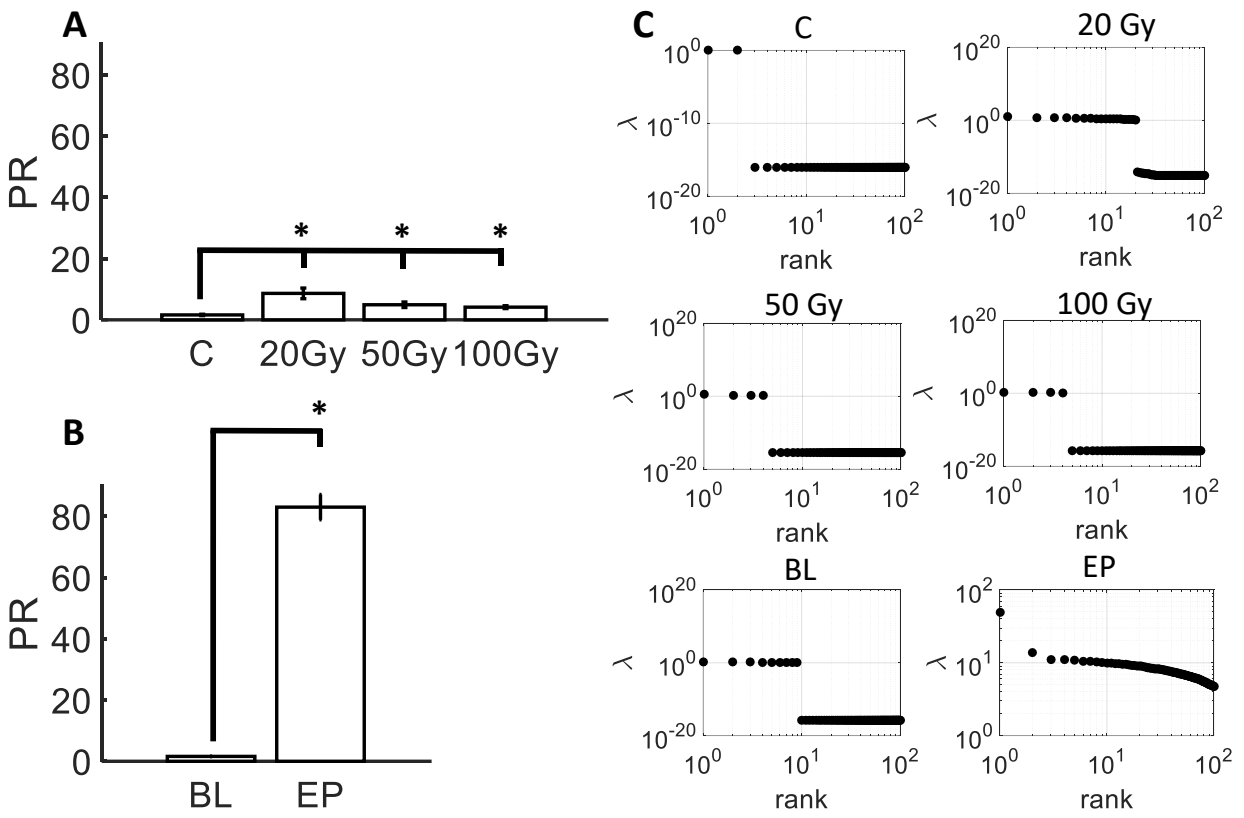

FIGURE 15. NEURONAL COMPLEXITY OF CORTICAL NETWORKS.

(**A**) Participation ratio (PR) in radiated slices, (**B**) PR in slices treated with PE solution, (**C**) Distribution of eigenvalues across experimental conditions.

QUANTIFYING CELL DEATH FOLLOWING RADIATION

A subset of slices was stained with PI following radiation or sham radiation (control) conditions (Figure 16A). The mean pixel intensity across radiation conditions revealed a trend whereby higher doses resulted in a higher level of cell death (Figure 16B). In this way, 20 Gy yielded higher intensity than controls ($p = 1.8954e-10$), 50 Gy was above 20 Gy ($p = 4.1943e-12$), and 100 Gy above 50 Gy ($p = 2.426e-12$). Thus, cell death was directly linked to the radiation dose delivered to PFC neurons. At higher doses, particularly 100 Gy, we observed a clustered spatial arrangement of pixels with higher intensity, suggesting an area

where neuronal damage was more pronounced (Figure 16A, arrow). Interestingly, this area is in the vicinity of the secondary motor area (M2), a region known to yield increased cell death following radiation (Hnilicová et al., 2022; Ueno et al., 2019). Limitations of the hd-MEAs, however, did not allow us to record activity from slices after imaging, hence it remains an open question whether these areas displayed aberrant neuronal activity.

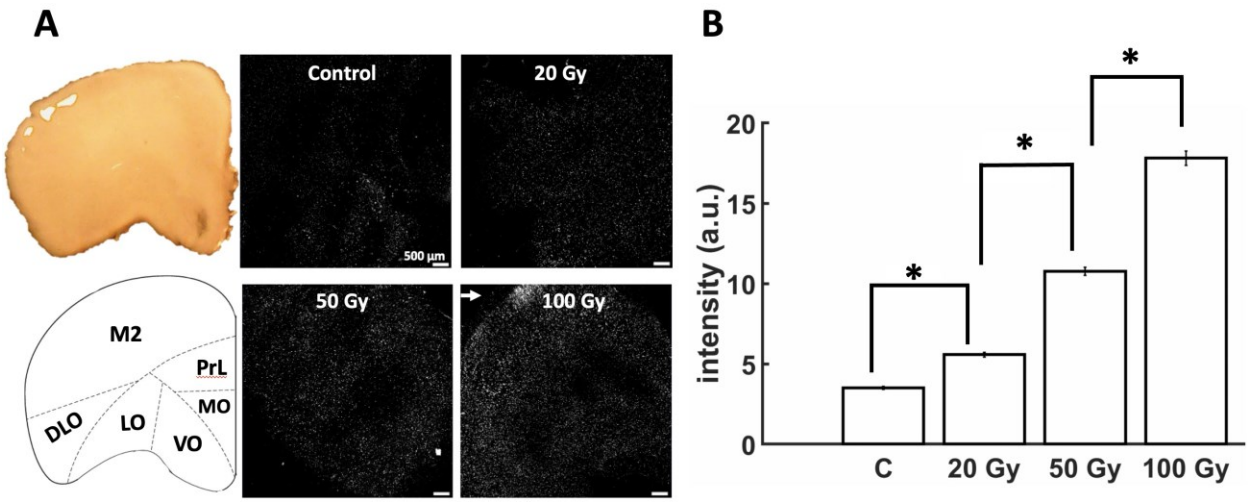

FIGURE 16. PROPIDIUM IODIDE (PI) STAINING OF PREFRONTAL SLICES FOLLOWING RADIATION

(**A**) Representative samples showing a graded increase in PI intensity with radiation dose. Arrow shows clustering of PI intensity at 100 Gy. Left panel shows approximate location of secondary motor cortex (M2), Prelimbic cortex (PrL), medial orbital cortex (MO), ventral orbital cortex (VO), lateral orbital cortex (LO), and dorsolateral orbital cortex (DLO), (**B**) Mean PI intensity ("a.u.": arbitrary units).

DISCUSSION

This study aimed to investigate the neuromodulatory effects of radiation on the firing rate, functional connectivity, complexity, and survival of *in vitro* PFC cells, and to compare

the results with those obtained during epileptiform activity (Postnikova et al., 2020). We found a marked increase in neuronal activity following acute doses of radiation (Zhang et al., 2020), accompanied by an increase in complexity, as well as in the density and in some cases the strength of functional connectivity. Finally, radiation induced a dose-dependent cell death where damage was selectively localized to areas surrounding M2, a region particularly vulnerable to radiation damage (Hnilicová et al., 2022; Ueno et al., 2019). These results were distinct from epileptiform activity, where complexity was markedly higher, and functional connections were strong but exhibited a lower density than radiated slices due to the restricted spatial focus of epileptic seizures. Differences between radiated slices and epileptiform activity highlight clear distinctions between the effects obtained in these two conditions: while neuronal activity and complexity were elevated in both radiated and PE slices, functional connections were more widely spread in radiation than under PE treatment. This work proposes a novel assay to test the impact of clinically relevant doses of radiation (Redmond et al., 2021; Tuleasca et al., 2021) on neural dynamics and cellular apoptosis.

Past research has established that firing rate and cross-correlations can increase together (de la Rocha et al., 2007) making it difficult to separate the two. However, it is worth noting that these two markers do not always increase together. For instance, during epileptiform activity, firing rates and the mean strength correlations are elevated compared to radiated slices, yet the density of functional connections was markedly lower. This is explained by the fact that waves of epileptiform activity occupied a spatially delimited region of the array (Figure 14B) (Boucher-Routhier and Thivierge, 2023). In cortical networks,

correlations are modulated by a balance of excitatory and inhibitory synaptic transmission, making them an intricate marker of activity across broad populations of neurons (Mazzoni et al., 2007).

The effects of radiation on neural dynamics within PFC networks remain to be fully elucidated, with past literature showing increased firing rates (Zhang et al., 2020), changes in synaptic morphology (Kempf et al., 2015; Zhang et al., 2020), inhibited synaptic function and disruptions in synaptic plasticity (Wu et al., 2012; Zhang et al., 2018). To date, however, scant attention has been devoted to intra- or inter-areal functional connectivity. Further, much of the literature has focused on the effect of radiation on the hippocampus, leaving a growing need to study the PFC due to its involvement in the hippocampal-PFC pathway. This pathway is believed to play a key role in the cognitive deficits/impairments experienced following radiation (Chen et al., 2017; Hnilicová et al., 2022; Kovalchuk and Kolb, 2017; Zhang et al., 2020). Moreover, the PFC has been identified as one of the areas that are most sensitive to radiation (Hnilicová et al., 2022; Kornev et al., 2005; Kovalchuk and Kolb, 2017).

Given established links between functional connectivity and cognitive outcomes (Hawellek et al., 2011; Konstantinou et al., 2019; Lang et al., 2017), examining the effects of radiation on functional connectivity in reduced hd-MEA preparations is of critical importance to understanding the neurophysiological mechanisms of radiation-induced damage and their impact in clinical settings. It is worth noting that the scale of the functional connectivity measured with hd-MEA preparations is significantly smaller than large-scale neural population level recordings that are used to access functional connectivity in human patients. For large-scale neural population level recordings, a single voxel is typically several

cubic millimetres in size and the network structure is comprised of sets of fiber bundles linking neuronal populations between regions and long-range intra-regional horizontal fibres (Honey et al., 2010). Hd-MEAs such as the one employed in this study have an active area of 7.22 mm^2 (Ferrea et al., 2012; Imfeld et al., 2008), which is smaller than a single voxel and the network structure is comprised of inter-neuronal connections (Honey et al., 2010)

Despite this, our findings of a dose-dependent disruption in functional connectivity are aligned with human imaging studies showing altered functional connectivity among regions that receive radiation (Chen et al., 2017; Kovács et al., 2015; Ma et al., 2016; Mitchell et al., 2020). In turn, higher doses of radiation are associated with worse long-term cognitive prognoses (Brière et al., 2008). Understanding the cellular origins of functional connectivity in healthy and radiated brain circuits provides a fruitful avenue to develop interventions that limit radiation-induced cognitive damage.

Because the current study focused on the acute effects of radiation, the timescale of alterations in activity and functional connectivity following radiation remains limited. *In vitro* acute brain slices under standard experimental conditions have a typical lifespan of 6-12 hours (Buskila et al., 2014). As a result, this study was limited to a window of only a few hours post-radiation and could not examine early delayed or late delayed radiation-induced injuries (Greene-Schloesser et al., 2012; Zhang et al., 2018). Despite this limitation, it is reasonable to assume that a majority of the injuries induced by radiosurgery are acute in nature given that extremely high doses are delivered within a brief time period. These findings are also consistent with previous investigations of the acute effects of radiation on PFC neurons (Zhang et al., 2020). Further research on early and late delayed radiation-

induced injuries suggests differential effects based on the timescale following radiation whereby an initial increase in firing rate is eventually followed by a decrease in activity (Zaer et al., 2022; Zhang et al., 2020). Similar results have been reported in human nasopharyngeal carcinoma patients (Ding et al., 2018), showing an acute increase in local activity which was associated with a decrease in functional connections and higher levels of necrosis in the late-delayed stage.

It is also worth noting that there are some key differences between acute brain slices that are irradiated *in vitro* and *in vivo* irradiation of the brain within a live rodent. For example, radiation delivered directly to a brain slice does not have to pass through the skull, membranes such as the meninx, dura mater, arachnoid membrane, pia mater, or cerebrospinal fluid before reaching the target location (Cefaro et al., 2013). The networks within the slices are more isolated as the connections to adjacent regions are severed during the slicing process, which may impact the effect radiation has on these networks when compared to *in vivo* networks. On the other hand, *in vitro* preparations allowed us to control the exact dose that was delivered to the PFC without the influence of adjacent tissue.

Further work will be needed to investigate the intracellular mechanisms involved in radiation-induced alterations in neuronal activity, functional connectivity, and cellular apoptosis, as hd-MEAs are restricted to tracking extracellular voltage deflections in the vicinity of cells. For example, ionic channel kinetics or patch clamp experiments may prove fruitful in determining why PFC neurons become hyperexcitable as these mechanisms are not accessible via hd-MEA recordings. Past research has shown acute downregulation in excitatory NR2A subunits of the N-methyl-D-aspartate receptors (NMDAR) and increases in

inhibitory gamma-aminobutyric acid receptors ($GABA_ARs$), leading to changes in synaptic function and inhibiting long-term potentiation (Wu et al., 2012). It is unclear how these phenomena are linked to broader effects on neuronal networks such as alterations in the density and strength of functional connections. Simultaneous intra/extracellular recordings, though technically difficult, may offer insights in this regard (Dipalo et al., 2017; Hamilton et al., 2018).

Given that hd-MEAs revealed markers of radiation-induced damage in neuronal activity and network interactions, it would be beneficial to examine the potential impact of pharmacological preconditioning in preventing these alterations. Past research has shown that pre-treating brain slices with memantine, an NMDAR antagonist (Wu et al., 2012) or administering oral doses of epigallocatechin-3-gallate (EGCG), the main polyphenolic compound in green tea (El-Missiry et al., 2018), and Quercetin, a flavonoid that is found in several vegetables and fruits (Kale et al., 2018), can provide neuroprotective effects against radiation damage.

One limitation of hd-MEA recordings is that it is not logistically possible to deliver fractionated doses of radiation that are used in typical radiation therapy protocols. Although implantable *in vivo* arrays are available, there are significant concerns regarding the radiosensitivity of the hd-MEA platform. In addition, the use of anaesthetics during *in vivo* protocols is known to influence brain activity and alter neuronal functioning (Huang et al., 2014; Sorrenti et al., 2021), which may impact recordings. As such, we opted for large single doses of radiation such as those used for stereotactic radiosurgery, pulsed high-dose-rate brachytherapy and certain hypofractionated palliative treatment protocols (Redmond et al.,

2021; Tuleasca et al., 2021; Yuan et al., 2006). These doses also provided a benchmark to compare the effects of standard dose rates (5-10 Gy/min) to ultrafast dose rates (>40 Gy/s) on various markers of neural activity and cell death.

Alternate dose ranges such as those below 20 Gy or above 100 Gy could be employed in future studies to determine whether the same neural dynamics and dose-dependent cellular apoptosis would be observed. Notably, doses above 60 Gy have been shown to produce radiation-induced necrosis (radionecrosis) and lesions in animal models (Zaer et al., 2022, 2020); however, clinical studies have revealed radionecrosis in normal tissues exposed to doses as low as 12 Gy (Blonigen et al., 2010; Korytko et al., 2006; Reynolds et al., 2020). Similar to these findings, our results revealed that cell death occurred in a dose-dependent manner beginning at doses as low as 20 Gy. Finally, future studies should examine different regions of the brain using the methods employed in this study to determine whether there are area-specific impacts of these doses.

Conclusions

In conclusion, hd-MEAs revealed radiation-induced changes in broad networks of the PFC that were characterized by increased firing rates, higher complexity, disrupted functional connectivity, and dose-dependent apoptosis. These markers were distinct from those observed in hd-MEA recordings of epileptiform activity, thus showing that radiation does not merely induce an epileptic state. These results point to hd-MEAs as a novel and promising tool for studying the interactions of clinically relevant doses of radiation and potential targets for radioprotection.

References

Altan, E., Solla, S. A., Miller, L. E., & Perreault, E. J. (2021). Estimating the dimensionality of the manifold underlying multi-electrode neural recordings. *PLoS Computational Biology*, *17*(11), e1008591. https://doi.org/10.1371/journal.pcbi.1008591

Avoli, M., D'Antuono, M., Louvel, J., Köhling, R., Biagini, G., Pumain, R., D'Arcangelo, G., & Tancredi, V. (2002). Network and pharmacological mechanisms leading to epileptiform synchronization in the limbic system in vitro. *Progress in Neurobiology*, *68*(3), 167–207. https://doi.org/10.1016/S0301-0082(02)00077-1

Bansal, A. K., Vargas-Irwin, C. E., Truccolo, W., & Donoghue, J. P. (2011). Relationships among low-frequency local field potentials, spiking activity, and three-dimensional reach and grasp kinematics in primary motor and ventral premotor cortices. *Journal of Neurophysiology*, *105*(4), 1603–1619. https://doi.org/10.1152/jn.00532.2010

Blonigen, B. J., Steinmetz, R. D., Levin, L., Lamba, M. A., Warnick, R. E., & Breneman, J. C. (2010). Irradiated Volume as a Predictor of Brain Radionecrosis After Linear Accelerator Stereotactic Radiosurgery. *International Journal of Radiation Oncology*Biology*Physics*, *77*(4), 996–1001. https://doi.org/10.1016/j.ijrobp.2009.06.006

Boucher-Routhier, M., & Thivierge, J.-P. (2023). A deep generative adversarial network capturing complex spiral waves in disinhibited circuits of the cerebral cortex. *BMC Neuroscience*, *24*(1), 22. https://doi.org/10.1186/s12868-023-00792-6

Brière, M.-E., Scott, J. G., McNall-Knapp, R. Y., & Adams, R. L. (2008). Cognitive outcome in pediatric brain tumor survivors: Delayed attention deficit at long-term follow-up. *Pediatric Blood & Cancer*, *50*(2), 337–340. https://doi.org/10.1002/pbc.21223

Bringmann, L. F., Scholte, H. S., & Waldorp, L. J. (2013). Matching Structural, Effective, and Functional Connectivity: A Comparison Between Structural Equation Modeling and Ancestral Graphs. *Brain Connectivity*, *3*(4), 375–385. https://doi.org/10.1089/brain.2012.0130

Bullmann, T., Radivojevic, M., Huber, S. T., Deligkaris, K., Hierlemann, A., & Frey, U. (2019). Large-Scale Mapping of Axonal Arbors Using High-Density Microelectrode Arrays. *Frontiers in Cellular Neuroscience*, *13*. https://www.frontiersin.org/articles/10.3389/fncel.2019.00404

Bullmore, E., & Sporns, O. (2009). Complex brain networks: Graph theoretical analysis of structural and functional systems. *Nature Reviews Neuroscience*, *10*(3), 186–198. https://doi.org/10.1038/nrn2575

Buskila, Y., Breen, P. P., Tapson, J., van Schaik, A., Barton, M., & Morley, J. W. (2014). Extending the viability of acute brain slices. *Scientific Reports*, *4*(1), Article 1. https://doi.org/10.1038/srep05309

Buzsáki, G., & Mizuseki, K. (2014). The log-dynamic brain: How skewed distributions affect network operations. *Nature Reviews Neuroscience*, *15*(4), 264–278. https://doi.org/10.1038/nrn3687

Carlén, M. (2017). What constitutes the prefrontal cortex? *Science*, *358*(6362), 478–482. https://doi.org/10.1126/science.aan8868

Cefaro, G. A., Genovesi, D., & Perez, C., A. (2013). Delineating Organs at Risk in Radiation Therapy. In *Delineating organs at risk in radiation therapy*. Springer.

Chapin, J. K., & Nicolelis, M. A. (1999). Principal component analysis of neuronal ensemble activity reveals multidimensional somatosensory representations. *Journal of Neuroscience Methods*, *94*(1), 121–140. https://doi.org/10.1016/s0165-0270(99)00130-2

Chen, S. C.-J., Abe, Y., Fang, P.-T., Hsieh, Y.-J., Yang, Y.-I., Lu, T.-Y., Oda, S., Mitani, H., Lian, S.-L., Tyan, Y.-C., Huang, C.-J., & Hisatsune, T. (2017). Prognosis of Hippocampal Function after Sub-lethal Irradiation Brain Injury in Patients with Nasopharyngeal Carcinoma. *Scientific Reports*, *7*(1). https://doi.org/10.1038/s41598-017-13972-2

Compte, A., Sanchez-Vives, M. V., McCormick, D. A., & Wang, X.-J. (2003). Cellular and Network Mechanisms of Slow Oscillatory Activity (<1 Hz) and Wave Propagations in a Cortical Network Model. *Journal of Neurophysiology*, *89*(5), 2707–2725. https://doi.org/10.1152/jn.00845.2002

Craddock, R. C., Holtzheimer III, P. E., Hu, X. P., & Mayberg, H. S. (2009). Disease state prediction from resting state functional connectivity. *Magnetic Resonance in Medicine*, *62*(6), 1619–1628. https://doi.org/10.1002/mrm.22159

Davis, Z. W., Muller, L., & Reynolds, J. H. (2022). Spontaneous Spiking Is Governed by Broadband Fluctuations. *Journal of Neuroscience*, *42*(26), 5159–5172. https://doi.org/10.1523/JNEUROSCI.1899-21.2022

de la Rocha, J., Doiron, B., Shea-Brown, E., Josić, K., & Reyes, A. (2007). Correlation between neural spike trains increases with firing rate. *Nature*, *448*(7155), 802–806. https://doi.org/10.1038/nature06028

Ding, Z., Zhang, H., Lv, X.-F., Xie, F., Liu, L., Qiu, S., Li, L., & Shen, D. (2018). Radiation-induced brain structural and functional abnormalities in presymptomatic phase and outcome prediction. *Human Brain Mapping*, *39*(1), 407–427. https://doi.org/10.1002/hbm.23852

Dipalo, M., Amin, H., Lovato, L., Moia, F., Caprettini, V., Messina, G. C., Tantussi, F., Berdondini, L., & De Angelis, F. (2017). Intracellular and Extracellular Recording of Spontaneous Action Potentials in Mammalian Neurons and Cardiac Cells with 3D Plasmonic Nanoelectrodes. *Nano Letters*, *17*(6), 3932–3939. https://doi.org/10.1021/acs.nanolett.7b01523

El-Missiry, M. A., Othman, A. I., El-Sawy, M. R., & Lebede, M. F. (2018). Neuroprotective effect of epigallocatechin-3-gallate (EGCG) on radiation-induced damage and apoptosis in the rat hippocampus. *International Journal of Radiation Biology*, *94*(9), 798–808. https://doi.org/10.1080/09553002.2018.1492755

Favaudon, V., Caplier, L., Monceau, V., Pouzoulet, F., Sayarath, M., Fouillade, C., Poupon, M.-F., Brito, I., Hupé, P., Bourhis, J., Hall, J., Fontaine, J.-J., & Vozenin, M.-C. (2014). Ultrahigh dose-rate FLASH irradiation increases the differential response between normal and tumor tissue in mice. *Science Translational Medicine*, *6*(245), 245ra93-245ra93. https://doi.org/10.1126/scitranslmed.3008973

Ferrea, E., Maccione, A., Medrihan, L., Nieus, T., Ghezzi, D., Baldelli, P., Benfenati, F., & Berdondini, L. (2012). Large-scale, high-resolution electrophysiological imaging of field potentials in brain slices with microelectronic multielectrode arrays. *Frontiers in Neural Circuits*, *6*. https://www.frontiersin.org/articles/10.3389/fncir.2012.00080

Friston, K. J. (2011). Functional and Effective Connectivity: A Review. *Brain Connectivity*, *1*(1), 13–36. https://doi.org/10.1089/brain.2011.0008

Friston, K. J., Harrison, L., & Penny, W. (2003). Dynamic causal modelling. *NeuroImage*, *19*(4), 1273–1302. https://doi.org/10.1016/S1053-8119(03)00202-7

Gonzalez-Sulser, A., Wang, J., Motamedi, G. K., Avoli, M., Vicini, S., & Dzakpasu, R. (2011). THE 4-AMINOPYRIDINE IN VITRO EPILEPSY MODEL ANALYZED WITH A PERFORATED MULTI-ELECTRODE ARRAY. *Neuropharmacology*, *60*(7–8), 1142–1153. https://doi.org/10.1016/j.neuropharm.2010.10.007

Gould, J. (2018). Breaking down the epidemiology of brain cancer. *Nature*, *561*(7724), S40–S41. https://doi.org/10.1038/d41586-018-06704-7

Greene-Schloesser, D., Robbins, M., Peiffer, A., Shaw, E., Chan, M., & Wheeler, K. (2012). Radiation-induced brain injury: A review. *Frontiers in Oncology*, *2*. https://www.frontiersin.org/articles/10.3389/fonc.2012.00073

Guye, M., Bartolomei, F., & Ranjeva, J.-P. (2008). Imaging structural and functional connectivity: Towards a unified definition of human brain organization?: *Current Opinion in Neurology*, *24*(4), 393–403. https://doi.org/10.1097/WCO.0b013e3283065cfb

Hamilton, F., Berry, T., & Sauer, T. (2018). Tracking intracellular dynamics through extracellular measurements. *PLOS ONE*, *13*(10), e0205031. https://doi.org/10.1371/journal.pone.0205031

Hawellek, D. J., Hipp, J. F., Lewis, C. M., Corbetta, M., & Engel, A. K. (2011). Increased functional connectivity indicates the severity of cognitive impairment in multiple sclerosis. *Proceedings of the National Academy of Sciences*, *108*(47), 19066–19071. https://doi.org/10.1073/pnas.1110024108

He, Y., & Evans, A. (2010). Graph theoretical modeling of brain connectivity. *Current Opinion in Neurology*, *23*(4), 341–350. https://doi.org/10.1097/WCO.0b013e32833aa567

Hilgen, G., Sorbaro, M., Pirmoradian, S., Muthmann, J.-O., Kepiro, I. E., Ullo, S., Ramirez, C. J., Encinas, A. P., Maccione, A., Berdondini, L., Murino, V., Sona, D., Zanacchi, F. C., Sernagor, E., & Hennig, M. H. (2017). Unsupervised Spike Sorting for Large-Scale, High-Density Multielectrode Arrays. *Cell Reports*, *18*(10), 2521–2532. https://doi.org/10.1016/j.celrep.2017.02.038

Hnilicová, P., Bálentová, S., Kalenská, D., Muríň, P., Hajtmanová, E., & Lehotský, J. (2022). Anatomic and metabolic alterations in the rodent frontal cortex caused by clinically relevant fractionated whole-brain irradiation. *Neurochemistry International*, *154*, 105293. https://doi.org/10.1016/j.neuint.2022.105293

Honey, C. J., Thivierge, J.-P., & Sporns, O. (2010). Can structure predict function in the human brain? *NeuroImage*, *52*(3), 766–776. https://doi.org/10.1016/j.neuroimage.2010.01.071

Hu, Y., & Sompolinsky, H. (2020). The spectrum of covariance matrices of randomly connected recurrent neuronal networks. *bioRxiv*.

Huang, S., & Uusisaari, M. Y. (2013). Physiological temperature during brain slicing enhances the quality of acute slice preparations. *Frontiers in Cellular Neuroscience*, *7*. https://doi.org/10.3389/fncel.2013.00048

Huang, Z., Wang, Z., Zhang, J., Dai, R., Wu, J., Li, Y., Liang, W., Mao, Y., Yang, Z., Holland, G., Zhang, J., & Northoff, G. (2014). Altered temporal variance and neural synchronization of spontaneous brain activity in anesthesia. *Human Brain Mapping*, *35*(11), 5368–5378. https://doi.org/10.1002/hbm.22556

Hughes, J. R., & Parsons, J. L. (2020). FLASH Radiotherapy: Current Knowledge and Future Insights Using Proton-Beam Therapy. *International Journal of Molecular Sciences*, *21*(18), Article 18. https://doi.org/10.3390/ijms21186492

Imfeld, K., Neukom, S., Maccione, A., Bornat, Y., Martinoia, S., Farine, P.-A., Koudelka-Hep, M., & Berdondini, L. (2008). Large-Scale, High-Resolution Data Acquisition System for Extracellular Recording of Electrophysiological Activity. *IEEE Transactions on Biomedical Engineering*, *55*(8), 2064–2073. IEEE Transactions on Biomedical Engineering. https://doi.org/10.1109/TBME.2008.919139

Johansen-Berg, H., & Behrens, T. E. (2006). Just pretty pictures? What diffusion tractography can add in clinical neuroscience. *Current Opinion in Neurology*, *19*(4), 379–385. https://doi.org/10.1097/01.wco.0000236618.82086.01

Kale, A., Pişkin, Ö., Baş, Y., Aydın, B. G., Can, M., Elmas, Ö., & Büyükuysal, Ç. (2018). Neuroprotective effects of Quercetin on radiation-induced brain injury in rats. *Journal of Radiation Research*, *59*(4), 404–410. https://doi.org/10.1093/jrr/rry032

Kempf, S. J., Sepe, S., von Toerne, C., Janik, D., Neff, F., Hauck, S. M., Atkinson, M. J., Mastroberardino, P. G., & Tapio, S. (2015). Neonatal Irradiation Leads to Persistent Proteome Alterations Involved in Synaptic Plasticity in the Mouse Hippocampus and Cortex. *Journal of Proteome Research*, *14*(11), 4674–4686. https://doi.org/10.1021/acs.jproteome.5b00564

Konstantinou, N., Pettemeridou, E., Stamatakis, E. A., Seimenis, I., & Constantinidou, F. (2019). Altered Resting Functional Connectivity Is Related to Cognitive Outcome in Males With Moderate-Severe Traumatic Brain Injury. *Frontiers in Neurology*, *9*. https://www.frontiersin.org/articles/10.3389/fneur.2018.01163

Kornev, M. A., Kulikova, E. A., & Kul'bakh, O. S. (2005). The Cellular Composition of the Cerebral Cortex of Rat Fetuses after Fractionated Low-Dose Irradiation. *Neuroscience and Behavioral Physiology*, *35*(6), 635–638. https://doi.org/10.1007/s11055-005-0104-3

Korytko, T., Radivoyevitch, T., Colussi, V., Wessels, B. W., Pillai, K., Maciunas, R. J., & Einstein, D. B. (2006). 12 Gy gamma knife radiosurgical volume is a predictor for radiation necrosis in non-AVM intracranial tumors. *International Journal of Radiation Oncology*Biology*Physics*, *64*(2), 419–424. https://doi.org/10.1016/j.ijrobp.2005.07.980

Kovács, Á., Emri, M., Opposits, G., Pisák, T., Vandulek, C., Glavák, C., Szalai, Z., Biró, G., Bajzik, G., & Repa, I. (2015). Changes in functional MRI signals after 3D based radiotherapy of glioblastoma multiforme. *Journal of Neuro-Oncology*, *125*(1), 157–166. https://doi.org/10.1007/s11060-015-1882-2

Kovalchuk, A., & Kolb, B. (2017). Low dose radiation effects on the brain – from mechanisms and behavioral outcomes to mitigation strategies. *Cell Cycle*, *16*(13), 1266–1270. https://doi.org/10.1080/15384101.2017.1320003

Kuebler, E. S., Tauskela, J. S., Aylsworth, A., Zhao, X., & Thivierge, J.-P. (2015). Burst predicting neurons survive an in vitro glutamate injury model of cerebral ischemia. *Scientific Reports*, *5*(1), Article 1. https://doi.org/10.1038/srep17718

Lang, S., Gaxiola-Valdez, I., Opoku-Darko, M., Partlo, L. A., Goodyear, B. G., Kelly, J. J. P., & Federico, P. (2017). Functional Connectivity in Frontoparietal Network: Indicator of Preoperative Cognitive Function and Cognitive Outcome Following Surgery in Patients with Glioma. *World Neurosurgery*, *105*, 913-922.e2. https://doi.org/10.1016/j.wneu.2017.05.149

Legatt, A. D., Arezzo, J., & Vaughan, H. G. (1980). Averaged multiple unit activity as an estimate of phasic changes in local neuronal activity: Effects of volume-conducted potentials. *Journal of Neuroscience Methods*, *2*(2), 203–217. https://doi.org/10.1016/0165-0270(80)90061-8

Lewicki, M. S. (1998). *A review of methods for spike sorting: The detection and classification of neural action potentials*. *9*(4), R53-77.

Lipton, P., Aitken, P. G., Dudek, F. E., Eskessen, K., Espanol, M. T., Ferchmin, P. A., Kelly, J. B., Kreisman, N. R., Landfield, P. W., Larkman, P. M., Leybaert, L., Newman, G. C., Panizzon, K. L., Payne, R. S., Phillips, P., Raley-Susman, K. M., Rice, M. E., Santamaria, R., Sarvey, J. M., … Wallis, R. (1995). Making the best of brain slices: Comparing preparative methods. *Journal of Neuroscience Methods*, *59*(1), 151–156. https://doi.org/10.1016/0165-0270(94)00205-U

Litwin-Kumar, A., Harris, K. D., Axel, R., Sompolinsky, H., & Abbott, L. F. (2017). Optimal Degrees of Synaptic Connectivity. *Neuron*, *93*(5), 1153-1164.e7. https://doi.org/10.1016/j.neuron.2017.01.030

Ma, Q., Wu, D., Zeng, L.-L., Shen, H., Hu, D., & Qiu, S. (2016). Radiation-induced functional connectivity alterations in nasopharyngeal carcinoma patients with radiotherapy. *Medicine*, *95*(29), e4275. https://doi.org/10.1097/MD.0000000000004275

Matuszak, N., Suchorska, W. M., Milecki, P., Kruszyna-Mochalska, M., Misiarz, A., Pracz, J., & Malicki, J. (2022). FLASH radiotherapy: An emerging approach in radiation therapy. *Reports of Practical Oncology and Radiotherapy*, *27*(2), Article 2. https://doi.org/10.5603/RPOR.a2022.0038

Mazzoni, A., Broccard, F. D., Garcia-Perez, E., Bonifazi, P., Ruaro, M. E., & Torre, V. (2007). On the Dynamics of the Spontaneous Activity in Neuronal Networks. *PLOS ONE*, *2*(5), e439. https://doi.org/10.1371/journal.pone.0000439

Mazzucato, L., Fontanini, A., & La Camera, G. (2016). Stimuli Reduce the Dimensionality of Cortical Activity. *Frontiers in Systems Neuroscience*, *10*, 11. https://doi.org/10.3389/fnsys.2016.00011

Miller, E. K., & Cohen, J. D. (2001). An Integrative Theory of Prefrontal Cortex Function. *Annual Review of Neuroscience*, *24*(1), 167–202. https://doi.org/10.1146/annurev.neuro.24.1.167

Mitchell, T. J., Seitzman, B. A., Ballard, N., Petersen, S. E., Shimony, J. S., & Leuthardt, E. C. (2020). Human Brain Functional Network Organization Is Disrupted After Whole-Brain Radiation Therapy. *Brain Connectivity*, *10*(1), 29–38. https://doi.org/10.1089/brain.2019.0713

Mitzdorf, U. (1985). Current source-density method and application in cat cerebral cortex: Investigation of evoked potentials and EEG phenomena. *Physiological Reviews*, *65*(1), 37–100. https://doi.org/10.1152/physrev.1985.65.1.37

Montay-Gruel, P., Petersson, K., Jaccard, M., Boivin, G., Germond, J.-F., Petit, B., Doenlen, R., Favaudon, V., Bochud, F., Bailat, C., Bourhis, J., & Vozenin, M.-C. (2017). Irradiation in a flash: Unique sparing of memory in mice after whole brain irradiation with dose rates above 100Gy/s. *Radiotherapy and Oncology*, *124*(3), 365–369. https://doi.org/10.1016/j.radonc.2017.05.003

Mulhern, R. K., Merchant, T. E., Gajjar, A., Reddick, W. E., & Kun, L. E. (2004). Late neurocognitive sequelae in survivors of brain tumours in childhood. *The Lancet Oncology*, *5*(7), 399–408. https://doi.org/10.1016/S1470-2045(04)01507-4

Postnikova, T. Y., Amakhin, D. V., Trofimova, A. M., & Zaitsev, A. V. (2020). Calcium-permeable AMPA receptors are essential to the synaptic plasticity induced by epileptiform activity in rat hippocampal slices. *Biochemical and Biophysical*

Research Communications, *529*(4), 1145–1150. https://doi.org/10.1016/j.bbrc.2020.06.121

Prentice, J. S., Homann, J., Simmons, K. D., Tkačik, G., Balasubramanian, V., & Nelson, P. C. (2011). Fast, Scalable, Bayesian Spike Identification for Multi-Electrode Arrays. *PLOS ONE*, *6*(7), e19884. https://doi.org/10.1371/journal.pone.0019884

Quigg, M., Rolston, J., & Barbaro, N. M. (2012). Radiosurgery for epilepsy: Clinical experience and potential antiepileptic mechanisms. *Epilepsia*, *53*(1), 7–15. https://doi.org/10.1111/j.1528-1167.2011.03339.x

Redmond, K. J., Gui, C., Benedict, S., Milano, M. T., Grimm, J., Vargo, J. A., Soltys, S. G., Yorke, E., Jackson, A., El Naqa, I., Marks, L. B., Xue, J., Heron, D. E., & Kleinberg, L. R. (2021). Tumor Control Probability of Radiosurgery and Fractionated Stereotactic Radiosurgery for Brain Metastases. *International Journal of Radiation Oncology*Biology*Physics*, *110*(1), 53–67. https://doi.org/10.1016/j.ijrobp.2020.10.034

Reynolds, T. A., Jensen, A. R., Bellairs, E. E., & Ozer, M. (2020). Dose Gradient Index for Stereotactic Radiosurgery/Radiation Therapy. *International Journal of Radiation Oncology*Biology*Physics*, *106*(3), 604–611. https://doi.org/10.1016/j.ijrobp.2019.11.408

Rossant, C., Kadir, S. N., Goodman, D. F. M., Schulman, J., Hunter, M. L. D., Saleem, A. B., Grosmark, A., Belluscio, M., Denfield, G. H., Ecker, A. S., Tolias, A. S., Solomon, S., Buzsáki, G., Carandini, M., & Harris, K. D. (2016). Spike sorting for large, dense

electrode arrays. *Nature Neuroscience*, *19*(4), 634–641. https://doi.org/10.1038/nn.4268

Rykhlevskaia, E., Gratton, G., & Fabiani, M. (2008). Combining structural and functional neuroimaging data for studying brain connectivity: A review. *Psychophysiology*, *45*(2), 173–187. https://doi.org/10.1111/j.1469-8986.2007.00621.x

Sanchez-Vives, M., & Mattia, M. (2014). Slow wave activity as the default mode of the cerebral cortex. *Archives Italiennes de Biologie*, *152*, 147–155. https://doi.org/10.12871/000298292014239

Sanchez-Vives, M. V. (2020). Origin and dynamics of cortical slow oscillations. *Current Opinion in Physiology*, *15*, 217–223. https://doi.org/10.1016/j.cophys.2020.04.005

Sanchez-Vives, M. V., Massimini, M., & Mattia, M. (2017). Shaping the Default Activity Pattern of the Cortical Network. *Neuron*, *94*(5), 993–1001. https://doi.org/10.1016/j.neuron.2017.05.015

Sanchez-Vives, M. V., & McCormick, D. A. (2000). Cellular and network mechanisms of rhythmic recurrent activity in neocortex. *Nature Neuroscience*, *3*(10), 1027–1035. https://doi.org/10.1038/79848

Simmons, D. A., Lartey, F. M., Schüler, E., Rafat, M., King, G., Kim, A., Ko, R., Semaan, S., Gonzalez, S., Jenkins, M., Pradhan, P., Shih, Z., Wang, J., von Eyben, R., Graves, E. E., Maxim, P. G., Longo, F. M., & Loo, B. W. (2019). Reduced cognitive deficits after FLASH irradiation of whole mouse brain are associated with less hippocampal dendritic spine loss and neuroinflammation. *Radiotherapy and Oncology*, *139*, 4–10. https://doi.org/10.1016/j.radonc.2019.06.006

Song, S., Sjöström, P. J., Reigl, M., Nelson, S., & Chklovskii, D. B. (2005). Highly Nonrandom Features of Synaptic Connectivity in Local Cortical Circuits. *PLOS Biology*, *3*(3), e68. https://doi.org/10.1371/journal.pbio.0030068

Sorrenti, V., Cecchetto, C., Maschietto, M., Fortinguerra, S., Buriani, A., & Vassanelli, S. (2021). Understanding the Effects of Anesthesia on Cortical Electrophysiological Recordings: A Scoping Review. *International Journal of Molecular Sciences*, *22*(3), Article 3. https://doi.org/10.3390/ijms22031286

Stark, E., & Abeles, M. (2007). Predicting Movement from Multiunit Activity. *Journal of Neuroscience*, *27*(31), 8387–8394. https://doi.org/10.1523/JNEUROSCI.1321-07.2007

Stevenson, I. H., & Kording, K. P. (2011). How advances in neural recording affect data analysis. *Nature Neuroscience*, *14*(2), Article 2. https://doi.org/10.1038/nn.2731

Thierry, A.-M., Gioanni, Y., Dégénétais, E., & Glowinski, J. (2000). Hippocampo-prefrontal cortex pathway: Anatomical and electrophysiological characteristics. *Hippocampus*, *10*(4), 411–419. https://doi.org/10.1002/1098-1063(2000)10:4<411::AID-HIPO7>3.0.CO;2-A

Tournier, J.-D., Mori, S., & Leemans, A. (2011). Diffusion Tensor Imaging and Beyond. *Magnetic Resonance in Medicine*, *65*(6), 1532–1556. https://doi.org/10.1002/mrm.22924

Trautmann, E. M., Stavisky, S. D., Lahiri, S., Ames, K. C., Kaufman, M. T., O'Shea, D. J., Vyas, S., Sun, X., Ryu, S. I., Ganguli, S., & Shenoy, K. V. (2019). Accurate Estimation of

Neural Population Dynamics without Spike Sorting. *Neuron*, *103*(2), 292-308.e4. https://doi.org/10.1016/j.neuron.2019.05.003

Tuleasca, C., Vermandel, M., & Reyns, N. (2021). Stereotactic Radiosurgery: From a Prescribed Physical Radiation Dose Toward Biologically Effective Dose. *Mayo Clinic Proceedings*, *96*(5), 1114–1116. https://doi.org/10.1016/j.mayocp.2021.03.027

Ueno, H., Suemitsu, S., Murakami, S., Kitamura, N., Wani, K., Matsumoto, Y., Okamoto, M., & Ishihara, T. (2019). Region-specific reduction of parvalbumin neurons and behavioral changes in adult mice following single exposure to cranial irradiation. *International Journal of Radiation Biology*, *95*(5), 611–625. https://doi.org/10.1080/09553002.2019.1564081

Wang, K., Liang, M., Wang, L., Tian, L., Zhang, X., Li, K., & Jiang, T. (2007). Altered functional connectivity in early Alzheimer's disease: A resting-state fMRI study. *Human Brain Mapping*, *28*(10), 967–978. https://doi.org/10.1002/hbm.20324

Wu, P., Coultrap, S., Pinnix, C., Davies, K. D., Tailor, R., Ang, K. K., Browning, M. D., & Grosshans, D. R. (2012). Radiation Induces Acute Alterations in Neuronal Function. *PLOS ONE*, *7*(5), e37677. https://doi.org/10.1371/journal.pone.0037677

Xia, Y. (2020). Chapter Eleven—Correlation and association analyses in microbiome study integrating multiomics in health and disease. In J. Sun (Ed.), *Progress in Molecular Biology and Translational Science* (Vol. 171, pp. 309–491). Academic Press. https://doi.org/10.1016/bs.pmbts.2020.04.003

Yuan, H., Gaber, M. W., Boyd, K., Wilson, C. M., Kiani, M. F., & Merchant, T. E. (2006). Effects of fractionated radiation on the brain vasculature in a murine model: Blood–brain

barrier permeability, astrocyte proliferation, and ultrastructural changes. *International Journal of Radiation Oncology*Biology*Physics*, *66*(3), 860–866. https://doi.org/10.1016/j.ijrobp.2006.06.043

Zaer, H., Fan, W., Orlowski, D., Glud, A. N., Jensen, M. B., Worm, E. S., Lukacova, S., Mikkelsen, T. W., Fitting, L. M., Jacobsen, L. M., Portmann, T., Hsieh, J.-Y., Noel, C., Weidlich, G., Chung, W., Riley, P., Jenkins, C., Adler, J. R., Schneider, M. B., … Stroh, A. (2022). Non-ablative doses of focal ionizing radiation alters function of central neural circuits. *Brain Stimulation*, *15*(3), 586–597. https://doi.org/10.1016/j.brs.2022.04.001

Zaer, H., Glud, A. N., Schneider, B. M., Lukacova, S., Vang Hansen, K., Adler, J. R., Høyer, M., Jensen, M. B., Hansen, R., Hoffmann, L., Worm, E. S., Sørensen, J. C. H., & Orlowski, D. (2020). Radionecrosis and cellular changes in small volume stereotactic brain radiosurgery in a porcine model. *Scientific Reports*, *10*(1), 16223. https://doi.org/10.1038/s41598-020-72876-w

Zhang, D., Zhou, W., Lam, T. T., Li, Y., Duman, J. G., Dougherty, P. M., & Grosshans, D. R. (2020). Cranial irradiation induces axon initial segment dysfunction and neuronal injury in the prefrontal cortex and impairs hippocampal coupling. *Neuro-Oncology Advances*, *2*(1), vdaa058. https://doi.org/10.1093/noajnl/vdaa058

Zhang, D., Zhou, W., Lam, T. T., Weng, C., Bronk, L., Ma, D., Wang, Q., Duman, J. G., Dougherty, P. M., & Grosshans, D. R. (2018). Radiation induces age-dependent deficits in cortical synaptic plasticity. *Neuro-Oncology*, *20*(9), 1207–1214. https://doi.org/10.1093/neuonc/noy052

CHAPTER 4: GENERAL DISCUSSION

This thesis aimed to describe and compare radiation-induced effects on neural networks and epileptiform network dynamics using hd-MEAs. To begin, we investigated the neural dynamics of PFC networks that were perfused with a PE solution containing 4-AP, reduced extracellular magnesium (Mg^{2+}) and increased extracellular potassium (K^{+})(Postnikova et al., 2020). Subsequently, we trained a deep GAN to generate novel exemplars and compared the exemplars produced by the GAN to our original data. Following this, we investigated the effect of varying radiation doses (20, 50, 100 Gy) on healthy cortical neurons located within the PFC. We then analyzed changes in firing rate and functional connectivity within irradiated networks of neurons based on the data we collected with our hd-MEAs. We also quantified the amount of cell death that occurs following radiation doses using PI staining and imaged the slices. Finally, we compared the network dynamics of the pro-epileptiform PFC networks, as measured by firing rates and functional connectivity, to the dynamics of the irradiated PFC networks.

We found that applying the PE solution resulted in cortical disinhibition whereby networks showed increased firing rates but a lower density of functional connections. Interestingly, past research has shown that cross-correlations and firing rates can increase in parallel, making it difficult to separate the two (de la Rocha et al., 2007). Consistent with this, we saw an increase in the strength of functional connections amongst both irradiated and PE networks. However, one aspect of functional connectivity that is not considered in de la Rocha et al. is the density of connections across a network. When looking at the density

of connections, we found a lower density of functional connections accompanied by an increase in firing rate in disinhibited PE networks, which can be explained by the fact that this activity typically occupies a spatially delimited region of the array (Boucher-Routhier & Thivierge, 2023). By comparison, irradiated networks showed an increase in both the density of connections and firing rates. Other work by Huang and collaborators (2019) investigated shared spiking variability during spatiotemporal patterns of neural population activity. The authors found that attention-mediated changes in population variability between and within visual areas (C. Huang et al., 2019); however, they did not investigate the density of functional connections.

In addition, we discovered complex spatiotemporal patterns of activation within our epileptiform-induced networks which included spiral and planar waves. These spiral waves showed stereotypical characteristics in terms of the phase distribution, center of mass, neural complexity and spatial correlations that were consistent with previous research (X. Huang, 2004; Rule et al., 2018). We were also successful in training our deep GAN to produce novel exemplars that captured the main features of the spiral waves that were seen in our experimental dataset. Together, these results point to neural complexity existing on a continuum whereby lower values are associated with healthy brain states and higher complexity values are associated with disinhibited or diseased brain states (Boucher-Routhier & Thivierge, 2023).

Following our investigation of epileptiform activity within large-scale PFC networks, we turned our attention to radiation-induced changes within healthy PFC networks. We

found that radiation produced marked increases in firing rate within previously healthy cortical networks. These findings are consistent with previous studies investigating the acute effects of radiation on PFC neurons (Zhang et al., 2020). Other studies that have investigated late-delayed have shown a decrease in firing with doses above 60 Gy (Zaer et al., 2022), which may point to differential effects based on the timescale following radiation. These differences are likely also due to increases in apoptotic cells and/or radionecrosis (Zaer et al., 2020, 2022).

Research in human nasopharyngeal carcinoma patients comparing early to late-delayed effects of radiation showed a change in the effects of radiation over time. A study conducted by Ding and colleagues (2018) showed that patients experience an initial increase in local brain activity which is often predictive of higher levels of necrosis in the late-delayed stages. Additionally, a comparison of the acute effects to late-delayed effects of radiation revealed an eventual decrease in functional connections within the medial PFC (mPFC) (Ding et al., 2018). Vincent and collaborators (2013) found similar results in a study involving cultured neurons preconditioned with 4-AP and bicuculline, which revealed a homeostatic rebound effect on firing rates. The authors observed a rebound effect that consisted of a marked increase in firing rate within 24 hours of preconditioning which eventually decreased 4 days post-washout (Vincent et al., 2013). This rebound effect, which has been linked to homeostatic regulation mechanisms, may also account for the differences in firing rate seen immediately after radiation exposure compared to firing rates several months post-irradiation. Thus, one may obtain different experimental results depending on when neural activity is recorded.

Irradiated networks also showed an increase in the density and in some cases the strength of functional connections within the PFC. It is important to note that these results were distinct from the pro-epileptiform networks which showed an increase in firing rate but reduced density in the functional connections. Thus, we concluded that the doses of radiation were not merely inducing a state of epileptic activity but rather they produced a distinct cortical state.

Finally, we discovered a dose-dependent rate of cell death whereby networks that received higher doses of radiation showed a higher rate of cell death. PI imaging revealed a higher rate of cell death in the slice that received 100 Gy which appeared to be localized to areas surrounding M2. This pattern was not seen in the lower doses that we examined (20 and 50 Gy), which may be because doses above 60 Gy have been shown to be lesional (Zaer et al., 2022). More specifically, doses above 60 Gy were shown to produce white matter necrosis, whereas doses above 100 Gy were shown to produce grey matter necrosis (Zaer et al., 2020). These results may offer some insight as to why we saw higher cell death in M2 following a dose of 100 Gy but not 20 or 50 Gy. The above result was only observed in a single slice as there was only a single slice that was imaged per condition. Thus, further investigation would be needed to determine whether selective damage would occur in M2 across slices.

M2 has previously been shown to be vulnerable to radiation-induced injuries (Hnilicová et al., 2022; Ueno et al., 2019). The M2 in rodents, which is a subdivision of the mPFC, receives afferent connections from several thalamic nuclei (Reep & Corwin, 1999)

and cortical regions including somatosensory, visual, parietal, auditory, orbital and retrosplenial areas (Hoover & Vertes, 2007; Reep et al., 1990; Yamawaki et al., 2016; Zingg et al., 2014). Neurons within M2 project to a wide variety of cortical and subcortical regions (Barthas & Kwan, 2017; Reep et al., 1987) and are speculated to play a key role in producing organized motor output from multimodal sensory inputs (Reep et al., 1987).

Although the behavioural role of M2 remains to be fully elucidated, lesion studies have shown that M2 is involved in initiating voluntary actions by integrating sensory information through reciprocal connections, providing action signals within the frontal cortex, and producing adaptive behaviour through a dependency on context-related information (Barthas & Kwan, 2017). Whole-brain mapping studies have also suggested that M2 is impacted by chronic stress and could be involved in brain disorders such as depression (Barthas & Kwan, 2017; Bernard & Mittal, 2015; Duncan et al., 1999; Kim et al., 2016; Miyamoto et al., 2000). Studies have suggested that the rodent M2 may be homologous to the supplementary motor cortex, premotor cortex or frontal eye field, however; further research is needed to clarify whether humans or non-human primates possess an equivalent region (Barthas & Kwan, 2017).

CONTRIBUTIONS TO FIELD

Our work provided a unique insight into the application of GANs in producing novel exemplars of varying neural complexity. The ability to produce a variety of exemplars of large-scale neural networks can potentially be used to inform future treatment protocols. We have shown that neural complexity can be explored by adjusting the variance and amplitude of the input injected into our model. As a result, GANs or other generative

networks may be used to produce pathological brain activity, then subsequently tuned in such a way that suppresses that pathological activity within the model network. The results from these models could therefore help inform neurostimulation protocols that aim to suppress pathological activity such as epileptiform brain activity (Scheid et al., 2021). In addition to informing potential treatment protocols, GANs can also be employed to produce large datasets of plausible exemplars of phenomena such as epileptic brain activity that are typically infrequent. This can help inform our understanding of key properties of the neural dynamics that occur during pathological brain states.

We also provided valuable insight into the effect of radiation on underlying PFC networks. Previously, the field primarily focused on the effect of radiation-induced brain injuries on the hippocampus, however; the PFC has been identified as one of the brain regions that is most sensitive to radiation (Hnilicová et al., 2022; Kornev et al., 2005; Kovalchuk & Kolb, 2017). The PFC also shares a direct monosynaptic pathway with the hippocampus which is believed to be implicated in the cognitive impairments and deficits seen in patients following RT (S. C.-J. Chen et al., 2017; Hnilicová et al., 2022; Kovalchuk & Kolb, 2017; Zhang et al., 2020).

We showed that radiation does not simply induce an epileptic state which is evident in the difference in network dynamics that are seen in the irradiated slices compared to the slices treated with our PE solution. Our results showed that radiation leads to an increase in the firing rate that is accompanied by an increase in the density of functional connections within irradiated networks. This is contrasted with the pro-epileptiform networks which

showed an increase in firing rate, and a lower density of functional connections within the network.

LIMITATIONS OF CURRENT WORKS

ACUTE BRAIN SLICE PREPARATIONS

In vitro brain slice preparations are one of the most used procedures for studying the electrophysiological properties of neurons and are used in a wide variety of experimental circumstances (Buskila et al., 2014). The preparation of acute brain slices has several advantages including shorter exposure to anaesthetics due to rapid preparation times, superior recording stability because the respiration and heartbeat of the animal are no longer present, the ability to locally apply drugs that would otherwise not cross the blood-brain barrier, and superior maintenance of the structural integrity of neural circuits compared to cell cultures or homogenates (Buskila et al., 2014; Gul et al., 2020).

On the other hand, acute brain slices have a limited lifespan that typically ranges from 4-12 hours depending on the brain region and thickness of the slice (Buskila et al., 2014; Fukuda et al., 1995). Other limitations include sensitivity to changes in the medium in which slices are kept (changes in pH, oxygen and glucose levels, and temperature) and the use of non-sterile environments that lead to bacteria build-up over time and eventually increased cell death (Buskila et al., 2014). Past research has shown that standard slicing procedures lead to a passive influx of sodium followed by water entering the cells leading to swelling. This swelling often results in poor survival of neurons, especially those located in the superficial layers that are more directly impacted by the blade during the cutting

procedure (Ting et al., 2014, 2018). Although exposure to anaesthetics is limited in acute slice preparations, it is worth noting that volatile anaesthetics such as isoflurane have been shown to block LTP and long-term depression (LTD) and produce a reversible depression of glutamatergic synaptic transmission by increasing $GABA_A$ receptor currents (Koltchine et al., 1999; Simon et al., 2001). Consequently, these effects may have an impact on subsequent findings.

Another limitation that results from collecting acute brain slices is the severing of connections with adjacent brain regions. During the slicing procedure, networks are susceptible to a loss of extrinsic connections between neurons and adjacent regions which can lead to significant changes in the normal functioning of these networks (Dailey, 2002). Tissue within the collected slices can also begin to deteriorate causing additional structural and/or physiological damage which is accompanied by the release of excitatory amino acids and other toxicants. These toxicants are known to produce excitotoxicity and increased vulnerability within the surviving cells (Buskila et al., 2014; Dailey, 2002; Schurr et al., 1995). Consequently, we were unable to study altered cortical brain states in their entirety as hd-MEA recordings of acute brain slices did not provide access to activity across the entire brain, but rather gave us insight to the activity of local cortical networks.

RADIATION TIMESCALE AND DOSING

As previously discussed, radiation-induced brain injuries happen on a variety of time scales (acute, early-delayed and late-delayed). However, we were unable to examine the early and late-delayed effects of RT on cortical networks due to limitations in the lifespan of

acute brain slices and limitations in producing brain slices from adult rodents (Buskila et al., 2014; Fukuda et al., 1995; Ting et al., 2014). Past research has shown that brain slices from adult animals experience heightened levels of oxidative stress during the slicing procedure as well as edema when incubated in standard ACSF (Ting et al., 2014). There are also some key differences between irradiating an acute brain slice compared to a live animal.

Another limitation of our work is that we were unable to deliver fractionated doses of radiation that are typically used for tumour treatments due to the length of viability of acute brain slices. For instance, a dose of 40 Gy would be fractionated into daily doses of 2 Gy that are delivered five days per week for four weeks in clinical settings (Yuan et al., 2006), which is not possible in acute brain slices. Large single doses of radiation, such as those employed in our study, are used in different clinical circumstances such as in the case of pulsed high-dose-rate brachytherapy, stereotactic radiosurgery, and some hypofractionated palliative treatment protocols (Redmond et al., 2021; Tuleasca et al., 2021; Yuan et al., 2006). Research comparing single-dose to fractionated treatments found that single doses resulted in rapid molecular responses which were reduced in the fractionated condition (Gaber et al., 2003). However, these findings fail to account for the long-term side effects that typically follow fractionated dose regimes, which may point to delayed effects (Gaber et al., 2003; Yuan et al., 2006). Finally, we were unable to investigate sex differences in the effect of radiation, which is something that has been highlighted in the literature (Armstrong et al., 2007; Carroll et al., 2013; Panwala et al., 2019).

LIMITATIONS OF HD-MEA DATA

The use of hd-MEA recordings as an electrophysiological measure also limited our ability to study laminar differences in radiosensitivity. Although current research remains to fully elucidate the impact of radiosensitivity in the various layers of cortex, some studies have shown varying radiosensitivity among certain regions of the brain. For example, Siebert and colleagues (2017) found heightened sensitivity in the entorhinal, inferior parietal, inferior temporal, isthmus cingulate, middle temporal, parahippocampal, superior frontal, superior temporal, and temporal pole regions of the brain. Nagtegaal and collaborators (2020) also found dose-dependent thinning in the right inferior parietal, superior parietal, and supramarginal, the right posterior cingulate and paracentral regions and the right lateral orbital regions. Another study by Karunamuni et al (2016) showed the most radiosensitivity in the temporal and limbic cortices compared to frontal, parietal, and occipital regions. They also alluded to the fact that the pattern of radiosensitivity is similar to the pattern of degeneration seen in Alzheimer's disease (Brun & Englund, 1981), which suggests there may be an inherent cellular property in certain regions that make them more vulnerable to injury (Karunamuni et al., 2016). Finally, we were unable to investigate the intracellular mechanism involved in the radiation or epileptiform-induced network changes that we saw as hd-MEAs provide extracellular measures.

BROADER IMPLICATIONS

This work has proven valuable in increasing our understanding of the effects of radiation on healthy neural networks. This provides preliminary insight into the neural mechanisms that may underlie the cognitive impairments experienced by patients, which

are currently poorly understood. This opens the doors to the use of hd-MEAs in guiding RT protocols that attempt to minimize the side effects of neuronal death and dysregulated activity. We also provided a deeper characterization of spiral waves including descriptions of the direction of consecutive spirals (clockwise or counter-clockwise) which had not been previously done.

Several models of spiral waves have been developed that rely on different measures to identify spiral waves. To begin, Ermentrout and Kleinfeld (2001) were able to spontaneously generate spiral waves using a 2D network that models a 40x40 array of phase oscillators coupled to their closest neighbour. Spiral waves consisted of nonsynchronous activity that surrounded phase singularities or "pinwheel" centers (Ermentrout & Kleinfeld, 2001). Huang (2004) developed a model that produced spiral waves by disrupting wavefronts with an inhibitory stimulus resulting in free ends capable of initiating a rotation. The results from this model were consistent with their experimental findings that showed a reduction in amplitude around a phase singularity at the center of the spiral (X. Huang, 2004). Keane and Gong (2015) developed a 2D spatially extended, conductance-based integrate-and-fire neural network with balanced excitation and inhibition. They found that spiral waves developed in circumstances where the network was unbalanced, and excitation dominated resulting in more global patterns such as rotating waves (Keane & Gong, 2015). Townsend and Gong (2018) developed a method based on critical points within a velocity vector field (a measure of local speed and direction of propagating neural activity) where both the x and y components of the velocity were equal to zero. These critical points were analogous to the center point of a spiral wave where local activity rotates around this

point (Perry & Chong, 1987; Townsend et al., 2015; Townsend & Gong, 2018). Hajian and colleagues (2023) were able to produce and disrupt spiral waves using a 200 x 200 lattice of FitzHugh–Nagumo neurons that were chemically coupled. The authors found that the emergence of spiral waves within chemical synapses was dependent on an interaction between the firing threshold, critical sigmoidal slope value and synaptic reversal potential (Hajian et al., 2023). It is difficult to differentiate which model is better at capturing spiral waves in a way that best represents how they occur physiologically. The ability to capture the direction of spiral waves and switch between directions (clockwise or counter-clockwise) may help elucidate which model is most biologically plausible. This is an aspect of experimentally-observed spiral waves that is described in our work but has yet to be targeted by computational simulations.

In addition, we provided a novel application of GANs in neuroscience whereby we used a deep GAN to generate novel exemplars as well as explore a range of cortical states from healthy to disinhibited or pathological activity. It is worth noting that there are alternative models that can be employed for these purposes such as variational autoencoders (VAEs) (Harshvardhan et al., 2020; Kingma & Welling, 2019), U-nets (Chen et al., 2021; Siddique et al., 2021), and diffusion models (Dhariwal & Nichol, 2021). Despite these alternative models, we chose to use a GAN to capture key aspects of complex spiral waves for a variety of reasons. One primary reason is that GANs offer advanced image generation capabilities which allowed us to produce realistic exemplars that mimic the fundamental characteristics of spiral waves.

VAEs take data as initial input and find lower dimensional latent space representations of the data before reconstructing it (Doersch, 2021; Harshvardhan et al., 2020; Kingma & Welling, 2019). In general, these models tend to produce inferior-quality data when compared to GANs. U-nets were primarily designed for image segmentation and consist of two paths. The first is the analysis or encoder path, which resembles a regular convolution network and thus provides information on classification. The second is the synthesis or decoder path allows the network to learn local classification information and increases the resolution of the output (Chen et al., 2021; Ronneberger et al., 2015; Siddique et al., 2021). One limitation of these models is that the input and output dimensions of the network must be the same. Finally, diffusion models are a type of likelihood-based model that can generate high-quality images by progressively adding noise to a sample dataset, followed by a gradual reversal to less noisy samples (Dhariwal & Nichol, 2021). These models have recently been shown to produce high-quality images and avoid the mode collapse problem that can occur when using GANs. However, they tend to require more intervention by the user via classifier guidance which involves training an additional classifier model that modifies the diffusion score to include the log-likelihood gradient of the classifier (Dhariwal & Nichol, 2021; Ho & Salimans, 2022).

FUTURE DIRECTIONS

One area that would be important to explore is pharmacological preconditioning prior to administering a dose of radiation. This has been previously shown to be effective using an ischemic model that was investigated via MEA recordings (Tauskela et al., 2021; Vincent et al., 2013); however, it would be beneficial to determine whether neuroprotective

substances would be able to mitigate the damage caused by radiation. Previous research has shown that oral doses of the main polyphenolic compound in green tea, EGCG (El-Missiry et al., 2018), or the flavonoid Quercetin (Kale et al., 2018) which is found in several fruits and vegetables can provide neuroprotective effects against radiation. In addition, pre-treating hippocampal slices with the NMDAR antagonist memantine also showed neuroprotective effects against radiation (P. Wu et al., 2012). It would be beneficial to determine whether these compounds can provide neuroprotective effects on neural network dynamics as measured by an hd-MEA as well as across different brain regions such as the M2 which was shown to experience increased cell death. It would also be beneficial to further our understanding of the role that more radiosensitive regions, such as the M2, play in the cognitive deficits experienced following radiation.

More recently, the use of FLASH radiation has shown promise in reducing radiation-induced toxicity in healthy tissue and the associated side effects while maintaining the effectiveness of the treatment (Favaudon et al., 2014; Hughes & Parsons, 2020; Matuszak et al., 2022; Montay-Gruel et al., 2017; Simmons et al., 2019). FLASH radiation involves an ultra-fast delivery at a dose rate several orders of magnitude greater (> 40 Gy/s) than conventional clinical RT (~ 5 Gy/min) (Favaudon et al., 2014; Hughes & Parsons, 2020; Matuszak et al., 2022). Future work could benefit from studying the effects of FLASH radiation compared to conventional dose rates on acute brain slices to determine if there are differences in network dynamics or cellular apoptosis.

It would be beneficial for future studies to include rodents of each sex to investigate sex differences in radiation-induced brain injuries that may underlie the higher rates of cognitive impairments in female survivors of brain tumours (Armstrong et al., 2007; Carroll et al., 2013; Panwala et al., 2019). Another avenue to explore would be a comparison among different age groups (juvenile vs. adult rodents), although there are limitations to the viability of acute slices that are collected from older rats (Lipton et al., 1995). For instance, acute slices from younger animals tend to have a better survival rate than older animals (Lipton et al., 1995), thus providing more accurate investigations of the effects of radiation. It is also worth noting that the neurons of younger animals tend to be more resistant to a variety of insults such as exposure to radiation, which may result in more reliable effects of radiation exposure (S. Huang & Uusisaari, 2013). Investigations into these effects on adult rodent neurons may yield more pronounced effects.

Recent studies have investigated various protective mechanisms that can be employed to aid in the recovery of brain slices collected from adult animals. These techniques involve replacing sodium ions during the initial recovery stages of the slice via a protective N-methyl-D-glucamine (NMDG) ACSF and adding 20 mM HEPES during slice incubation to reduce edema and oxidative damage (Chen et al., 2012; Peca et al., 2011; Ting et al., 2014; Zhao et al., 2020). Additional research has investigated the impact of preparing acute slices at physiological temperature (PT) rather than the standard ice-cold temperature (CT), which produced higher quality cerebellar and hindbrain slices in adult rodents (Eguchi et al., 2020; Fried et al., 2014; S. Huang & Uusisaari, 2013). These methods

could be employed in future research to aid in the investigation of RT effects on adult brain slices.

It would also be helpful to study the effects of radiation in adjacent brain regions or brain slices that maintain connections between regions (for example PFC to hippocampus) to determine whether the impact is consistent across regions. Related to this, future research should investigate both regional and laminar differences in radiosensitivity among brain regions. Another avenue to explore would be the contribution of various neuronal subtypes such as vasoactive intestinal peptide, parvalbumin-expressing and somatostatin inhibitory neuron subtypes (Ren et al., 2022; Rudy et al., 2011). It is worth noting that PI staining alone is not able to distinguish between cell types, rather it can only be used to quantify the amount of cell death within a given slice. Future work could employ cell-specific dyes in combination with PI staining to help identify which cell types are most sensitive to radiation-induced apoptosis. For example, parvalbumin-expressing interneurons (PV neurons) in the cerebral cortex are believed to play a role in radiation-induced cognitive impairments due to their involvement in gamma oscillations (Gouwens et al., 2010; Lewis et al., 2005; Ueno et al., 2019; Zhou et al., 2012) and vulnerability to oxidative stress (Cabungcal et al., 2013; Steullet et al., 2017; Ueno et al., 2019), which can be induced by radiation. Co-labelling PV cells with PI and a cell-specific marker such as Alexa Fluor-488 (Ueno et al., 2019) may help determine whether radiation is causing apoptosis in a higher proportion of PV cells or whether the cell death can be attributed to different cell types.

Hd-MEAs provide global patterns of firing rates and functional connectivity based on MUA that have been shown to capture the key properties of activity in neural circuits. Past research has shown that MUA can be used to adequately infer cross-correlations and firing rates even in the absence of spike sorting methods or single-cell resolution data (Trautmann et al., 2019). The use of simultaneous intracellular and extracellular recordings (Dipalo et al., 2017; Hamilton et al., 2018; D. Xu et al., 2021) could be used to complement the MUA data recorded from hd-MEAs. This type of experiment is technically very challenging; however, it would likely provide very fruitful insight into the intracellular mechanisms that are underlying the changes in network dynamics seen following RT. The use of cultured neurons could provide additional insight into the long-term effects (early delayed or late delayed radiation-induced brain injuries) of RT. These cultures could then be recorded via hd-MEAs to determine whether the changes in network dynamics that we discovered are also present on a longer timescale or whether networks exhibit different changes in their dynamics as time goes on.

Although cultured slices would provide the ability to track radiation-induced injuries across longer periods of time, there are also several disadvantages to this method. First, the preparation and maintenance of slice cultures require much more work compared to acute slices (Lein et al., 2011). There is also a risk of neuronal injury and/or death, as well as a loss of anatomical organization within the slice (Humpel, 2015). During preparation, synapses are reorganized and the culture experiences dendritic and axonal remodeling resulting in a disruption of afferent and efferent connections (Coltman et al., 1995; Lein et al., 2011).

Future studies investigating pro-epileptiform activity could benefit from studying surrounding brain regions. It is currently unclear whether other brain regions would show a similar pattern of increased complexity during disinhibited cortical activity or how adjacent regions would interact under these conditions. It would also be beneficial to further explore the role of excitatory and inhibitory cells in propagating and sustaining spiral waves. Although we were able to examine the dynamics of both spiral and planar waves, future research could also benefit from exploring other wave types such as sink, source or saddle waves to determine if they exhibit the same level of complexity. It would also be beneficial to develop a systematic way of extracting spiral waves from continuous recordings of population activity as none currently exist. Another area that could provide interesting findings would be to combine a pro-epileptic model with high doses of radiation as radiosurgery has previously been used to treat epileptic lesions in cases where lesions are difficult to reach by other treatment measures (McGonigal et al., 2017; Quigg et al., 2012). It is worth noting that several challenges may present themselves including issues with identifying the brain site where seizures commence and verifying whether a network is indeed epileptic before applying radiation. This is because acute brain slices cannot be recorded prior to applying radiation as radiation would damage the hd-MEAs.

FINAL CONCLUSIONS

The results from this thesis highlight the role of hd-MEAs in providing a novel and viable assay to investigate cortical network dynamics within PE and irradiated networks. This has provided valuable insight into the characteristics of the complex spatiotemporal patterns of activity that are present in PE networks. Successfully training a deep GAN to

generate novel exemplars of this otherwise rare form of neural activity has increased our understanding of complexity as a marker of the health of neural activity. To illustrate, results obtained from the deep GAN highlighted the fact that the complexity of population activity exists on a continuum from healthy to disinhibited or diseased. These findings can help inform future work aimed at designing neurostimulation protocols to suppress pathological neural activity such as cortical seizures. Further, hd-MEA recordings of previously healthy irradiated cortical tissue have also provided valuable insight into the acute effects of clinically-relevant doses of radiation. We discovered a dose-dependent increase in cell death, increased firing rates, an increase in the density of functional connections and in some cases an increase in the strength of functional connections within irradiated networks. The pattern of activity observed following radiation was distinct from PE networks which highlights that radiation does not merely induce an epileptic brain state. This work paves the way for future investigations of potential pharmacological preconditional aimed at reducing radiation-induced brain injuries such as cellular apoptosis, and alterations in network dynamics.

REFERENCES

Aggarwal, A., Mittal, M., & Battineni, G. (2021). Generative adversarial network: An overview of theory and applications. *International Journal of Information Management Data Insights*, *1*(1), 100004. https://doi.org/10.1016/j.jjimei.2020.100004

Altan, E., Solla, S. A., Miller, L. E., & Perreault, E. J. (2021). Estimating the dimensionality of the manifold underlying multi-electrode neural recordings. *PLoS Computational Biology*, *17*(11), e1008591. https://doi.org/10.1371/journal.pcbi.1008591

Amit, D. J., & Brunel, N. (1997). Model of global spontaneous activity and local structured activity during delay periods in the cerebral cortex. *Cerebral Cortex (New York, N.Y.: 1991)*, *7*(3), 237–252. https://doi.org/10.1093/cercor/7.3.237

Ammann, C., Dileone, M., Pagge, C., Catanzaro, V., Mata-Marín, D., Hernández-Fernández, F., Monje, M. H. G., Sánchez-Ferro, Á., Fernández-Rodríguez, B., Gasca-Salas, C., Máñez-Miró, J. U., Martínez-Fernández, R., Vela-Desojo, L., Alonso-Frech, F., Oliviero, A., Obeso, J. A., & Foffani, G. (2020). Cortical disinhibition in Parkinson's disease. *Brain*, *143*(11), 3408–3421. https://doi.org/10.1093/brain/awaa274

Amunts, K., & Zilles, K. (2015). Architectonic Mapping of the Human Brain beyond Brodmann. *Neuron*, *88*(6), 1086–1107. https://doi.org/10.1016/j.neuron.2015.12.001

Anastasiades, P. G., & Carter, A. G. (2021). Circuit organization of the rodent medial prefrontal cortex. *Trends in Neurosciences*, *44*(7), 550–563. https://doi.org/10.1016/j.tins.2021.03.006

Arakaki, T., Barello, G., & Ahmadian, Y. (2017). Capturing the diversity of biological tuning curves using generative adversarial networks. *arXiv Preprint arXiv:1707.04582*.

Araújo, N. S., Reyes-Garcia, S. Z., Brogin, J. A. F., Bueno, D. D., Cavalheiro, E. A., Scorza, C. A., & Faber, J. (2022). Chaotic and stochastic dynamics of epileptiform-like activities in sclerotic hippocampus resected from patients with pharmacoresistant epilepsy. *PLoS Computational Biology*, *18*(4), e1010027. https://doi.org/10.1371/journal.pcbi.1010027

Arjovsky, M., Chintala, S., & Bottou, L. (2017). Wasserstein Generative Adversarial Networks. *Proceedings of the 34th International Conference on Machine Learning*, 214–223. https://proceedings.mlr.press/v70/arjovsky17a.html

Armstrong, G. T., Sklar, C. A., Hudson, M. M., & Robison, L. L. (2007). Long-Term Health Status Among Survivors of Childhood Cancer: Does Sex Matter? *Journal of Clinical Oncology*, *25*(28), 4477–4489. https://doi.org/10.1200/JCO.2007.11.2003

Avena-Koenigsberger, A., Misic, B., & Sporns, O. (2018). Communication dynamics in complex brain networks. *Nature Reviews Neuroscience*, *19*(1), 17–34. https://doi.org/10.1038/nrn.2017.149

Avoli, M., Barbarosie, M., Lücke, A., Nagao, T., Lopantsev, V., & Köhling, R. (1996). Synchronous GABA-mediated potentials and epileptiform discharges in the rat limbic system in vitro. *The Journal of Neuroscience: The Official Journal of the Society for Neuroscience*, *16*(12), 3912–3924.

Avoli, M., D'Antuono, M., Louvel, J., Köhling, R., Biagini, G., Pumain, R., D'Arcangelo, G., & Tancredi, V. (2002). Network and pharmacological mechanisms leading to

epileptiform synchronization in the limbic system in vitro. *Progress in Neurobiology*, *68*(3), 167–207. https://doi.org/10.1016/S0301-0082(02)00077-1

Baker, A., Kalmbach, B., Morishima, M., Kim, J., Juavinett, A., Li, N., & Dembrow, N. (2018). Specialized Subpopulations of Deep-Layer Pyramidal Neurons in the Neocortex: Bridging Cellular Properties to Functional Consequences. *Journal of Neuroscience*, *38*(24), 5441–5455. https://doi.org/10.1523/JNEUROSCI.0150-18.2018

Balentova, S., & Adamkov, M. (2015). Molecular, Cellular and Functional Effects of Radiation-Induced Brain Injury: A Review. *International Journal of Molecular Sciences*, *16*(11), Article 11. https://doi.org/10.3390/ijms161126068

Bansal, A. K., Vargas-Irwin, C. E., Truccolo, W., & Donoghue, J. P. (2011). Relationships among low-frequency local field potentials, spiking activity, and three-dimensional reach and grasp kinematics in primary motor and ventral premotor cortices. *Journal of Neurophysiology*, *105*(4), 1603–1619. https://doi.org/10.1152/jn.00532.2010

Barbas, H., & Blatt, G. J. (1995). Topographically specific hippocampal projections target functionally distinct prefrontal areas in the rhesus monkey. *Hippocampus*, *5*(6), 511–533. https://doi.org/10.1002/hipo.450050604

Barbero-Castillo, A., Mateos-Aparicio, P., Dalla Porta, L., Camassa, A., Perez-Mendez, L., & Sanchez-Vives, M. V. (2021). Impact of $GABA_A$ and $GABA_B$ Inhibition on Cortical Dynamics and Perturbational Complexity during Synchronous and Desynchronized States. *The Journal of Neuroscience*, *41*(23), 5029–5044. https://doi.org/10.1523/JNEUROSCI.1837-20.2021

Barthas, F., & Kwan, A. C. (2017). Secondary Motor Cortex: Where 'Sensory' Meets 'Motor' in the Rodent Frontal Cortex. *Trends in Neurosciences*, *40*(3), 181–193. https://doi.org/10.1016/j.tins.2016.11.006

Bast, T., Pezze, M., & McGarrity, S. (2017). Cognitive deficits caused by prefrontal cortical and hippocampal neural disinhibition. *British Journal of Pharmacology*, *174*(19), 3211–3225. https://doi.org/10.1111/bph.13850

Bear, J., & Lothman, E. W. (1993). An in vitro study of focal epileptogenesis in combined hippocampal-parahippocampal slices. *Epilepsy Research*, *14*(3), 183–193. https://doi.org/10.1016/0920-1211(93)90043-7

Berdondini, L., Imfeld, K., Maccione, A., Tedesco, M., Neukom, S., Koudelka-Hep, M., & Martinoia, S. (2009). Active pixel sensor array for high spatio-temporal resolution electrophysiological recordings from single cell to large scale neuronal networks. *Lab on a Chip*, *9*(18), 2644–2651. https://doi.org/10.1039/b907394a

Bernard, J. A., & Mittal, V. A. (2015). Updating the research domain criteria: The utility of a motor dimension. *Psychological Medicine*, *45*(13), 2685–2689. https://doi.org/10.1017/S0033291715000872

Betzel, R. F., & Bassett, D. S. (2017). Generative models for network neuroscience: Prospects and promise. *Journal of the Royal Society Interface*, *14*(136), 20170623. https://doi.org/10.1098/rsif.2017.0623

Blonigen, B. J., Steinmetz, R. D., Levin, L., Lamba, M. A., Warnick, R. E., & Breneman, J. C. (2010). Irradiated Volume as a Predictor of Brain Radionecrosis After Linear Accelerator Stereotactic Radiosurgery. *International Journal of Radiation*

*Oncology*Biology*Physics*, *77*(4), 996–1001. https://doi.org/10.1016/j.ijrobp.2009.06.006

Boucher-Routhier, M., & Thivierge, J.-P. (2023). A deep generative adversarial network capturing complex spiral waves in disinhibited circuits of the cerebral cortex. *BMC Neuroscience*, *24*(1), 22. https://doi.org/10.1186/s12868-023-00792-6

Braakman, H. M. H., Vaessen, M. J., Hofman, P. A. M., Debeij-van Hall, M. H. J. A., Backes, W. H., Vles, J. S. H., & Aldenkamp, A. P. (2011). Cognitive and behavioral complications of frontal lobe epilepsy in children: A review of the literature. *Epilepsia*, *52*(5), 849–856. https://doi.org/10.1111/j.1528-1167.2011.03057.x

Bragin, A., Engel Jr, J., Wilson, C. L., Fried, I., & Buzsáki, G. (1999). High-frequency oscillations in human brain. *Hippocampus*, *9*(2), 137–142. https://doi.org/10.1002/(SICI)1098-1063(1999)9:2<137::AID-HIPO5>3.0.CO;2-0

Brière, M.-E., Scott, J. G., McNall-Knapp, R. Y., & Adams, R. L. (2008). Cognitive outcome in pediatric brain tumor survivors: Delayed attention deficit at long-term follow-up. *Pediatric Blood & Cancer*, *50*(2), 337–340. https://doi.org/10.1002/pbc.21223

Bringmann, L. F., Scholte, H. S., & Waldorp, L. J. (2013). Matching Structural, Effective, and Functional Connectivity: A Comparison Between Structural Equation Modeling and Ancestral Graphs. *Brain Connectivity*, *3*(4), 375–385. https://doi.org/10.1089/brain.2012.0130

Brock, A., Donahue, J., & Simonyan, K. (2018). Large scale GAN training for high fidelity natural image synthesis. *arXiv Preprint arXiv:1809.11096*.

Brun, A., & Englund, E. (1981). Regional pattern of degeneration in Alzheimer's disease: Neuronal loss and histopathological grading. *Histopathology*, *5*(5), 549–564. https://doi.org/10.1111/j.1365-2559.1981.tb01818.x

Bullmann, T., Radivojevic, M., Huber, S. T., Deligkaris, K., Hierlemann, A., & Frey, U. (2019). Large-Scale Mapping of Axonal Arbors Using High-Density Microelectrode Arrays. *Frontiers in Cellular Neuroscience*, *13*. https://www.frontiersin.org/articles/10.3389/fncel.2019.00404

Bullmore, E., & Sporns, O. (2009). Complex brain networks: Graph theoretical analysis of structural and functional systems. *Nature Reviews Neuroscience*, *10*(3), 186–198. https://doi.org/10.1038/nrn2575

Buskila, Y., Breen, P. P., Tapson, J., van Schaik, A., Barton, M., & Morley, J. W. (2014). Extending the viability of acute brain slices. *Scientific Reports*, *4*(1), Article 1. https://doi.org/10.1038/srep05309

Buzsáki, G., Anastassiou, C. A., & Koch, C. (2012). The origin of extracellular fields and currents—EEG, ECoG, LFP and spikes. *Nature Reviews. Neuroscience*, *13*(6), 407–420. https://doi.org/10.1038/nrn3241

Buzsáki, G., & Mizuseki, K. (2014). The log-dynamic brain: How skewed distributions affect network operations. *Nature Reviews Neuroscience*, *15*(4), 264–278. https://doi.org/10.1038/nrn3687

Cabungcal, J.-H., Steullet, P., Morishita, H., Kraftsik, R., Cuenod, M., Hensch, T. K., & Do, K. Q. (2013). Perineuronal nets protect fast-spiking interneurons against oxidative

stress. *Proceedings of the National Academy of Sciences*, *110*(22), 9130–9135. https://doi.org/10.1073/pnas.1300454110

Carlén, M. (2017). What constitutes the prefrontal cortex? *Science*, *358*(6362), 478–482. https://doi.org/10.1126/science.aan8868

Carroll, C., Clare, I., Watson, P., Hawkins, M. M., Spoudeas, H., Walker, D., Holland, A., & Ring, H. A. (2013). Effects of Early Childhood Posterior Fossa Tumours on Iq. *Journal of Neurology, Neurosurgery & Psychiatry*, *84*(9), e1–e1. https://doi.org/10.1136/jnnp-2013-306103.8

Cavada, C., Compañy, T., Tejedor, J., Cruz-Rizzolo, R. J., & Reinoso-Suárez, F. (2000). The Anatomical Connections of the Macaque Monkey Orbitofrontal Cortex. A Review. *Cerebral Cortex*, *10*(3), 220–242. https://doi.org/10.1093/cercor/10.3.220

Cavanagh, S. E., Hunt, L. T., & Kennerley, S. W. (2020). A Diversity of Intrinsic Timescales Underlie Neural Computations. *Frontiers in Neural Circuits*, *14*, 615626. https://doi.org/10.3389/fncir.2020.615626

Cefaro, G. A., Genovesi, D., & Perez, C., A. (2013). Delineating Organs at Risk in Radiation Therapy. In *Delineating organs at risk in radiation therapy /*. Springer.

Cenquizca, L. A., & Swanson, L. W. (2007). Spatial organization of direct hippocampal field CA1 axonal projections to the rest of the cerebral cortex. *Brain Research Reviews*, *56*(1), 1–26. https://doi.org/10.1016/j.brainresrev.2007.05.002

Chapin, J. K., & Nicolelis, M. A. (1999). Principal component analysis of neuronal ensemble activity reveals multidimensional somatosensory representations. *Journal of*

Neuroscience Methods, *94*(1), 121–140. https://doi.org/10.1016/s0165-0270(99)00130-2

Chen, Q., Cichon, J., Wang, W., Qiu, L., Lee, S.-J. R., Campbell, N. R., DeStefino, N., Goard, M. J., Fu, Z., Yasuda, R., Looger, L. L., Arenkiel, B. R., Gan, W.-B., & Feng, G. (2012). Imaging Neural Activity Using Thy1-GCaMP Transgenic Mice. *Neuron*, *76*(2), 297–308. https://doi.org/10.1016/j.neuron.2012.07.011

Chen, S. C.-J., Abe, Y., Fang, P.-T., Hsieh, Y.-J., Yang, Y.-I., Lu, T.-Y., Oda, S., Mitani, H., Lian, S.-L., Tyan, Y.-C., Huang, C.-J., & Hisatsune, T. (2017). Prognosis of Hippocampal Function after Sub-lethal Irradiation Brain Injury in Patients with Nasopharyngeal Carcinoma. *Scientific Reports*, *7*(1). Scopus. https://doi.org/10.1038/s41598-017-13972-2

Chen, X., Li, Y., Yao, L., Adeli, E., & Zhang, Y. (2021). Generative adversarial U-Net for domain-free medical image augmentation. *arXiv*. https://doi.org/10.48550/arXiv.2101.04793

Chini, M., & Hanganu-Opatz, I. L. (2021). Prefrontal Cortex Development in Health and Disease: Lessons from Rodents and Humans. *Trends in Neurosciences*, *44*(3), 227–240. https://doi.org/10.1016/j.tins.2020.10.017

Chirasani, S. K. R., & Manikandan, S. (2022). A deep neural network for the classification of epileptic seizures using hierarchical attention mechanism. *Soft Computing*, *26*(11), 5389–5397. https://doi.org/10.1007/s00500-022-07122-8

Clark, A., Donahue, J., & Simonyan, K. (2019). Adversarial video generation on complex datasets. *arXiv Preprint arXiv:1907.06571*.

Cohen–Jonathan, E., Bernhard, E. J., & McKenna, W. G. (1999). How does radiation kill cells? *Current Opinion in Chemical Biology*, *3*(1), 77–83. https://doi.org/10.1016/S1367-5931(99)80014-3

Coltman, B. W., Earley, E. M., Shahar, A., Dudek, F. E., & Ide, C. F. (1995). Factors influencing mossy fiber collateral sprouting in organotypic slice cultures of neonatal mouse hippocampus. *Journal of Comparative Neurology*, *362*(2), 209–222. https://doi.org/10.1002/cne.903620205

Compte, A., Sanchez-Vives, M. V., McCormick, D. A., & Wang, X.-J. (2003). Cellular and network mechanisms of slow oscillatory activity (<1 Hz) and wave propagations in a cortical network model. *Journal of Neurophysiology*, *89*(5), 2707–2725. https://doi.org/10.1152/jn.00845.2002

Constantinople, C. M., & Bruno, R. M. (2011). Effects and Mechanisms of Wakefulness on Local Cortical Networks. *Neuron*, *69*(6), 1061–1068. https://doi.org/10.1016/j.neuron.2011.02.040

Craddock, R. C., Holtzheimer III, P. E., Hu, X. P., & Mayberg, H. S. (2009). Disease state prediction from resting state functional connectivity. *Magnetic Resonance in Medicine*, *62*(6), 1619–1628. https://doi.org/10.1002/mrm.22159

Cuccurullo, V., Di Stasio, G. D., Cascini, G. L., Gatta, G., & Bianco, C. (2019). The Molecular Effects of Ionizing Radiations on Brain Cells: Radiation Necrosis vs. Tumor Recurrence. *Diagnostics*, *9*(4), 127. https://doi.org/10.3390/diagnostics9040127

Cunningham, J. P., & Yu, B. M. (2014). Dimensionality reduction for large-scale neural recordings. *Nature Neuroscience*, *17*(11), 1500–1510. https://doi.org/10.1038/nn.3776

Dagher, A. (2001). The role of the striatum and hippocampus in planning: A PET activation study in Parkinson's disease. *Brain*, *124*(5), 1020–1032. https://doi.org/10.1093/brain/124.5.1020

Dailey, M. E. (2002). 3 - Optical Imaging of Neural Structure and Physiology: Confocal Fluorescence Microscopy in Live Brain Slices. In A. W. Toga & J. C. Mazziotta (Eds.), *Brain Mapping: The Methods (Second Edition)* (pp. 49–76). Academic Press. https://doi.org/10.1016/B978-012693019-1/50005-8

D'Antuono, M., Benini, R., Biagini, G., D'Arcangelo, G., Barbarosie, M., Tancredi, V., & Avoli, M. (2002). Limbic network interactions leading to hyperexcitability in a model of temporal lobe epilepsy. *Journal of Neurophysiology*, *87*(1), 634–639. https://doi.org/10.1152/jn.00351.2001

Davis, Z. W., Muller, L., & Reynolds, J. H. (2022). Spontaneous Spiking Is Governed by Broadband Fluctuations. *Journal of Neuroscience*, *42*(26), 5159–5172. https://doi.org/10.1523/JNEUROSCI.1899-21.2022

De Curtis, M., & Gnatkovsky, V. (2009). Reevaluating the mechanisms of focal ictogenesis: The role of low-voltage fast activity. *Epilepsia*, *50*(12), 2514–2525. https://doi.org/10.1111/j.1528-1167.2009.02249.x

de la Rocha, J., Doiron, B., Shea-Brown, E., Josić, K., & Reyes, A. (2007). Correlation between neural spike trains increases with firing rate. *Nature*, *448*(7155), 802–806. https://doi.org/10.1038/nature06028

Dhariwal, P., & Nichol, A. (2021). Diffusion Models Beat GANs on Image Synthesis *Advances in Neural Information Processing Systems*, *34*, 8780–8794.. arXiv. https://doi.org/10.48550/arXiv.2105.05233

Ding, Z., Zhang, H., Lv, X.-F., Xie, F., Liu, L., Qiu, S., Li, L., & Shen, D. (2018). Radiation-induced brain structural and functional abnormalities in presymptomatic phase and outcome prediction. *Human Brain Mapping*, *39*(1), 407–427. https://doi.org/10.1002/hbm.23852

Dipalo, M., Amin, H., Lovato, L., Moia, F., Caprettini, V., Messina, G. C., Tantussi, F., Berdondini, L., & De Angelis, F. (2017). Intracellular and Extracellular Recording of Spontaneous Action Potentials in Mammalian Neurons and Cardiac Cells with 3D Plasmonic Nanoelectrodes. *Nano Letters*, *17*(6), 3932–3939. https://doi.org/10.1021/acs.nanolett.7b01523

Doersch, C. (2021). *Tutorial on Variational Autoencoders* (arXiv:1606.05908). arXiv. https://doi.org/10.48550/arXiv.1606.05908

Duncan, G. E., Miyamoto, S., Leipzig, J. N., & Lieberman, J. A. (1999). Comparison of brain metabolic activity patterns induced by ketamine, MK-801 and amphetamine in rats: Support for NMDA receptor involvement in responses to subanesthetic dose of ketamine. *Brain Research*, *843*(1), 171–183. https://doi.org/10.1016/S0006-8993(99)01776-X

Dzhala, V. I., & Staley, K. J. (2003). Transition from Interictal to Ictal Activity in Limbic Networks *In Vitro*. *The Journal of Neuroscience*, *23*(21), 7873–7880. https://doi.org/10.1523/JNEUROSCI.23-21-07873.2003

Ecker, A. S., Berens, P., Cotton, R. J., Subramaniyan, M., Denfield, G. H., Cadwell, C. R., Smirnakis, S. M., Bethge, M., & Tolias, A. S. (2014). State dependence of noise correlations in macaque primary visual cortex. *Neuron*, *82*(1), 235–248. https://doi.org/10.1016/j.neuron.2014.02.006

Eguchi, K., Velicky, P., Hollergschwandtner, E., Itakura, M., Fukazawa, Y., Danzl, J. G., & Shigemoto, R. (2020). Advantages of Acute Brain Slices Prepared at Physiological Temperature in the Characterization of Synaptic Functions. *Frontiers in Cellular Neuroscience*, *14*. https://www.frontiersin.org/articles/10.3389/fncel.2020.00063

El Boustani, S., & Destexhe, A. (2010). Brain dynamics at multiple scales: Can one reconcile the apparent low-dimensional chaos of macroscopic variables with the seemingly stochastic behavior of single neurons? *International Journal of Bifurcation and Chaos*, *20*(06), 1687–1702. https://doi.org/10.1142/S0218127410026769

El-Missiry, M. A., Othman, A. I., El-Sawy, M. R., & Lebede, M. F. (2018). Neuroprotective effect of epigallocatechin-3-gallate (EGCG) on radiation-induced damage and apoptosis in the rat hippocampus. *International Journal of Radiation Biology*, *94*(9), 798–808. https://doi.org/10.1080/09553002.2018.1492755

Engel, T. A., & Steinmetz, N. A. (2019). New perspectives on dimensionality and variability from large-scale cortical dynamics. *Current Opinion in Neurobiology*, *58*, 181–190. https://doi.org/10.1016/j.conb.2019.09.003

Ermentrout, G. B., & Kleinfeld, D. (2001). Traveling electrical waves in cortex: Insights from phase dynamics and speculation on a computational role. *Neuron*, *29*(1), 33–44. https://doi.org/10.1016/s0896-6273(01)00178-7

Esteban, C., Hyland, S. L., & Rätsch, G. (2017). Real-valued (medical) time series generation with recurrent conditional gans. *arXiv Preprint arXiv:1706.02633*.

Faisal, A. A., Selen, L. P. J., & Wolpert, D. M. (2008). Noise in the nervous system. *Nature Reviews Neuroscience*, *9*(4), 292–304.

Favaudon, V., Caplier, L., Monceau, V., Pouzoulet, F., Sayarath, M., Fouillade, C., Poupon, M.-F., Brito, I., Hupé, P., Bourhis, J., Hall, J., Fontaine, J.-J., & Vozenin, M.-C. (2014). Ultrahigh dose-rate FLASH irradiation increases the differential response between normal and tumor tissue in mice. *Science Translational Medicine*, *6*(245), 245ra93-245ra93. https://doi.org/10.1126/scitranslmed.3008973

Ferrea, E., Maccione, A., Medrihan, L., Nieus, T., Ghezzi, D., Baldelli, P., Benfenati, F., & Berdondini, L. (2012). Large-scale, high-resolution electrophysiological imaging of field potentials in brain slices with microelectronic multielectrode arrays. *Frontiers in Neural Circuits*, *6*, 80. https://doi.org/10.3389/fncir.2012.00080

Fink, S. L., & Cookson, B. T. (2005). Apoptosis, Pyroptosis, and Necrosis: Mechanistic Description of Dead and Dying Eukaryotic Cells. *Infection and Immunity*, *73*(4), 1907–1916. https://doi.org/10.1128/IAI.73.4.1907-1916.2005

Fried, N. T., Moffat, C., Seifert, E. L., & Oshinsky, M. L. (2014). Functional mitochondrial analysis in acute brain sections from adult rats reveals mitochondrial dysfunction in

a rat model of migraine. *American Journal of Physiology-Cell Physiology*, *307*(11), C1017–C1030. https://doi.org/10.1152/ajpcell.00332.2013

Friston, K. J. (2011). Functional and Effective Connectivity: A Review. *Brain Connectivity*, *1*(1), 13–36. https://doi.org/10.1089/brain.2011.0008

Friston, K. J., Harrison, L., & Penny, W. (2003). Dynamic causal modelling. *NeuroImage*, *19*(4), 1273–1302. https://doi.org/10.1016/S1053-8119(03)00202-7

Fukuda, A., Czurkó, A., Hida, H., Muramatsu, K., Lénárd, L., & Nishino, H. (1995). Appearance of deteriorated neurons on regional different time tables in rat brain thin slices maintained in physiological condition. *Neuroscience Letters*, *184*(1), 13–16. https://doi.org/10.1016/0304-3940(94)11156-D

Furuse, M., Nonoguchi, N., Kawabata, S., Miyatake, S., & Kuroiwa, T. (2015). Delayed brain radiation necrosis: Pathological review and new molecular targets for treatment. *Medical Molecular Morphology*, *48*(4), 183–190. https://doi.org/10.1007/s00795-015-0123-2

Fuster, J. M. (1997). The prefrontal cortex-anatomy. *Physiology and Neuropsychology of the Frontal Lobe*, 6–11.

Gaber, M. W., Sabek, O. M., Fukatsu, K., Wilcox, H. G., Kiani, M. F., & Merchant, T. E. (2003). Differences in ICAM-1 and TNF-α expression between large single fraction and fractionated irradiation in mouse brain. *International Journal of Radiation Biology*, *79*(5), 359–366. https://doi.org/10.1080/0955300031000114738

Godsil, B. P., Kiss, J. P., Spedding, M., & Jay, T. M. (2013). The hippocampal–prefrontal pathway: The weak link in psychiatric disorders? *European*

Neuropsychopharmacology, *23*(10), 1165–1181. https://doi.org/10.1016/j.euroneuro.2012.10.018

Golomb, D. (1998). Models of neuronal transient synchrony during propagation of activity through neocortical circuitry. *Journal of Neurophysiology*, *79*(1), 1–12. https://doi.org/10.1152/jn.1998.79.1.1

Gonzalez-Sulser, A., Wang, J., Motamedi, G. K., Avoli, M., Vicini, S., & Dzakpasu, R. (2011). THE 4-AMINOPYRIDINE IN VITRO EPILEPSY MODEL ANALYZED WITH A PERFORATED MULTI-ELECTRODE ARRAY. *Neuropharmacology*, *60*(7–8), 1142–1153. https://doi.org/10.1016/j.neuropharm.2010.10.007

Goodfellow, I., Pouget-Abadie, J., Mirza, M., Xu, B., Warde-Farley, D., Ozair, S., Courville, A., & Bengio, Y. (2014). Generative adversarial nets. *Advances in Neural Information Processing Systems*, *27*.

Gould, J. (2018). Breaking down the epidemiology of brain cancer. *Nature*, *561*(7724), S40–S41. https://doi.org/10.1038/d41586-018-06704-7

Gouwens, N. W., Zeberg, H., Tsumoto, K., Tateno, T., Aihara, K., & Robinson, H. P. C. (2010). Synchronization of firing in cortical fast-spiking interneurons at gamma frequencies: A phase-resetting analysis. *PLoS Computational Biology*, *6*(9). https://doi.org/10.1371/journal.pcbi.1000951

Grainger, A. I., King, M. C., Nagel, D. A., Parri, H. R., Coleman, M. D., & Hill, E. J. (2018). In vitro Models for Seizure-Liability Testing Using Induced Pluripotent Stem Cells. *Frontiers in Neuroscience*, *12*, 590. https://doi.org/10.3389/fnins.2018.00590

Gray, C. M., König, P., Engel, A. K., & Singer, W. (1989). Oscillatory responses in cat visual cortex exhibit inter-columnar synchronization which reflects global stimulus properties. *Nature*, *338*(6213), 334–337. https://doi.org/10.1038/338334a0

Greene-Schloesser, D., Robbins, M., Peiffer, A., Shaw, E., Chan, M., & Wheeler, K. (2012). Radiation-induced brain injury: A review. *Frontiers in Oncology*, *2*. https://www.frontiersin.org/articles/10.3389/fonc.2012.00073

Grenier, F., Timofeev, I., & Steriade, M. (2001). Focal Synchronization of Ripples (80–200 Hz) in Neocortex and Their Neuronal Correlates. *Journal of Neurophysiology*, *86*(4), 1884–1898. https://doi.org/10.1152/jn.2001.86.4.1884

Gross, G. W., Rieske, E., Kreutzberg, G. W., & Meyer, A. (1977). A new fixed-array multi-microelectrode system designed for long-term monitoring of extracellular single unit neuronal activity in vitro. *Neuroscience Letters*, *6*(2), 101–105. https://doi.org/10.1016/0304-3940(77)90003-9

Gui, J., Sun, Z., Wen, Y., Tao, D., & Ye, J. (2023). A Review on Generative Adversarial Networks: Algorithms, Theory, and Applications. *IEEE Transactions on Knowledge and Data Engineering*, *35*(4), 3313–3332. https://doi.org/10.1109/TKDE.2021.3130191

Gul, Z., Buyukuysal, M. C., & Buyukuysal, R. L. (2020). Brain slice viability determined under normoxic and oxidative stress conditions: Involvement of slice quantity in the medium. *Neurological Research*, *42*(3), 228–238. https://doi.org/10.1080/01616412.2020.1723299

Gulrajani, I., Ahmed, F., Arjovsky, M., Dumoulin, V., & Courville, A. C. (2017). Improved Training of Wasserstein GANs. *Advances in Neural Information Processing Systems*, *30*. https://proceedings.neurips.cc/paper/2017/hash/892c3b1c6dccd52936e27cbd0ff683d6-Abstract.html

Guye, M., Bartolomei, F., & Ranjeva, J.-P. (2008). Imaging structural and functional connectivity: Towards a unified definition of human brain organization?: *Current Opinion in Neurology*, *24*(4), 393–403. https://doi.org/10.1097/WCO.0b013e3283065cfb

Hajian, D. N., Parastesh, F., Rajagopal, K., Jafari, S., & Perc, M. (2023). When do chemical synapses modulate the formation of spiral waves? *Nonlinear Dynamics*, *111*(24), 22551–22565. https://doi.org/10.1007/s11071-023-08994-7

Hamilton, F., Berry, T., & Sauer, T. (2018). Tracking intracellular dynamics through extracellular measurements. *PLOS ONE*, *13*(10), e0205031. https://doi.org/10.1371/journal.pone.0205031

Han, C., Rundo, L., Araki, R., Nagano, Y., Furukawa, Y., Mauri, G., Nakayama, H., & Hayashi, H. (2019). Combining Noise-to-Image and Image-to-Image GANs: Brain MR Image Augmentation for Tumor Detection. *IEEE Access*, *7*, 156966–156977. https://doi.org/10.1109/ACCESS.2019.2947606

Han, F., Caporale, N., & Dan, Y. (2008). Reverberation of recent visual experience in spontaneous cortical waves. *Neuron*, *60*(2), 321–327. https://doi.org/10.1016/j.neuron.2008.08.026

Harshvardhan, G.M., Gourisaria, M. K., Pandey, M., & Rautaray, S. S. (2020). A comprehensive survey and analysis of generative models in machine learning. *Computer Science Review*, *38*, 100285. https://doi.org/10.1016/j.cosrev.2020.100285

Hawellek, D. J., Hipp, J. F., Lewis, C. M., Corbetta, M., & Engel, A. K. (2011). Increased functional connectivity indicates the severity of cognitive impairment in multiple sclerosis. *Proceedings of the National Academy of Sciences*, *108*(47), 19066–19071. https://doi.org/10.1073/pnas.1110024108

He, Y., & Evans, A. (2010). Graph theoretical modeling of brain connectivity. *Current Opinion in Neurology*, *23*(4), 341–350. https://doi.org/10.1097/WCO.0b013e32833aa567

Heusel, M., Ramsauer, H., Unterthiner, T., Nessler, B., & Hochreiter, S. (2017). Gans trained by a two time-scale update rule converge to a local nash equilibrium. *Advances in Neural Information Processing Systems*, *30*.

Hilgen, G., Sorbaro, M., Pirmoradian, S., Muthmann, J.-O., Kepiro, I. E., Ullo, S., Ramirez, C. J., Encinas, A. P., Maccione, A., Berdondini, L., Murino, V., Sona, D., Zanacchi, F. C., Sernagor, E., & Hennig, M. H. (2017). Unsupervised Spike Sorting for Large-Scale, High-Density Multielectrode Arrays. *Cell Reports*, *18*(10), 2521–2532. https://doi.org/10.1016/j.celrep.2017.02.038

Hnilicová, P., Bálentová, S., Kalenská, D., Muríň, P., Hajtmanová, E., & Lehotský, J. (2022). Anatomic and metabolic alterations in the rodent frontal cortex caused by clinically relevant fractionated whole-brain irradiation. *Neurochemistry International*, *154*, 105293. https://doi.org/10.1016/j.neuint.2022.105293

Ho, J., & Salimans, T. (2022). *Classifier-Free Diffusion Guidance* (arXiv:2207.12598). arXiv. https://doi.org/10.48550/arXiv.2207.12598

Honey, C. J., Thivierge, J.-P., & Sporns, O. (2010). Can structure predict function in the human brain? *NeuroImage*, *52*(3), 766–776. https://doi.org/10.1016/j.neuroimage.2010.01.071

Hong, G., & Lieber, C. M. (2019). Novel electrode technologies for neural recordings. *Nature Reviews Neuroscience*, *20*(6), 330–345. https://doi.org/10.1038/s41583-019-0140-6

Hoover, W. B., & Vertes, R. P. (2007). Anatomical analysis of afferent projections to the medial prefrontal cortex in the rat. *Brain Structure and Function*, *212*(2), 149–179. https://doi.org/10.1007/s00429-007-0150-4

Horvát, S., Gămănuț, R., Ercsey-Ravasz, M., Magrou, L., Gămănuț, B., Van Essen, D. C., Burkhalter, A., Knoblauch, K., Toroczkai, Z., & Kennedy, H. (2016). Spatial Embedding and Wiring Cost Constrain the Functional Layout of the Cortical Network of Rodents and Primates. *PLoS Biology*, *14*(7), e1002512. https://doi.org/10.1371/journal.pbio.1002512

Hu, Y., & Sompolinsky, H. (2020). The spectrum of covariance matrices of randomly connected recurrent neuronal networks. *bioRxiv*.

Huang, C., Ruff, D. A., Pyle, R., Rosenbaum, R., Cohen, M. R., & Doiron, B. (2019). Circuit Models of Low-Dimensional Shared Variability in Cortical Networks. *Neuron*, *101*(2), 337-348.e4. https://doi.org/10.1016/j.neuron.2018.11.034

Huang, S., & Uusisaari, M. Y. (2013). Physiological temperature during brain slicing enhances the quality of acute slice preparations. *Frontiers in Cellular Neuroscience*, *7*. https://doi.org/10.3389/fncel.2013.00048

Huang, X., Troy, W. C., Yang, Q., Ma, H., Laing, C. R., Schiff, S. J., & Wu, J.-Y. (2004). Spiral Waves in Disinhibited Mammalian Neocortex. *Journal of Neuroscience*, *24*(44), 9897–9902. https://doi.org/10.1523/JNEUROSCI.2705-04.2004

Huang, X., Xu, W., Liang, J., Takagaki, K., Gao, X., & Wu, J. (2010). Spiral Wave Dynamics in Neocortex. *Neuron*, *68*(5), 978–990. https://doi.org/10.1016/j.neuron.2010.11.007

Hughes, J. R., & Parsons, J. L. (2020). FLASH Radiotherapy: Current Knowledge and Future Insights Using Proton-Beam Therapy. *International Journal of Molecular Sciences*, *21*(18), Article 18. https://doi.org/10.3390/ijms21186492

Humpel, C. (2015). Organotypic brain slice cultures: A review. *Neuroscience*, *305*, 86–98. https://doi.org/10.1016/j.neuroscience.2015.07.086

Igelström, K. M., Shirley, C. H., & Heyward, P. M. (2011). Low-magnesium medium induces epileptiform activity in mouse olfactory bulb slices. *Journal of Neurophysiology*, *106*(5), 2593–2605. https://doi.org/10.1152/jn.00601.2011

Ilakiyaselvan, N., Nayeemulla Khan, A., & Shahina, A. (2020). Deep learning approach to detect seizure using reconstructed phase space images. *Journal of Biomedical Research*, *34*(3), 240–250. https://doi.org/10.7555/JBR.34.20190043

Ilias, L., Askounis, D., & Psarras, J. (2023). Multimodal detection of epilepsy with deep neural networks. *Expert Systems with Applications*, *213*, 119010. https://doi.org/10.1016/j.eswa.2022.119010

Imfeld, K., Garenne, A., Martinoia, S., Koudelka-Hep, M., & Berdondini, L. (2007). Motivations and APS-based solution for high-resolution extracellular recording from in-vitro neuronal networks. *2007 3rd International IEEE/EMBS Conference on Neural Engineering*, 225–228. https://doi.org/10.1109/CNE.2007.369652

Imfeld, K., Neukom, S., Maccione, A., Bornat, Y., Martinoia, S., Farine, P.-A., Koudelka-Hep, M., & Berdondini, L. (2008). Large-scale, high-resolution data acquisition system for extracellular recording of electrophysiological activity. *IEEE Transactions on Bio-Medical Engineering*, *55*(8), 2064–2073. https://doi.org/10.1109/TBME.2008.919139

Jabbar, A., Li, X., & Omar, B. (2021). A Survey on Generative Adversarial Networks: Variants, Applications, and Training. *ACM Computing Surveys*, *54*(8), 157:1-157:49. https://doi.org/10.1145/3463475

Jay, T. M., & Witter, M. P. (1991). Distribution of hippocampal CA1 and subicular efferents in the prefrontal cortex of the rat studied by means of anterograde transport of Phaseolus vulgaris-leucoagglutinin. *The Journal of Comparative Neurology*, *313*(4), 574–586. https://doi.org/10.1002/cne.903130404

Jirsa, V. K., Stacey, W. C., Quilichini, P. P., Ivanov, A. I., & Bernard, C. (2014). On the nature of seizure dynamics. *Brain: A Journal of Neurology*, *137*(Pt 8), 2210–2230. https://doi.org/10.1093/brain/awu133

Jiruska, P., de Curtis, M., Jefferys, J. G. R., Schevon, C. A., Schiff, S. J., & Schindler, K. (2013). Synchronization and desynchronization in epilepsy: Controversies and hypotheses. *The Journal of Physiology*, *591*(4), 787–797. https://doi.org/10.1113/jphysiol.2012.239590

Jobst, B. C., Siegel, A. M., Thadani, V. M., Roberts, D. W., Rhodes, H. C., & Williamson, P. D. (2000). Intractable Seizures of Frontal Lobe Origin: Clinical Characteristics, Localizing Signs, and Results of Surgery. *Epilepsia*, *41*(9), 1139–1152. https://doi.org/10.1111/j.1528-1157.2000.tb00319.x

Johansen-Berg, H., & Behrens, T. E. (2006). Just pretty pictures? What diffusion tractography can add in clinical neuroscience. *Current Opinion in Neurology*, *19*(4), 379–385. https://doi.org/10.1097/01.wco.0000236618.82086.01

Kale, A., Pişkin, Ö., Baş, Y., Aydın, B. G., Can, M., Elmas, Ö., & Büyükuysal, Ç. (2018). Neuroprotective effects of Quercetin on radiation-induced brain injury in rats. *Journal of Radiation Research*, *59*(4), 404–410. https://doi.org/10.1093/jrr/rry032

Kam, W. W.-Y., & Banati, R. B. (2013). Effects of ionizing radiation on mitochondria. *Free Radical Biology and Medicine*, *65*(Complete), 607–619. https://doi.org/10.1016/j.freeradbiomed.2013.07.024

Karras, T., Laine, S., & Aila, T. (2019). A style-based generator architecture for generative adversarial networks. *Proceedings of the IEEE/CVF Conference on Computer Vision and Pattern Recognition*, 4401–4410.

Karunamuni, R., Bartsch, H., White, N. S., Moiseenko, V., Carmona, R., Marshall, D. C., Seibert, T. M., McDonald, C. R., Farid, N., Krishnan, A., Kuperman, J., Mell, L., Brewer, J. B., Dale, A. M., & Hattangadi-Gluth, J. A. (2016). Dose-Dependent Cortical Thinning After Partial Brain Irradiation in High-Grade Glioma. *International Journal of Radiation Oncology*Biology*Physics*, *94*(2), 297–304. https://doi.org/10.1016/j.ijrobp.2015.10.026

Keane, A., & Gong, P. (2015). Propagating Waves Can Explain Irregular Neural Dynamics. *Journal of Neuroscience*, *35*(4), 1591–1605. https://doi.org/10.1523/JNEUROSCI.1669-14.2015

Kempf, S. J., Sepe, S., von Toerne, C., Janik, D., Neff, F., Hauck, S. M., Atkinson, M. J., Mastroberardino, P. G., & Tapio, S. (2015). Neonatal Irradiation Leads to Persistent Proteome Alterations Involved in Synaptic Plasticity in the Mouse Hippocampus and Cortex. *Journal of Proteome Research*, *14*(11), 4674–4686. https://doi.org/10.1021/acs.jproteome.5b00564

Kim, Y., Perova, Z., Mirrione, M. M., Pradhan, K., Henn, F. A., Shea, S., Osten, P., & Li, B. (2016). Whole-Brain Mapping of Neuronal Activity in the Learned Helplessness Model of Depression. *Frontiers in Neural Circuits*, *10*. https://doi.org/10.3389/fncir.2016.00003

Kingma, D. P., & Ba, J. (2014). Adam: A method for stochastic optimization. *arXiv Preprint arXiv:1412.6980*.

Kingma, D. P., & Welling, M. (2019). An introduction to variational autoencoders. *Foundations and Trends® in Machine Learning*, *12*(4), 307–392. https://doi.org/10.1561/2200000056

Kohn, A., Jasper, A. I., Semedo, J. D., Gokcen, E., Machens, C. K., & Yu, B. M. (2020). Principles of Corticocortical Communication: Proposed Schemes and Design Considerations. *Trends in Neurosciences*, *43*(9), 725–737. https://doi.org/10.1016/j.tins.2020.07.001

Koltchine, V. V., Finn, S. E., Jenkins, A., Nikolaeva, N., Lin, A., & Harrison, N. L. (1999). Agonist Gating and Isoflurane Potentiation in the Human γ-Aminobutyric Acid Type A Receptor Determined by the Volume of a Second Transmembrane Domain Residue. *Molecular Pharmacology*, *56*(5), 1087–1093. https://doi.org/10.1124/mol.56.5.1087

Konstantinou, N., Pettemeridou, E., Stamatakis, E. A., Seimenis, I., & Constantinidou, F. (2019). Altered Resting Functional Connectivity Is Related to Cognitive Outcome in Males With Moderate-Severe Traumatic Brain Injury. *Frontiers in Neurology*, *9*. https://www.frontiersin.org/articles/10.3389/fneur.2018.01163

Kornev, M. A., Kulikova, E. A., & Kul'bakh, O. S. (2005). The Cellular Composition of the Cerebral Cortex of Rat Fetuses after Fractionated Low-Dose Irradiation. *Neuroscience and Behavioral Physiology*, *35*(6), 635–638. https://doi.org/10.1007/s11055-005-0104-3

Korytko, T., Radivoyevitch, T., Colussi, V., Wessels, B. W., Pillai, K., Maciunas, R. J., & Einstein, D. B. (2006). 12 Gy gamma knife radiosurgical volume is a predictor for radiation necrosis in non-AVM intracranial tumors. *International Journal of Radiation Oncology*Biology*Physics*, *64*(2), 419–424. https://doi.org/10.1016/j.ijrobp.2005.07.980

Kovács, Á., Emri, M., Opposits, G., Pisák, T., Vandulek, C., Glavák, C., Szalai, Z., Biró, G., Bajzik, G., & Repa, I. (2015). Changes in functional MRI signals after 3D based radiotherapy of glioblastoma multiforme. *Journal of Neuro-Oncology*, *125*(1), 157–166. https://doi.org/10.1007/s11060-015-1882-2

Kovalchuk, A., & Kolb, B. (2017). Low dose radiation effects on the brain – from mechanisms and behavioral outcomes to mitigation strategies. *Cell Cycle*, *16*(13), 1266–1270. https://doi.org/10.1080/15384101.2017.1320003

Kramer, M. A., & Cash, S. S. (2012). Epilepsy as a Disorder of Cortical Network Organization. *The Neuroscientist*, *18*(4), 360–372. https://doi.org/10.1177/1073858411422754

Kramer, M. A., Eden, U. T., Kolaczyk, E. D., Zepeda, R., Eskandar, E. N., & Cash, S. S. (2010). Coalescence and Fragmentation of Cortical Networks during Focal Seizures. *Journal of Neuroscience*, *30*(30), 10076–10085. https://doi.org/10.1523/JNEUROSCI.6309-09.2010

Kuebler, E. S., Tauskela, J. S., Aylsworth, A., Zhao, X., & Thivierge, J.-P. (2015). Burst predicting neurons survive an in vitro glutamate injury model of cerebral ischemia. *Scientific Reports*, *5*(1), Article 1. https://doi.org/10.1038/srep17718

Lang, S., Gaxiola-Valdez, I., Opoku-Darko, M., Partlo, L. A., Goodyear, B. G., Kelly, J. J. P., & Federico, P. (2017). Functional Connectivity in Frontoparietal Network: Indicator of Preoperative Cognitive Function and Cognitive Outcome Following Surgery in Patients with Glioma. *World Neurosurgery*, *105*, 913-922.e2. https://doi.org/10.1016/j.wneu.2017.05.149

Laubach, M., Amarante, L. M., Swanson, K., & White, S. R. (2018). What, If Anything, Is Rodent Prefrontal Cortex? *eNeuro*, *5*(5). https://doi.org/10.1523/ENEURO.0315-18.2018

Le Van Quyen, M., Navarro, V., Martinerie, J., Baulac, M., & Varela, F. J. (2003). Toward a Neurodynamical Understanding of Ictogenesis. *Epilepsia*, *44*(s12), 30–43. https://doi.org/10.1111/j.0013-9580.2003.12007.x

Legatt, A. D., Arezzo, J., & Vaughan, H. G. (1980). Averaged multiple unit activity as an estimate of phasic changes in local neuronal activity: Effects of volume-conducted potentials. *Journal of Neuroscience Methods*, *2*(2), 203–217. https://doi.org/10.1016/0165-0270(80)90061-8

Lein, P. J., Barnhart, C. D., & Pessah, I. N. (2011). Acute Hippocampal Slice Preparation and Hippocampal Slice Cultures. *Methods in Molecular Biology (Clifton, N.J.)*, *758*, 115–134. https://doi.org/10.1007/978-1-61779-170-3_8

Letzkus, J. J., Wolff, S. B. E., & Lüthi, A. (2015). Disinhibition, a Circuit Mechanism for Associative Learning and Memory. *Neuron*, *88*(2), 264–276. https://doi.org/10.1016/j.neuron.2015.09.024

Levina, E., & Bickel, P. J. (2004). Maximum Likelihood Estimation of Intrinsic Dimension: Neural Information Processing Systems: NIPS. *Vancouver, CA*.

Levy, R. B., & Reyes, A. D. (2012). Spatial profile of excitatory and inhibitory synaptic connectivity in mouse primary auditory cortex. *The Journal of Neuroscience: The Official Journal of the Society for Neuroscience*, *32*(16), 5609–5619. https://doi.org/10.1523/JNEUROSCI.5158-11.2012

Lewicki, M. S. (1998). *A review of methods for spike sorting: The detection and classification of neural action potentials*. *9*(4), R53-77.

Lewis, D. A., Hashimoto, T., & Volk, D. W. (2005). Cortical inhibitory neurons and schizophrenia. *Nature Reviews Neuroscience*, *6*(4), 312–324. https://doi.org/10.1038/nrn1648

Lin, I.-C., Okun, M., Carandini, M., & Harris, K. D. (2015). The Nature of Shared Cortical Variability. *Neuron*, *87*(3), 644–656. https://doi.org/10.1016/j.neuron.2015.06.035

Liou, J., Smith, E. H., Bateman, L. M., Bruce, S. L., McKhann, G. M., Goodman, R. R., Emerson, R. G., Schevon, C. A., & Abbott, L. (2020). A model for focal seizure onset, propagation, evolution, and progression. *eLife*, *9*, e50927. https://doi.org/10.7554/eLife.50927

Lipton, P., Aitken, P. G., Dudek, F. E., Eskessen, K., Espanol, M. T., Ferchmin, P. A., Kelly, J. B., Kreisman, N. R., Landfield, P. W., Larkman, P. M., Leybaert, L., Newman, G. C., Panizzon, K. L., Payne, R. S., Phillips, P., Raley-Susman, K. M., Rice, M. E., Santamaria, R., Sarvey, J. M., … Wallis, R. (1995). Making the best of brain slices: Comparing preparative methods. *Journal of Neuroscience Methods*, *59*(1), 151–156. https://doi.org/10.1016/0165-0270(94)00205-U

Litwin-Kumar, A., Harris, K. D., Axel, R., Sompolinsky, H., & Abbott, L. F. (2017). Optimal Degrees of Synaptic Connectivity. *Neuron*, *93*(5), 1153-1164.e7. https://doi.org/10.1016/j.neuron.2017.01.030

Liu, M., Song, C., Liang, Y., Knöpfel, T., & Zhou, C. (2019). Assessing spatiotemporal variability of brain spontaneous activity by multiscale entropy and functional connectivity. *NeuroImage*, *198*, 198–220. https://doi.org/10.1016/j.neuroimage.2019.05.022

Logothetis, N. K., Pauls, J., Augath, M., Trinath, T., & Oeltermann, A. (2001). Neurophysiological investigation of the basis of the fMRI signal. *Nature*, *412*(6843), 150–157. https://doi.org/10.1038/35084005

Lyamzin, D. R., Macke, J. H., & Lesica, N. A. (2010). Modeling Population Spike Trains with Specified Time-Varying Spike Rates, Trial-to-Trial Variability, and Pairwise Signal and Noise Correlations. *Frontiers in Computational Neuroscience*, *4*, 144. https://doi.org/10.3389/fncom.2010.00144

Ma, Q., Wu, D., Zeng, L.-L., Shen, H., Hu, D., & Qiu, S. (2016). Radiation-induced functional connectivity alterations in nasopharyngeal carcinoma patients with radiotherapy. *Medicine*, *95*(29), e4275. https://doi.org/10.1097/MD.0000000000004275

Manford, M., Hart, Y., Sander, L., & Shorvon, S. (1992). National General Practice Study of Epilepsy (NGPSE): Partial seizure patterns in a general population. *Neurology*, *42*, 1911–1917. https://doi.org/10.1212/WNL.42.10.1911

Mariño, J., Schummers, J., Lyon, D. C., Schwabe, L., Beck, O., Wiesing, P., Obermayer, K., & Sur, M. (2005). Invariant computations in local cortical networks with balanced excitation and inhibition. *Nature Neuroscience*, *8*(2), 194–201. https://doi.org/10.1038/nn1391

Mathieu, M., Couprie, C., & LeCun, Y. (2015). Deep multi-scale video prediction beyond mean square error. *arXiv Preprint arXiv:1511.05440*.

Matuszak, N., Suchorska, W. M., Milecki, P., Kruszyna-Mochalska, M., Misiarz, A., Pracz, J., & Malicki, J. (2022). FLASH radiotherapy: An emerging approach in radiation therapy.

Reports of Practical Oncology and Radiotherapy, *27*(2), Article 2. https://doi.org/10.5603/RPOR.a2022.0038

Mazzoni, A., Broccard, F. D., Garcia-Perez, E., Bonifazi, P., Ruaro, M. E., & Torre, V. (2007). On the Dynamics of the Spontaneous Activity in Neuronal Networks. *PLOS ONE*, *2*(5), e439. https://doi.org/10.1371/journal.pone.0000439

Mazzucato, L., Fontanini, A., & La Camera, G. (2016). Stimuli Reduce the Dimensionality of Cortical Activity. *Frontiers in Systems Neuroscience*, *10*, 11. https://doi.org/10.3389/fnsys.2016.00011

McGonigal, A. (2022). Frontal lobe seizures: Overview and update. *Journal of Neurology*, *269*(6), 3363–3371. https://doi.org/10.1007/s00415-021-10949-0

McGonigal, A., Sahgal, A., De Salles, A., Hayashi, M., Levivier, M., Ma, L., Martinez, R., Paddick, I., Ryu, S., Slotman, B. J., & Régis, J. (2017). Radiosurgery for epilepsy: Systematic review and International Stereotactic Radiosurgery Society (ISRS) practice guideline. *Epilepsy Research*, *137*(Complete), 123–131. https://doi.org/10.1016/j.eplepsyres.2017.08.016

Menick, J., & Kalchbrenner, N. (2018). Generating high fidelity images with subscale pixel networks and multidimensional upscaling. *arXiv Preprint arXiv:1812.01608*.

Miller, E. K., & Cohen, J. D. (2001). An Integrative Theory of Prefrontal Cortex Function. *Annual Review of Neuroscience*, *24*(1), 167–202. https://doi.org/10.1146/annurev.neuro.24.1.167

Mitchell, T. J., Seitzman, B. A., Ballard, N., Petersen, S. E., Shimony, J. S., & Leuthardt, E. C. (2020). Human Brain Functional Network Organization Is Disrupted After Whole-

Brain Radiation Therapy. *Brain Connectivity*, *10*(1), 29–38. https://doi.org/10.1089/brain.2019.0713

Mitzdorf, U. (1985). Current source-density method and application in cat cerebral cortex: Investigation of evoked potentials and EEG phenomena. *Physiological Reviews*, *65*(1), 37–100. https://doi.org/10.1152/physrev.1985.65.1.37

Miyamoto, S., Leipzig, J. N., Lieberman, J. A., & Duncan, G. E. (2000). Effects of Ketamine, MK-801, and Amphetamine on Regional Brain 2-Deoxyglucose Uptake in Freely Moving Mice. *Neuropsychopharmacology*, *22*(4), 400–412. https://doi.org/10.1016/S0893-133X(99)00127-X

Miyatake, S.-I., Nonoguchi, N., Furuse, M., Yoritsune, E., Miyata, T., Kawabata, S., & Kuroiwa, T. (2015). Pathophysiology, Diagnosis, and Treatment of Radiation Necrosis in the Brain. *Neurologia Medico-Chirurgica*, *55*(1), 50–59. https://doi.org/10.2176/nmc.ra.2014-0188

Mogren, O. (2016). *C-RNN-GAN: Continuous recurrent neural networks with adversarial training*. https://doi.org/10.48550/arXiv.1611.09904

Mohajerani, M. H., Aminoltejari, K., & Murphy, T. H. (2011). Targeted mini-strokes produce changes in interhemispheric sensory signal processing that are indicative of disinhibition within minutes. *Proceedings of the National Academy of Sciences of the United States of America*, *108*(22), 8932–8933.

Monchi, O., Petrides, M., Mejia-Constain, B., & Strafella, A. P. (2006). Cortical activity in Parkinson's disease during executive processing depends on striatal involvement. *Brain*, *130*(1), 233–244. https://doi.org/10.1093/brain/awl326

Monje, M. (2008). Cranial radiation therapy and damage to hippocampal neurogenesis. *Developmental Disabilities Research Reviews*, *14*(3), 238–242. https://doi.org/10.1002/ddrr.26

Montay-Gruel, P., Petersson, K., Jaccard, M., Boivin, G., Germond, J.-F., Petit, B., Doenlen, R., Favaudon, V., Bochud, F., Bailat, C., Bourhis, J., & Vozenin, M.-C. (2017). Irradiation in a flash: Unique sparing of memory in mice after whole brain irradiation with dose rates above 100Gy/s. *Radiotherapy and Oncology*, *124*(3), 365–369. https://doi.org/10.1016/j.radonc.2017.05.003

Mulhern, R. K., Merchant, T. E., Gajjar, A., Reddick, W. E., & Kun, L. E. (2004). Late neurocognitive sequelae in survivors of brain tumours in childhood. *The Lancet Oncology*, *5*(7), 399–408. https://doi.org/10.1016/S1470-2045(04)01507-4

Muller, L., Chavane, F., Reynolds, J., & Sejnowski, T. J. (2018). Cortical travelling waves: Mechanisms and computational principles. *Nature Reviews Neuroscience*, *19*(5), Article 5. https://doi.org/10.1038/nrn.2018.20

Nadeau, S. E. (2020). Neural Population Dynamics and Cognitive Function. *Frontiers in Human Neuroscience*, *14*. https://www.frontiersin.org/articles/10.3389/fnhum.2020.00050

Nicolelis, M. A., Baccala, L. A., Lin, R. C., & Chapin, J. K. (1995). Sensorimotor encoding by synchronous neural ensemble activity at multiple levels of the somatosensory system. *Science (New York, N.Y.)*, *268*(5215), 1353–1358. https://doi.org/10.1126/science.7761855

Northoff, G. (2018). The brain's spontaneous activity and its psychopathological symptoms – "Spatiotemporal binding and integration." *Progress in Neuro-Psychopharmacology and Biological Psychiatry*, *80*, 81–90. https://doi.org/10.1016/j.pnpbp.2017.03.019

Obien, M. E. J., Deligkaris, K., Bullmann, T., Bakkum, D. J., & Frey, U. (2015). Revealing neuronal function through microelectrode array recordings. *Frontiers in Neuroscience*, *8*. https://www.frontiersin.org/articles/10.3389/fnins.2014.00423

Oka, H., Shimono, K., Ogawa, R., Sugihara, H., & Taketani, M. (1999). A new planar multielectrode array for extracellular recording: Application to hippocampal acute slice. *Journal of Neuroscience Methods*, *93*(1), 61–67. https://doi.org/10.1016/s0165-0270(99)00113-2

Pacico, N., & Mingorance-Le Meur, A. (2014). New in vitro phenotypic assay for epilepsy: Fluorescent measurement of synchronized neuronal calcium oscillations. *PloS One*, *9*(1), e84755. https://doi.org/10.1371/journal.pone.0084755

Palkar, G., Wu, J., & Ermentrout, B. (2023). The inhibitory control of traveling waves in cortical networks. *PLOS Computational Biology*, *19*(9), e1010697. https://doi.org/10.1371/journal.pcbi.1010697

Pang, R., Lansdell, B. J., & Fairhall, A. L. (2016). Dimensionality reduction in neuroscience. *Current Biology*, *26*(14), R656–R660. https://doi.org/10.1016/j.cub.2016.05.029

Paninski, L., & Cunningham, J. (2018). Neural data science: Accelerating the experiment-analysis-theory cycle in large-scale neuroscience. *Current Opinion in Neurobiology*, *50*, 232–241. https://doi.org/10.1016/j.conb.2018.04.007

Panwala, T. F., Fox, M. E., Tucker, T. D., & King, T. Z. (2019). The Effects of Radiation and Sex Differences on Adaptive Functioning in Adult Survivors of Pediatric Posterior Fossa Brain Tumors. *Journal of the International Neuropsychological Society*, *25*(7), 729–739. https://doi.org/10.1017/S135561771900033X

Panzeri, S., Brunel, N., Logothetis, N. K., & Kayser, C. (2010). Sensory neural codes using multiplexed temporal scales. *Trends in Neurosciences*, *33*(3), 111–120. https://doi.org/10.1016/j.tins.2009.12.001

Patrikelis, P., Angelakis, E., & Gatzonis, S. (2009). Neurocognitive and behavioral functioning in frontal lobe epilepsy: A review. *Epilepsy & Behavior*, *14*(1), 19–26. https://doi.org/10.1016/j.yebeh.2008.09.013

Peca, J., Feliciano, C., Ting, J. T., Wang, W., Wells, M. F., Venkatraman, T. N., Lascola, C. D., Fu, Z., & Feng, G. (2011). Shank3 mutant mice display autistic-like behaviours and striatal dysfunction. *Nature*, *472*(7344), 437–447. https://doi.org/10.1038/nature09965

Perry, A. E., & Chong, M. S. (1987). A Description of Eddying Motions and Flow Patterns Using Critical-Point Concepts. *Annual Review of Fluid Mechanics*, *19*(Volume 19, 1987), 125–155. https://doi.org/10.1146/annurev.fl.19.010187.001013

Pine, J. (1980). Recording action potentials from cultured neurons with extracellular microcircuit electrodes. *Journal of Neuroscience Methods*, *2*(1), 19–31. https://doi.org/10.1016/0165-0270(80)90042-4

Pinto, D. J., Patrick, S. L., Huang, W. C., & Connors, B. W. (2005). Initiation, propagation, and termination of epileptiform activity in rodent neocortex in vitro involve distinct

mechanisms. *The Journal of Neuroscience*, *25*(36), 8131–8140. https://doi.org/10.1523/JNEUROSCI.2278-05.2005

Postnikova, T. Y., Amakhin, D. V., Trofimova, A. M., & Zaitsev, A. V. (2020). Calcium-permeable AMPA receptors are essential to the synaptic plasticity induced by epileptiform activity in rat hippocampal slices. *Biochemical and Biophysical Research Communications*, *529*(4), 1145–1150. https://doi.org/10.1016/j.bbrc.2020.06.121

Poulet, J. F. A., & Crochet, S. (2019). The Cortical States of Wakefulness. *Frontiers in Systems Neuroscience*, *12*. https://www.frontiersin.org/articles/10.3389/fnsys.2018.00064

Prentice, J. S., Homann, J., Simmons, K. D., Tkačik, G., Balasubramanian, V., & Nelson, P. C. (2011). Fast, Scalable, Bayesian Spike Identification for Multi-Electrode Arrays. *PLOS ONE*, *6*(7), e19884. https://doi.org/10.1371/journal.pone.0019884

Quigg, M., Rolston, J., & Barbaro, N. M. (2012). Radiosurgery for epilepsy: Clinical experience and potential antiepileptic mechanisms. *Epilepsia*, *53*(1), 7–15. https://doi.org/10.1111/j.1528-1167.2011.03339.x

Rabinowitz, N. C., Goris, R. L., Cohen, M., & Simoncelli, E. P. (2015). Attention stabilizes the shared gain of V4 populations. *eLife*, *4*, e08998. https://doi.org/10.7554/eLife.08998

Rachmadi, M. F., Valdés-Hernández, M. del C., Makin, S., Wardlaw, J., & Komura, T. (2020). Automatic spatial estimation of white matter hyperintensities evolution in brain MRI using disease evolution predictor deep neural networks. *Medical Image Analysis*, *63*, 101712. https://doi.org/10.1016/j.media.2020.101712

Ramanathan, D. S., Guo, L., Gulati, T., Davidson, G., Hishinuma, A. K., Won, S.-J., Knight, R. T., Chang, E. F., Swanson, R. A., & Ganguly, K. (2018). Low frequency cortical activity is a neuromodulatory target that tracks recovery after stroke. *Nature Medicine*, *24*(8), 1257–1267. https://doi.org/10.1038/s41591-018-0058-y

Ranchet, M., Hoang, I., Cheminon, M., Derollepot, R., Devos, H., Perrey, S., Luauté, J., Danaila, T., & Paire-Ficout, L. (2020). Changes in Prefrontal Cortical Activity During Walking and Cognitive Functions Among Patients With Parkinson's Disease. *Frontiers in Neurology*, *11*. https://www.frontiersin.org/articles/10.3389/fneur.2020.601686

Ravi, D., Blumberg, S. B., Ingala, S., Barkhof, F., Alexander, D. C., & Oxtoby, N. P. (2022). Degenerative adversarial neuroimage nets for brain scan simulations: Application in ageing and dementia. *Medical Image Analysis*, *75*, 102257. https://doi.org/10.1016/j.media.2021.102257

Razavi, A., Van den Oord, A., & Vinyals, O. (2019). Generating diverse high-fidelity images with vq-vae-2. *Advances in Neural Information Processing Systems*, *32*.

Redmond, K. J., Gui, C., Benedict, S., Milano, M. T., Grimm, J., Vargo, J. A., Soltys, S. G., Yorke, E., Jackson, A., El Naqa, I., Marks, L. B., Xue, J., Heron, D. E., & Kleinberg, L. R. (2021). Tumor Control Probability of Radiosurgery and Fractionated Stereotactic Radiosurgery for Brain Metastases. *International Journal of Radiation Oncology*Biology*Physics*, *110*(1), 53–67. https://doi.org/10.1016/j.ijrobp.2020.10.034

Reep, R. L., & Corwin, J. V. (1999). Topographic organization of the striatal and thalamic connections of rat medial agranular cortex. *Brain Research*, *841*(1), 43–52. https://doi.org/10.1016/S0006-8993(99)01779-5

Reep, R. L., Corwin, J. V., Hashimoto, A., & Watson, R. T. (1987). Efferent Connections of the Rostral Portion of Medial Agranular Cortex in Rats. *Brain Research Bulletin*, *19*(2), 203–221. https://doi.org/10.1016/0361-9230(87)90086-4

Reep, R. L., Goodwin, G. S., & Corwin, J. V. (1990). Topographic organization in the corticocortical connections of medial agranular cortex in rats. *Journal of Comparative Neurology*, *294*(2), 262–280. https://doi.org/10.1002/cne.902940210

Reinhart, R. M. G., & Woodman, G. F. (2014). Oscillatory Coupling Reveals the Dynamic Reorganization of Large-scale Neural Networks as Cognitive Demands Change. *Journal of Cognitive Neuroscience*, *26*(1), 175–188. https://doi.org/10.1162/jocn_a_00470

Ren, C., Peng, K., Yang, R., Liu, W., Liu, C., & Komiyama, T. (2022). Global and subtype-specific modulation of cortical inhibitory neurons regulated by acetylcholine during motor learning. *Neuron*, *110*(14), 2334-2350.e8. https://doi.org/10.1016/j.neuron.2022.04.031

Reynolds, T. A., Jensen, A. R., Bellairs, E. E., & Ozer, M. (2020). Dose Gradient Index for Stereotactic Radiosurgery/Radiation Therapy. *International Journal of Radiation Oncology*Biology*Physics*, *106*(3), 604–611. https://doi.org/10.1016/j.ijrobp.2019.11.408

Rigotti, M., Barak, O., Warden, M. R., Wang, X.-J., Daw, N. D., Miller, E. K., & Fusi, S. (2013). The importance of mixed selectivity in complex cognitive tasks. *Nature*, *497*(7451), 585–590. https://doi.org/10.1038/nature12160

Robbins, T. W., & Arnsten, A. F. T. (2009). The Neuropsychopharmacology of Fronto-Executive Function: Monoaminergic Modulation. *Annual Review of Neuroscience*, *32*, 267–287. https://doi.org/10.1146/annurev.neuro.051508.135535

Ronneberger, O., Fischer, P., & Brox, T. (2015). *U-net: Convolutional networks for biomedical image segmentation*. 234–241.

Rose, J. E., & Woosley, C. N. (1948). The orbitofrontal cortex and its connections with the mediodorsal nucleus in rabbit, sheep and cat. *Research Publications - Association for Research in Nervous and Mental Disease*, *27 (1 vol.)*, 210–232.

Rossant, C., Kadir, S. N., Goodman, D. F. M., Schulman, J., Hunter, M. L. D., Saleem, A. B., Grosmark, A., Belluscio, M., Denfield, G. H., Ecker, A. S., Tolias, A. S., Solomon, S., Buzsáki, G., Carandini, M., & Harris, K. D. (2016). Spike sorting for large, dense electrode arrays. *Nature Neuroscience*, *19*(4), 634–641. https://doi.org/10.1038/nn.4268

Rudy, B., Fishell, G., Lee, S., & Hjerling-Leffler, J. (2011). Three groups of interneurons account for nearly 100% of neocortical GABAergic neurons. *Developmental Neurobiology*, *71*(1), 45–61. https://doi.org/10.1002/dneu.20853

Rule, M. E., Vargas-Irwin, C., Donoghue, J. P., & Truccolo, W. (2018). Phase reorganization leads to transient β-LFP spatial wave patterns in motor cortex during steady-state

movement preparation. *Journal of Neurophysiology*, *119*(6), 2212–2228. https://doi.org/10.1152/jn.00525.2017

Rykhlevskaia, E., Gratton, G., & Fabiani, M. (2008). Combining structural and functional neuroimaging data for studying brain connectivity: A review. *Psychophysiology*, *45*(2), 173–187. https://doi.org/10.1111/j.1469-8986.2007.00621.x

Saberi, A., Paquola, C., Wagstyl, K., Hettwer, M. D., Bernhardt, B. C., Eickhoff, S. B., & Valk, S. L. (2023). The regional variation of laminar thickness in the human isocortex is related to cortical hierarchy and interregional connectivity. *PLoS Biology*, *21*(11), e3002365–e3002365. https://doi.org/10.1371/journal.pbio.3002365

Saito, M., Matsumoto, E., & Saito, S. (2017). Temporal generative adversarial nets with singular value clipping. *Proceedings of the IEEE International Conference on Computer Vision*, 2830–2839.

Salehi, P., Chalechale, A., & Taghizadeh, M. (2020). *Generative Adversarial Networks (GANs): An Overview of Theoretical Model, Evaluation Metrics, and Recent Developments* (arXiv:2005.13178). arXiv. https://doi.org/10.48550/arXiv.2005.13178

Salimans, T., Goodfellow, I., Zaremba, W., Cheung, V., Radford, A., & Chen, X. (2016, June 10). *Improved Techniques for Training GANs*. arXiv.Org. https://doi.org/10.48550/arXiv.1606.03498

Sanchez-Vives, M., & Mattia, M. (2014). Slow wave activity as the default mode of the cerebral cortex. *Archives Italiennes de Biologie*, *152*, 147–155. https://doi.org/10.12871/000298292014239

Sanchez-Vives, M. V. (2020). Origin and dynamics of cortical slow oscillations. *Current Opinion in Physiology*, *15*, 217–223. https://doi.org/10.1016/j.cophys.2020.04.005

Sanchez-Vives, M. V., Massimini, M., & Mattia, M. (2017). Shaping the Default Activity Pattern of the Cortical Network. *Neuron*, *94*(5), 993–1001. https://doi.org/10.1016/j.neuron.2017.05.015

Sanchez-Vives, M. V., & McCormick, D. A. (2000). Cellular and network mechanisms of rhythmic recurrent activity in neocortex. *Nature Neuroscience*, *3*(10), 1027–1035. https://doi.org/10.1038/79848

Sato, Bergmann, T. O., & Borich, M. R. (2015). Opportunities for concurrent transcranial magnetic stimulation and electroencephalography to characterize cortical activity in stroke. *Frontiers in Human Neuroscience*, *9*. https://www.frontiersin.org/articles/10.3389/fnhum.2015.00250

Sato, T. K., Nauhaus, I., & Carandini, M. (2012). Traveling Waves in Visual Cortex. *Neuron*, *75*(2), 218–229. https://doi.org/10.1016/j.neuron.2012.06.029

Saxena, D., & Cao, J. (2021). Generative Adversarial Networks (GANs): Challenges, Solutions, and Future Directions. *ACM Computing Surveys*, *54*(3), 63:1-63:42. https://doi.org/10.1145/3446374

Scheid, B. H., Ashourvan, A., Stiso, J., Davis, K. A., Mikhail, F., Pasqualetti, F., Litt, B., & Bassett, D. S. (2021). Time-evolving controllability of effective connectivity networks during seizure progression. *Proceedings of the National Academy of Sciences of the United States of America*, *118*(5), e2006436118. https://doi.org/10.1073/pnas.2006436118

Schindler, K. A., Bialonski, S., Horstmann, M.-T., Elger, C. E., & Lehnertz, K. (2008). Evolving functional network properties and synchronizability during human epileptic seizures. *Chaos: An Interdisciplinary Journal of Nonlinear Science*, *18*(3), 033119. https://doi.org/10.1063/1.2966112

Schindler, K., Amor, F., Gast, H., Müller, M., Stibal, A., Mariani, L., & Rummel, C. (2010). Peri-ictal correlation dynamics of high-frequency (80–200Hz) intracranial EEG. *Epilepsy Research*, *89*(1), 72–81. https://doi.org/10.1016/j.eplepsyres.2009.11.006

Schlegl, T., Seeböck, P., Waldstein, S. M., Langs, G., & Schmidt-Erfurth, U. (2019). f-AnoGAN: Fast unsupervised anomaly detection with generative adversarial networks. *Medical Image Analysis*, *54*, 30–44. https://doi.org/10.1016/j.media.2019.01.010

Schurr, A., Payne, R. S., Heine, M. F., & Rigor, B. M. (1995). Hypoxia, excitotoxicity, and neuroprotection in the hippocampal slice preparation. *Journal of Neuroscience Methods*, *59*(1), 129–138. https://doi.org/10.1016/0165-0270(94)00203-S

Seeliger, K., Güçlü, U., Ambrogioni, L., Güçlütürk, Y., & van Gerven, M. A. (2018). Generative adversarial networks for reconstructing natural images from brain activity. *NeuroImage*, *181*, 775–785.

Siddique, N., Paheding, S., Elkin, C. P., & Devabhaktuni, V. (2021). U-Net and Its Variants for Medical Image Segmentation: A Review of Theory and Applications. *IEEE Access*, *9*, 82031–82057. https://doi.org/10.1109/ACCESS.2021.3086020

Simmons, D. A., Lartey, F. M., Schüler, E., Rafat, M., King, G., Kim, A., Ko, R., Semaan, S., Gonzalez, S., Jenkins, M., Pradhan, P., Shih, Z., Wang, J., von Eyben, R., Graves, E. E.,

Maxim, P. G., Longo, F. M., & Loo, B. W. (2019). Reduced cognitive deficits after FLASH irradiation of whole mouse brain are associated with less hippocampal dendritic spine loss and neuroinflammation. *Radiotherapy and Oncology*, *139*, 4–10. https://doi.org/10.1016/j.radonc.2019.06.006

Simon, W., Hapfelmeier, G., Kochs, E., Zieglgänsberger, W., & Rammes, G. (2001). Isoflurane Blocks Synaptic Plasticity in the Mouse Hippocampus. *Anesthesiology*, *94*(6), 1058–1065. https://doi.org/10.1097/00000542-200106000-00021

Song, S., Sjöström, P. J., Reigl, M., Nelson, S., & Chklovskii, D. B. (2005). Highly nonrandom features of synaptic connectivity in local cortical circuits. *PLoS Biology*, *3*(3), e68. https://doi.org/10.1371/journal.pbio.0030068

Spedding, M., Chattarji, S., Spedding, C., & Jay, T. M. (2021). Brain circuits at risk in psychiatric diseases and pharmacological pathways. *Thérapie*, *76*(2), 75–86. https://doi.org/10.1016/j.therap.2020.12.005

Spiegler, A., Hansen, E. C. A., Bernard, C., McIntosh, A. R., & Jirsa, V. K. (2016). Selective Activation of Resting-State Networks following Focal Stimulation in a Connectome-Based Network Model of the Human Brain. *eNeuro*, *3*(5), ENEURO.0068-16.2016. https://doi.org/10.1523/ENEURO.0068-16.2016

Spira, M. E., & Hai, A. (2013). Multi-electrode array technologies for neuroscience and cardiology. *Nature Nanotechnology*, *8*(2), 83–94. https://doi.org/10.1038/nnano.2012.265

Stark, E., & Abeles, M. (2007). Predicting Movement from Multiunit Activity. *Journal of Neuroscience*, *27*(31), 8387–8394. https://doi.org/10.1523/JNEUROSCI.1321-07.2007

Stein, R. B., Gossen, E. R., & Jones, K. E. (2005). Neuronal variability: Noise or part of the signal? *Nature Reviews Neuroscience*, *6*(5), 389–398. https://doi.org/10.1038/nrn1668

Steullet, P., Cabungcal, J.-H., Coyle, J., Didriksen, M., Gill, K., Grace, A. A., Hensch, T. K., LaMantia, A.-S., Lindemann, L., Maynard, T. M., Meyer, U., Morishita, H., O&amp, P., apos, Donnell, Puhl, M., Cuenod, M., & Do, K. Q. (2017). Oxidative stress-driven parvalbumin interneuron impairment as a common mechanism in models of schizophrenia. *Molecular Psychiatry*, *22*(7), 936–936. https://doi.org/10.1038/mp.2017.47

Stevenson, I. H., & Kording, K. P. (2011). How advances in neural recording affect data analysis. *Nature Neuroscience*, *14*(2), Article 2. https://doi.org/10.1038/nn.2731

Stringer, C., Pachitariu, M., Steinmetz, N. A., Okun, M., Bartho, P., Harris, K. D., Sahani, M., & Lesica, N. A. (2016). Inhibitory control of correlated intrinsic variability in cortical networks. *eLife*, *5*, e19695. https://doi.org/10.7554/eLife.19695

Stringer, C., Pachitariu, M., Steinmetz, N., Carandini, M., & Harris, K. D. (2019). High-dimensional geometry of population responses in visual cortex. *Nature*, *571*(7765), 361–365. https://doi.org/10.1038/s41586-019-1346-5

Stringer, C., Pachitariu, M., Steinmetz, N., Reddy, C. B., Carandini, M., & Harris, K. D. (2019). Spontaneous behaviors drive multidimensional, brainwide activity. *Science (New York, N.Y.)*, *364*(6437), 255. https://doi.org/10.1126/science.aav7893

Tauskela, J. S., Kuebler, E. S., Thivierge, J.-P., Aylsworth, A., Hewitt, M., Zhao, X., Mielke, J. G., & Martina, M. (2021). Resilience of network activity in preconditioned neurons exposed to 'stroke-in-a-dish' insults. *Neurochemistry International*, *146*, 105035. https://doi.org/10.1016/j.neuint.2021.105035

Thierry, A.-M., Gioanni, Y., Dégénétais, E., & Glowinski, J. (2000). Hippocampo-prefrontal cortex pathway: Anatomical and electrophysiological characteristics. *Hippocampus*, *10*(4), 411–419. https://doi.org/10.1002/1098-1063(2000)10:4<411::AID-HIPO7>3.0.CO;2-A

Thivierge, J.-P. (2020). Frequency-separated principal component analysis of cortical population activity. *Journal of Neurophysiology*, *124*(3), 668–681. https://doi.org/10.1152/jn.00167.2020

Thomas, C. A., Springer, P. A., Loeb, G. E., Berwald-Netter, Y., & Okun, L. M. (1972). A miniature microelectrode array to monitor the bioelectric activity of cultured cells. *Experimental Cell Research*, *74*(1), 61–66. https://doi.org/10.1016/0014-4827(72)90481-8

Ting, J. T., Daigle, T. L., Chen, Q., & Feng, G. (2014). Acute brain slice methods for adult and aging animals: Application of targeted patch clampanalysis and optogenetics. *Methods in Molecular Biology (Clifton, N.J.)*, *1183*, 221–242. https://doi.org/10.1007/978-1-4939-1096-0_14

Ting, J. T., Lee, B. R., Chong, P., Soler-Llavina, G., Cobbs, C., Koch, C., Zeng, H., & Lein, E. (2018). Preparation of Acute Brain Slices Using an Optimized N-Methyl-D-glucamine Protective Recovery Method. *JoVE (Journal of Visualized Experiments)*, *132*, e53825. https://doi.org/10.3791/53825

Tournier, J.-D., Mori, S., & Leemans, A. (2011). Diffusion Tensor Imaging and Beyond. *Magnetic Resonance in Medicine*, *65*(6), 1532–1556. https://doi.org/10.1002/mrm.22924

Townsend, R. G., & Gong, P. (2018). Detection and analysis of spatiotemporal patterns in brain activity. *PLOS Computational Biology*, *14*(12), e1006643. https://doi.org/10.1371/journal.pcbi.1006643

Townsend, R. G., Solomon, S. S., Chen, S. C., Pietersen, A. N. J., Martin, P. R., Solomon, S. G., & Gong, P. (2015). Emergence of Complex Wave Patterns in Primate Cerebral Cortex. *Journal of Neuroscience*, *35*(11), 4657–4662. https://doi.org/10.1523/JNEUROSCI.4509-14.2015

Trautmann, E. M., Stavisky, S. D., Lahiri, S., Ames, K. C., Kaufman, M. T., O'Shea, D. J., Vyas, S., Sun, X., Ryu, S. I., Ganguli, S., & Shenoy, K. V. (2019). Accurate Estimation of Neural Population Dynamics without Spike Sorting. *Neuron*, *103*(2), 292-308.e4. https://doi.org/10.1016/j.neuron.2019.05.003

Traynelis, S. F., & Dingledine, R. (1988). Potassium-induced spontaneous electrographic seizures in the rat hippocampal slice. *Journal of Neurophysiology*, *59*(1), 259–276. https://doi.org/10.1152/jn.1988.59.1.259

Trevarrow, M. P., Reelfs, A., Ott, L. R., Penhale, S. H., Lew, B. J., Goeller, J., Wilson, T. W., & Kurz, M. J. (2022). Altered spontaneous cortical activity predicts pain perception in individuals with cerebral palsy. *Brain Communications*, *4*(2), fcac087. https://doi.org/10.1093/braincomms/fcac087

Trevelyan, A. J., Sussillo, D., Watson, B. O., & Yuste, R. (2006). Modular propagation of epileptiform activity: Evidence for an inhibitory veto in neocortex. *The Journal of Neuroscience: The Official Journal of the Society for Neuroscience*, *26*(48), 12447–12455. https://doi.org/10.1523/JNEUROSCI.2787-06.2006

Trevelyan, A. J., Sussillo, D., & Yuste, R. (2007). Feedforward Inhibition Contributes to the Control of Epileptiform Propagation Speed. *Journal of Neuroscience*, *27*(13), 3383–3387. https://doi.org/10.1523/JNEUROSCI.0145-07.2007

Tuleasca, C., Vermandel, M., & Reyns, N. (2021). Stereotactic Radiosurgery: From a Prescribed Physical Radiation Dose Toward Biologically Effective Dose. *Mayo Clinic Proceedings*, *96*(5), 1114–1116. https://doi.org/10.1016/j.mayocp.2021.03.027

Tulyakov, S., Liu, M.-Y., Yang, X., & Kautz, J. (2018). Mocogan: Decomposing motion and content for video generation. *Proceedings of the IEEE Conference on Computer Vision and Pattern Recognition*, 1526–1535.

Ueno, H., Suemitsu, S., Murakami, S., Kitamura, N., Wani, K., Matsumoto, Y., Okamoto, M., & Ishihara, T. (2019). Region-specific reduction of parvalbumin neurons and behavioral changes in adult mice following single exposure to cranial irradiation. *International Journal of Radiation Biology*, *95*(5), 611–625. https://doi.org/10.1080/09553002.2019.1564081

Uhlhaas, P., Pipa, G., Lima, B., Melloni, L., Neuenschwander, S., Nikolić, D., & Singer, W. (2009). Neural synchrony in cortical networks: History, concept and current status. *Frontiers in Integrative Neuroscience*, *3*. https://www.frontiersin.org/articles/10.3389/neuro.07.017.2009

Uylings, H. B. M., Groenewegen, H. J., & Kolb, B. (2003). Do rats have a prefrontal cortex? *Behavioural Brain Research*, *146*(1), 3–17. https://doi.org/10.1016/j.bbr.2003.09.028

Verche, E., San Luis, C., & Hernández, S. (2018). Neuropsychology of frontal lobe epilepsy in children and adults: Systematic review and meta-analysis. *Epilepsy & Behavior*, *88*, 15–20. https://doi.org/10.1016/j.yebeh.2018.08.008

Vincent, K., Tauskela, J. S., Mealing, G. A., & Thivierge, J.-P. (2013). Altered Network Communication Following a Neuroprotective Drug Treatment. *PLoS ONE*, *8*(1), e54478. Gale Academic OneFile.

Viventi, J., Kim, D.-H., Vigeland, L., Frechette, E. S., Blanco, J. A., Kim, Y.-S., Avrin, A. E., Tiruvadi, V. R., Hwang, S.-W., Vanleer, A. C., Wulsin, D. F., Davis, K., Gelber, C. E., Palmer, L., Van der Spiegel, J., Wu, J., Xiao, J., Huang, Y., Contreras, D., … Litt, B. (2011). Flexible, foldable, actively multiplexed, high-density electrode array for mapping brain activity in vivo. *Nature Neuroscience*, *14*(12), 1599–1605. https://doi.org/10.1038/nn.2973

von Economo, C., Koskanis, G., & Triarhou, L. (2008). *Atlas of cytoarchitectonics of the adult human cerebral cortex* (Vol. 10). Basel:Karger. https://cir.nii.ac.jp/crid/1130000798224627200

Vondrick, C., Pirsiavash, H., & Torralba, A. (2016). Generating videos with scene dynamics. *Advances in Neural Information Processing Systems*, *29*.

Wang, K., Liang, M., Wang, L., Tian, L., Zhang, X., Li, K., & Jiang, T. (2007). Altered functional connectivity in early Alzheimer's disease: A resting-state fMRI study. *Human Brain Mapping*, *28*(10), 967–978. https://doi.org/10.1002/hbm.20324

Wang, R., Bashyam, V., Yang, Z., Yu, F., Tassopoulou, V., Chintapalli, S. S., Skampardoni, I., Sreepada, L. P., Sahoo, D., Nikita, K., Abdulkadir, A., Wen, J., & Davatzikos, C. (2023). Applications of generative adversarial networks in neuroimaging and clinical neuroscience. *NeuroImage*, *269*, 119898. https://doi.org/10.1016/j.neuroimage.2023.119898

Wang, S., Kfoury, C., Marion, A., Lévesque, M., & Avoli, M. (2022). Modulation of in vitro epileptiform activity by optogenetic stimulation of parvalbumin-positive interneurons. *Journal of Neurophysiology*, *128*(4), 837–846. https://doi.org/10.1152/jn.00192.2022

Wei, W., Poirion, E., Bodini, B., Tonietto, M., Durrleman, S., Colliot, O., Stankoff, B., & Ayache, N. (2020). Predicting PET-derived myelin content from multisequence MRI for individual longitudinal analysis in multiple sclerosis. *NeuroImage*, *223*, 117308. https://doi.org/10.1016/j.neuroimage.2020.117308

Wenzel, M., Hamm, J. P., Peterka, D. S., & Yuste, R. (2017). Reliable and Elastic Propagation of Cortical Seizures In Vivo. *Cell Reports*, *19*(13), 2681–2693. https://doi.org/10.1016/j.celrep.2017.05.090

Wenzel, M., Hamm, J. P., Peterka, D. S., & Yuste, R. (2019). Acute Focal Seizures Start As Local Synchronizations of Neuronal Ensembles. *Journal of Neuroscience*, *39*(43), 8562–8575. https://doi.org/10.1523/JNEUROSCI.3176-18.2019

Wu, J.-Y, Huang, X., & Zhang, C. (2008). Propagating Waves of Activity in the Neocortex: What They Are, What They Do. *The Neuroscientist*, *14*(5), 487–502. https://doi.org/10.1177/1073858408317066

Wu, P., Coultrap, S., Pinnix, C., Davies, K. D., Tailor, R., Ang, K. K., Browning, M. D., & Grosshans, D. R. (2012). Radiation Induces Acute Alterations in Neuronal Function. *PLOS ONE*, *7*(5), e37677. https://doi.org/10.1371/journal.pone.0037677

Xia, T., Chartsias, A., Wang, C., & Tsaftaris, S. A. (2021). Learning to synthesise the ageing brain without longitudinal data. *Medical Image Analysis*, *73*, 102169. https://doi.org/10.1016/j.media.2021.102169

Xia, Y. (2020). Chapter Eleven—Correlation and association analyses in microbiome study integrating multiomics in health and disease. In J. Sun (Ed.), *Progress in Molecular Biology and Translational Science* (Vol. 171, pp. 309–491). Academic Press. https://doi.org/10.1016/bs.pmbts.2020.04.003

Xiao, Y., Huang, X.-Y, Van Wert, S., Barreto, E., Wu, J.-Y., Gluckman, B. J., & Schiff, S. J. (2012). The role of inhibition in oscillatory wave dynamics in the cortex. *European Journal of Neuroscience*, *36*(2), 2201–2212. https://doi.org/10.1111/j.1460-9568.2012.08132.x

Xu, D., Fang, J., Zhang, M., Wang, H., Zhang, T., Hang, T., Xie, X., & Hu, N. (2021). Synchronized intracellular and extracellular recording of action potentials by three-

dimensional nanoroded electroporation. *Biosensors and Bioelectronics*, *192*, 113501. https://doi.org/10.1016/j.bios.2021.113501

Xu, W., Huang, X., Takagaki, K., & Wu, J. (2007). Compression and reflection of visually evoked cortical waves. *Neuron*, *55*(1), 119–129. https://doi.org/10.1016/j.neuron.2007.06.016

Yamawaki, N., Radulovic, J., & Shepherd, G. M. G. (2016). A Corticocortical Circuit Directly Links Retrosplenial Cortex to M2 in the Mouse. *Journal of Neuroscience*, *36*(36), 9365–9374. https://doi.org/10.1523/JNEUROSCI.1099-16.2016

Yan, Z., & Rein, B. (2022). Mechanisms of synaptic transmission dysregulation in the prefrontal cortex: Pathophysiological implications. *Molecular Psychiatry*, *27*(1), Article 1. https://doi.org/10.1038/s41380-021-01092-3

Yuan, H., Gaber, M. W., Boyd, K., Wilson, C. M., Kiani, M. F., & Merchant, T. E. (2006). Effects of fractionated radiation on the brain vasculature in a murine model: Blood–brain barrier permeability, astrocyte proliferation, and ultrastructural changes. *International Journal of Radiation Oncology*Biology*Physics*, *66*(3), 860–866. https://doi.org/10.1016/j.ijrobp.2006.06.043

Zaer, H., Fan, W., Orlowski, D., Glud, A. N., Jensen, M. B., Worm, E. S., Lukacova, S., Mikkelsen, T. W., Fitting, L. M., Jacobsen, L. M., Portmann, T., Hsieh, J.-Y., Noel, C., Weidlich, G., Chung, W., Riley, P., Jenkins, C., Adler, J. R., Schneider, M. B., … Stroh, A. (2022). Non-ablative doses of focal ionizing radiation alters function of central neural circuits. *Brain Stimulation*, *15*(3), 586–597. https://doi.org/10.1016/j.brs.2022.04.001

Zaer, H., Glud, A. N., Schneider, B. M., Lukacova, S., Vang Hansen, K., Adler, J. R., Høyer, M., Jensen, M. B., Hansen, R., Hoffmann, L., Worm, E. S., Sørensen, J. C. H., & Orlowski, D. (2020). Radionecrosis and cellular changes in small volume stereotactic brain radiosurgery in a porcine model. *Scientific Reports*, *10*(1), 16223. https://doi.org/10.1038/s41598-020-72876-w

Zhang, D., Zhou, W., Lam, T. T., Li, Y., Duman, J. G., Dougherty, P. M., & Grosshans, D. R. (2020). Cranial irradiation induces axon initial segment dysfunction and neuronal injury in the prefrontal cortex and impairs hippocampal coupling. *Neuro-Oncology Advances*, *2*(1), vdaa058. https://doi.org/10.1093/noajnl/vdaa058

Zhang, D., Zhou, W., Lam, T. T., Weng, C., Bronk, L., Ma, D., Wang, Q., Duman, J. G., Dougherty, P. M., & Grosshans, D. R. (2018). Radiation induces age-dependent deficits in cortical synaptic plasticity. *Neuro-Oncology*, *20*(9), 1207–1214. https://doi.org/10.1093/neuonc/noy052

Zhao, J., Huang, J., Zhi, D., Yan, W., Ma, X., Yang, X., Li, X., Ke, Q., Jiang, T., Calhoun, V. D., & Sui, J. (2020). Functional network connectivity (FNC)-based generative adversarial network (GAN) and its applications in classification of mental disorders. *Journal of Neuroscience Methods*, *341*, 108756. https://doi.org/10.1016/j.jneumeth.2020.108756

Zhong, Y.-M., Yukie, M., & Rockland, K. S. (2006). Distinctive morphology of hippocampal CA1 terminations in orbital and medial frontal cortex in macaque monkeys. *Experimental Brain Research*, *169*(4), 549–553. https://doi.org/10.1007/s00221-005-0187-7

Zhou, Z., Zhang, G., Li, X., Yang, C., & Yang, J. (2012). Fast-spiking interneurons and gamma oscillations may be involved in the antidepressant effects of ketamine. *Medical Hypotheses*, *79*(1), 85–86. https://doi.org/10.1016/j.mehy.2012.04.007

Zingg, B., Hintiryan, H., Gou, L., Song, M. Y., Bay, M., Bienkowski, M. S., Foster, N. N., Yamashita, S., Bowman, I., Toga, A. W., & Dong, H.-W. (2014). Neural Networks of the Mouse Neocortex. *Cell*, *156*(5), 1096–1111. https://doi.org/10.1016/j.cell.2014.02.023

Zirkle, J., & Rubchinsky, L. L. (2021). Noise effect on the temporal patterns of neural synchrony. *Neural Networks*, *141*, 30–39.